

---

# **Aerodynamic Characteristics of Two-Dimensional Wing Configurations at Angles of Attack Near $-90^\circ$**

---

Martin Maisel, Georgene Laub, and W.J. McCroskey

---

December 1986

(NASA-TM-88373) AERODYNAMIC CHARACTERISTICS  
OF TWO-DIMENSIONAL WING CONFIGURATIONS AT  
ANGLES OF ATTACK NEAR  $-90^\circ$  DEG (NASA) 84 p  
CSCL 01A

N87-15182

G3/02 40347  
Unclas

**NASA**  
National Aeronautics and  
Space Administration

United States Army  
Aviation Systems  
Command



---

# **Aerodynamic Characteristics of Two-Dimensional Wing Configurations at Angles of Attack Near $-90^\circ$**

---

Martin Maisel,

Georgene Laub,

W. J. McCroskey, Aeroflightdynamics Directorate, U.S. Army Aviation Research  
and Technology Activity,  
Ames Research Center, Moffett Field, California



National Aeronautics and  
Space Administration

**Ames Research Center**

Moffett Field, California 94035

United States Army  
Aviation Systems  
Command  
St. Louis, Missouri 63120



## SYMBOLS

$b$	ratio of model wing chord to test section lateral dimension
$c$	wing chord, ft (reference chord = 1 ft)
$c_e$	effective chord length, projection on chord line of distance from leading edge to trailing edge, ft
$C_D$	drag coefficient, $D/qS$
$C_L$	lift coefficient, $L/qS$
$C_M$	pitching moment coefficient, $M/qSc$
$C_p$	pressure coefficient, $(p_{\text{local}} - p_{\text{tunnel static}})/q$
$D$	drag force, lb
$L$	lift force, lb
$M$	pitching moment about quarter chord, ft-lb
$p$	pressure, lb/ft <sup>2</sup>
$q$	dynamic pressure, $(1/2)\rho V^2$ , lb/ft <sup>2</sup>
$Re$	Reynolds number, $\rho(Vc)/\mu$
$S$	wing reference area, ft <sup>2</sup> (reference area = 5 ft <sup>2</sup> )
$v$	tunnel velocity, ft/sec
$x$	chordwise distance from leading edge/ $c$
$y$	distance normal to chord line/ $c$
$\alpha$	angle of attack, referenced to chord line, deg
$\delta_F$	flap deflection angle, deg
$\delta_S$	slat deflection angle, deg
$\epsilon$	constant
$\mu$	coefficient of viscosity, slugs/ft-sec

$\rho$  mass density of air, slugs/ft<sup>3</sup>

Subscripts:

base pertains to conditions at the most downstream (leeward) surface of a body

force value derived from wind tunnel balance system data

o uncorrected value

local pertains to condition at a point on the surface of the model

lower pertains to the lower wing surface (-y)

pressure value derived from model surface pressure data

upper pertains to the upper wing surface (+y)

# AERODYNAMIC CHARACTERISTICS OF TWO-DIMENSIONAL WING CONFIGURATIONS

AT ANGLES OF ATTACK NEAR  $-90^\circ$

M. D. Maisel, G. H. Laub, and W. J. McCroskey

Aeroflightdynamics Directorate, U.S. Army Aviation and Technology Activity  
Ames Research Center, Moffett Field, California

## SUMMARY

Wind tunnel tests were conducted to determine the drag of two-dimensional wing sections operating in a near-vertical flow condition. Various leading- and trailing-edge configurations, including plain flaps of 25, 30, and 35% chord were tested at angles of attack from  $-75$  to  $-105^\circ$ . Reynolds Numbers examined ranged from approximately  $0.6 \times 10^6$  to  $1.4 \times 10^6$ . The data were obtained using a wind tunnel force and moment balance system and arrays of chordwise pressure orifices. The results showed that significant reductions in drag, beyond what would be expected by virtue of the decreased frontal area, were obtainable with geometries that delayed flow separation. Rapid changes in drag with angle of attack were noted for many configurations. The results, however, were fairly insensitive to Reynolds Number variations. Drag values computed from the pressure data generally agreed with the force data within 2%.

## INTRODUCTION

Several vertical take-off and landing (VTOL) rotorcraft configurations place a wing surface in the wake of the lifting rotor during hover conditions. Two examples of this are the compound helicopter which uses wing surfaces to reduce the rotor mean loads in high-speed cruise flight and the tilt rotor aircraft which places the rotor axes at the wing tips. It is essential for all types of vertical take-off rotorcraft to minimize the vertical drag of airframe components immersed in the rotor wake to increase the lift available for useful load. To that end, flow visualization investigations were conducted employing tufts and smoke on the XV-15 Tilt Rotor Research Aircraft at NASA Ames Research Center and on a scale tilt-rotor model in the Army 7- by 10-Foot Subsonic Wind Tunnel at Ames to determine the general nature of the flow over the wing. These tests revealed that a portion of the wing is exposed to a flow field which, after approaching from above, forms a stagnation bubble near the midchord, and then spills over the leading and trailing edges of the wing in a chordwise direction (fig. 1). This flow condition is so uncommon that there exists little information in the literature on the resulting vertical drag and the influence of leading- and trailing-edge geometry and passive devices on the magnitude of that drag. Examples of the available data are presented in references 1, 2, and 3. Recognizing the potentially significant gains in hover payload

that could be obtained with even modest reductions in wing download for vehicles such as the tilt rotor aircraft, an experimental investigation was conducted in the U. S. Army Aeromechanics Laboratory (currently the Aeroflightdynamics Directorate, U. S. Army Aviation Research and Technology Activity, AVSCOM) 7- by 10-Foot Subsonic Wind Tunnel at Ames Research Center. The effort focused on the chordwise two-dimensional flow condition noted above. This report presents the test results for a series of two-dimensional wing sections operating in a near-vertical flow field (i.e., at angles of attack near  $-90^\circ$ ). The data is intended to provide some insight into the effects of wing geometry on near-vertical drag and to provide guidance in the design of the portion of the wing immersed in a rotor wake which experiences primarily chordwise flow.

## TEST OBJECTIVES

The two-dimensional model wind tunnel test focused on the following objectives for the near  $-90^\circ$  angle-of-attack flow condition:

1. Establishment of the relative vertical drag of various wing (leading- and trailing-edge) configurations to identify the significant factors which influence the reduction of drag and to enable meaningful trade-off design studies between the structural-mechanical (weight) and aerodynamic requirements of wings for application to rotorcraft.
2. Establishment of values for drag coefficients of the various two-dimensional wing sections for use in analysis of download performance losses.
3. Assessment of the sensitivity of the drag coefficient to inflow angle (angle of attack).
4. Assessment of the effect of Reynolds number on drag coefficient.

## MODEL AND APPARATUS

Figure 2 illustrates the installation of the two-dimensional model in the wind tunnel. The model spar is cantilevered from the frame of the force and moment balance system located below the wind tunnel floor, which places the span vertically and the chord horizontally (approximately normal to the flow) in the test section. A turntable in the balance frame permitted remote adjustment of the model angle of attack  $\pm 20^\circ$ . Large endplates (located 1 ft from the wind tunnel floor and ceiling) were used to separate the wing section from the wind-tunnel-wall boundary layer. The endplate size was based on the observations and recommendations of reference 4. Both endplates were mounted to the wind tunnel walls and did not physically contact the wing model. A fairing between the lower endplate and the wind tunnel floor prevented the development of significant airloads on the nonaerodynamic support portion of the wing spar.

A 12-in. chord was selected to obtain Reynolds numbers on the order of one million within the model structural limits, although it was recognized that the blockage correction would be fairly large (approximately 10%) for some of the higher drag configurations. An array of detachable leading- and trailing-edge configurations were fabricated. All movable surfaces (flaps, slats) were manually set using slotted linkages attached to tiedown points on the wing's lower surface. Figure 3 illustrates the cross section of the various shapes tested, which are based on the NACA-64A223 airfoil used on the XV-15 Tilt Rotor Research Aircraft. The flap chord reference used in this report is based on the overall length of the flap. For comparison, when the hinge center to trailing-edge distance is used to define the flap length, the 25, 30, and 35% flap chord ratios reported here become 20, 25, and 30% respectively. In addition, equilateral triangular cylinders with 12-in. sides (same as the basic wing chord) and 8.5-in. sides were tested with the base to the wind and with the apex to the wind to aid in assessing the wall correction method by comparison with prior data. Wind-tunnel-wall pressure signatures were obtained during a portion of the tests.

For the basic airfoil with plain flaps, 15 upper- and 10 lower-surface pressure orifices were placed at three spanwise locations--midspan and 12 in. from each endplate. The distribution of the pressure orifices is shown in figure 4. Tubing connected to these orifices was routed out from the top of the model through the upper fairing to the six-transducer scanivalve package located on top of the tunnel.

## TESTS

Test section dynamic pressure ( $q$ ) ranged from 11 to 53 lb/ft<sup>2</sup> (giving an air-speed range of approximately 100 to 220 ft/sec). The maximum speed, which varied for each configuration, was limited by model deflections or by vibratory oscillations. Except for the Reynolds number evaluation, the data presented in this report were obtained at a dynamic pressure of 31 lb/ft<sup>2</sup> (yielding a Reynolds number of about  $1.0 \times 10^6$ ).

## REDUCTION OF DATA

### Data Acquisition

Data acquisition and reduction were performed using the 7- by 10-Foot (No. 2) wind tunnel data acquisition system. Data reduction was performed online and the data were stored following each run for further analysis. This data acquisition system recorded the model pressure and force data, tunnel dynamic pressure, static pressure, settling chamber temperature, and forces from the tunnel's external balance system. Model angle of attack (positioned using the tunnel turntable system) was entered manually into the program.

Model pressures were acquired at three spanwise stations using a six-transducer scanivalve package. The pressure acquisition program controlled the scanivalve stepping, sampled all the data channels at each scanivalve step, and averaged all the tunnel flow and force measurements taken at the 17 scanivalve steps. The online program yielded the model pressure data as differential pressures relative to the tunnel static pressure and presented forces and moments in coefficient form. An off-line version of the program converted the pressures to coefficient form.

The force acquisition program was a modified version of the pressure program with the exception that only three readings were averaged for each data point. As with the pressure program, the forces were presented in coefficient form. Neither on-line program included tunnel wall corrections.

#### Accuracy of Measurements

The accuracy of the measured force, moment, and pressure data were determined to be within the following limits.

Lift	$\pm 0.2$ lb
Drag	$\pm 0.2$ lb
Pitching Moment	$\pm 1.0$ ft-lb
Model pressure	$\pm 0.1$ lb/ft <sup>2</sup>
Wind tunnel pressure	$\pm 0.1$ lb/ft <sup>2</sup>
Angle of Attack	$\pm 0.5$ deg
Flap/slat deflection	$\pm 2.0$ deg

Some of the bluff bodies tested during this investigation produce an unsteady, turbulent-wake and/or model-dynamic oscillations that could affect the repeatability of the test data. Multiple data points for most of the test conditions revealed that a hysteresis condition exists for some configurations where flow separation was imminent or unstable.

#### FORCE/MOMENT DATA REDUCTION

The six-component, wind-tunnel scale data was reduced to standard aerodynamic coefficient form, based on the reference 1-ft chord length, the 5-ft span, and the dynamic pressure which was corrected for blockage. Moments are referenced to the one-quarter chord location.

The sign convention as applied to the data presented here is in accordance with standard practice with respect to the flow direction and the airfoil orientation at low (conventional) angles of attack. Therefore, it should be noted that positive values of lift coefficient at angles of attack near  $-90^\circ$  represent a force directed toward the airfoil's trailing edge.



## RESULTS AND DISCUSSION

The investigation examined a 25, 30, and 35% chord plain flap with the basic airfoil leading edge, and an array of leading edge configurations with the 30% trailing edge flap. A range of inflow angles from  $-75$  to  $-105^\circ$  angle of attack was examined for most test models. Except where noted, the models were run with the flap slot unsealed. A listing of the model configurations tested and the resulting data plots are given in table 1.

Confirmation that the tested inflow angles included the angle-of-attack range of interest was provided by obtaining photographs of tufts in the near wake of the XV-15 rotor while the aircraft was mounted on a tiedown stand. The results of this test are shown in figure 5. The predominant inflow lies between  $-80$  and  $-88^\circ \alpha$ , with a mean value of approximately  $-84^\circ$ . (Note that the XV-15 rotor was operating at a height-to-diameter ratio of about 0.75 during the tiedown test and that the direction of the rotor rotation is from the wing leading edge to the trailing edge.) Opposite rotation of the rotor would be expected to provide a mean angle of attack of about  $-96^\circ$ .

### Trailing Edge Variations for a 30% Flap

#### Plain Flap, 30% c

Figure 6 presents the 30% plain flap with the basic airfoil leading edge (configuration b of fig. 3). The variation of the aerodynamic coefficients with angle of attack for various flap angles is shown in figure 6a.

In figure 6b the drag coefficient is seen to decrease with flap deflection until a  $C_D$  level of about 1.0 is reached. A cross plot at pertinent inflow angles is given in figure 6c. The steady reduction in drag coefficient with increasing flap angle is interrupted by a sharp drag coefficient increase at the onset of flow separation on the upper surface of the flap. This separation is indicated by unstable and reversed surface tufts, and by sharp local pressure changes. Figures 6b and c also show that the flap angle at which separation occurs varies with wing angle of attack. Moreover, the separation appeared to be dependent on the orientation of the flap upper-surface angle with respect to the free-stream direction.

The lift and moment coefficient generally increases in value with decreasing angle of attack but remains small for all flap positions tested. At the minimum drag configuration ( $\delta_F = 60^\circ$  at  $-85^\circ \alpha$ ), the lift coefficient is about 0.1. The moment coefficient decreases in value with increasing flap deflection and approaches zero at the  $60^\circ \delta_F$  minimum drag point. As a reference, for comparison with other data, the drag coefficient for the 30% plain flap at  $-85^\circ$  angle of attack is 1.0.

Figure 6d shows that the reduction in drag coefficient with flap deflection is greater than the associated reduction of the wing frontal area. This figure

TABLE 1.- MODEL CONFIGURATION AND DATA LOG

Model configuration	Cross section	Flap chord, %	$C_L$ , $C_D$ , $C_M$ vs $\alpha$	$C_D$ vs $\alpha$	Other force data	Pressure data
Plain flap	Fig. 3(a)	25	Fig. 24(a) Fig. 24(c) + upper surface spoiler	Fig. 24(b) Fig. 24(d) + upper surface spoiler		Figs. 27, 28, 29, 30 (with spoiler) 31(a), 32(a)
Plain flap	Fig. 3(b)	30	Fig. 6(a)	Fig. 6(b)	Fig. 6(c), $C_D$ vs $\delta_F$ Fig. 6(d), $C_D$ & $c_e$ Reduction vs $\delta_F$ Fig. 26, $C_D$ vs $Re_6$ $0.6 \times 10^6$ to $1.4 \times 10^6$	Fig. 31(b), 32(b)
Plain flap	Fig. 3(c)	35	Fig. 25(a)	Fig. 25(b)		Fig. 31(c), 32(c)
Plain flap with upper-surface spoiler	Fig. 3(d)	30	Fig. 7(a)	Fig. 7(b)	Fig. 7(c), $C_D$ vs spoiler location	
Modified flap	Fig. 3(e)	30	Fig. 8(a)	Fig. 8(b)		
Slot forward of flap	Fig. 3(f)	30	Fig. 9(a) Fig. 10(a) vs slot size	Fig. 9(b)	Fig. 10(b) $C_D$ vs slot size	
Lower flap hinge	Fig. 3(g)	30	Fig. 11(a)	Fig. 11(b)		
Umbrella leading edge	Fig. 3(h), Fig. 12	30	Fig. 13(a), (b), (c) Fig. 13(h) blockage in slot	Fig. 13(d), (e), (f), (g) Fig. 13(i) blockage in slot		
Umbrella leading edge + modified flap	Fig. 3(i)	30	Fig. 14(a)	Fig. 14(b)		

TABLE 1.- CONCLUDED

Model configuration	Cross section	Flap chord, %	$C_L$ , $C_D$ , $C_M$ vs $\alpha$	$C_D$ vs $\alpha$	Other force data	Pressure data
Lower leading-edge slat	Fig. 3(j), Fig. 15	30	Fig. 16(a), (b)	Fig. 16(c)		
Upper leading slat, forward hinge	Fig. 3(k), Fig. 17	30	Fig. 18(a)	Fig. 18(b)	Fig. 18(c), $C_D$ vs slat angle	
Upper leading-edge slat, aft hinge	Fig. 3(l)	30	Fig. 19(a)	Fig. 19(b), Fig. 20	Fig. 19(c), $C_D$ vs slat angle	
Upper leading-edge slat, increased slot	Fig. 3(m)	30	Fig. 21(a)	Fig. 21(b)		
Upper leading-edge slat, increased slot, modified flap	Fig. 3(n)	30	Fig. 22(a)	Fig. 22(b)		
Leading-edge slat removed, modified flap	Fig. 3(o)	30	Fig. 23(a)	Fig. 23(b)		
8.5 in. triangle flat face to wind	Fig. 3(p)				Table B2, $C_{D_o}$ & $C_D$	
12 in. triangle flat face to wind	Fig. 3(q)				Table B2, $C_{D_o}$ & $C_D$	
8.5 in. triangle apex to wind	Fig. 3(r)				Table B2, $C_{D_o}$ & $C_D$	
12 in. triangle apex to wind	Fig. 3(s)				Table B2, $C_{D_o}$ & $C_D$	

indicates that even when the actual or frontal chord is used to calculate the drag coefficient, the coefficient diminishes more than twice as rapidly as the frontal surface area (or chord length). For the plain flap configuration with attached flow on the upper surface, nearly one-half of the drag reduction observed is attributable to the area change in the two-dimensional flow environment.

### Upper Surface Spoiler

The separation phenomenon became the subject of additional experiments. Observation of the tufts applied to the configuration b flap indicated that chordwise flow, rather than the free-stream flow, dominated in the vicinity of the leading-edge of the flap. This results in the inability of the flow field to remain attached aft of the flap leading-edge radius at high flap angles. An attempt was made, therefore, to reduce the strength of the chordwise flow component, thus changing the flow angle approaching the flap upper surface. This was done by placing a spoiler normal to the wing's upper surface forward of the flap's leading edge (configuration d, fig. 3). The spoiler's chordwise location and height above the wing surface were varied to determine the most effective arrangement. Figure 7 shows the drag coefficient obtained with this approach (at a  $75^\circ$  flap angle) was reduced by as much as 0.2 at angles of attack between  $-75^\circ$  and  $-90^\circ$ . Attached flow was maintained at an angle of attack of about  $10^\circ$  lower than what was possible for the untreated airfoil. When compared to the basic plain flap configuration, the spoiler causes an increase in the lift coefficient and little change in moment values.

The minimum drag coefficient was reduced by 0.1 (to approximately  $0.9 C_D$  at  $\alpha = -85^\circ$ ) by using the upper surface spoiler. Figure 7c depicts the effects of the spoiler position on the drag coefficient.

### Modified Flap Contour

The second attempt to delay separation used a modified flap upper-surface (configuration e, of fig. 3). The modification employed a (convex) curved flap surface faired into the constant radius flap leading edge, rather than the nearly flat surface defined by the airfoil coordinates. This method not only altered the separation point but it also provided a small drag reduction (less than 0.1) throughout the range of inflow angles examined, when compared to the unmodified configuration. The practical aspect of this approach (i.e., no additional weight or mechanical complexity) makes it an attractive candidate for download reduction. However, a determination needs to be made of the effects of this flap shape on the airfoil's aerodynamics for the range of inflow angles and Mach numbers encountered in airplane mode flight. Figure 8 illustrates the gains achieved with the 30% chord modified flap.

## Flap Slot

A variant of the 30% plain flap, shown in configuration f of figure 3, provides a large slot forward of the flap's leading edge. It was anticipated that flow through the slot would be sufficient to delay separation.

The performance of this model is shown in figure 9. When compared to the drag of the basic airfoil (configuration b), the large slot produced significant drag reductions for the lower flap angles ( $0^\circ$  to  $45^\circ$ ) for which attached flow existed through ventilation of the lower surface. For the  $60^\circ$  flap angle, however, the slot had essentially no effect on the drag in the attached-flow region ( $\alpha < -85^\circ$ ). In the formerly separated zone ( $\alpha > -85^\circ$ ), the slot enabled the flow to remain attached, and an associated drag reduction was produced. At  $75^\circ$  flap angle, however, the slot could not maintain fully attached flow on the flap's upper surface. The small radius of the forward corner of the slot was found to be too sharp to permit adequate flow turning. The drag coefficient for the  $\delta_F = 75^\circ$  configuration at an angle of attack of  $-85^\circ$  is slightly below 1.0.

The influence of the flap slot size on drag can be evaluated by comparing the drag coefficients produced by the large slot of configuration f and the small slot of configuration b with the closed slot variant of the configuration b airfoil. This effect is shown in figure 10.

## Flap Hinge Location

Configuration g (fig. 3) investigated the effects of relocating the flap hinge line to the lower surface of the airfoil. Using the same flap shape as in configuration b, the lower hinge produces an increase in the slot size as flap angle is increased while moving the flap's leading edge above the wing's upper surface contour.

As in configuration f, the flap slot created by this arrangement was ineffective in maintaining attached flow at the high flap angles. Furthermore, the elevated flap leading edge, coupled with its relatively small radius, apparently contributes to an earlier onset of the separated-flow condition. The results, shown in figure 11, indicate a minimum  $C_D$  of about 1.1 at  $-85^\circ \alpha$  and  $60^\circ \delta_F$ . This design approach would probably have been more effective if the flap shape and hinge point were arranged to provide a large radius leading edge which fairs smoothly into the wing's upper surface contour.

## Leading-Edge Variations

A number of leading-edge variations were examined. The two basic themes of the leading-edge designs were the reduction of frontal (chordwise) area and the delay of separation through the use of leading-edge slats or the modification of the leading-edge contour. These approaches were used either separately or in combination with each other.

## Umbrella Flap

Configuration h (fig. 3) employs a device referred to as the "umbrella flap." The upper and lower segments of this device are hinged at the leading edge. A near-constant radius fairing was selected for the wing's fixed leading edge (forming a slot between the umbrella flap and the wing). The upper and lower flap segments were independently and systematically varied to identify the optimum arrangement. The various positions tested are illustrated in figure 12. Figure 13 shows that with the rather large (25% c) umbrella flap, the minimum drag coefficient can be reduced to approximately 0.4 at  $-85^\circ$   $\alpha$  with a  $60^\circ$  trailing-edge flap angle (umbrella flap set at  $-30^\circ$  upper surface and  $-10^\circ$  lower surface). Although this is the lowest level of drag obtained during this test series, it should be noted that the umbrella flap also produces high lift coefficients (which would alter the aircraft's force and moment trim in hover). This negative lift coefficient represents an aircraft positive thrust force. In addition, the leading edge must be designed to permit flap operation (i.e., hinged segments) while maintaining a stringent leading-edge contour to obtain the desired cruise mode performance. Therefore, the umbrella flap, while quite effective in reducing download, must be assessed in view of the aforementioned potential problems.

Also interesting to note is the complex shape of some of the umbrella flap lift and drag coefficient curves. This is due to the multiple possibilities for flow separation (i.e., separation may occur on the flap's upper surface, the umbrella's upper and lower segments, and the wing's leading edge).

The effect of additional blockage within the leading-edge slot was simulated by placing a 1/4-in. (2% x) diameter rod approximately 1/4-in. forward of the wing's leading-edge surface (representing, for example, a tilt conversion system cross-shaft or a bundle of hydraulic lines). Figure 13h depicts the drag increase (from  $C_D = 0.4$  to  $C_D = 0.5$  at  $\alpha = -85^\circ$ ) resulting from the additional blockage and the associated premature flow separation. Clearly, the leading-edge slot and, of course, the leading-edge surface must remain clean to obtain the lowest download values.

The effect of the modified flap's upper surface on the performance of the umbrella flap (illustrated in configuration i of fig. 3) is presented in figure 14. The data, obtained at a  $75^\circ$  flap angle shows that, similar to the prior application of this flap, separation is delayed and drag is reduced.

## Leading Edge Slat

Two leading-edge slats which maintained a smooth-nose-radius contour were investigated. The configuration-j slat would form the lower leading-edge surface of the wing when retracted for cruise flight, and the configuration-k and -l slats would form the upper surface of the leading edge in cruise flight.

### Lower Surface Slat

The position of the configuration-j, lower-surface slat was varied to determine the optimum orientation. Chordwise locations include: alignment with the airfoil's leading edge, and a position forward of the original leading edge. At the original leading-edge chord location, the slat was operated with the nose pivoted around the center point of the leading-edge radius and at an elevated position. Various angles were examined at each slat setting. Figure 15 illustrates the range of slat positions tested.

The performance of all slat positions yielded reasonably low drag coefficients in the  $-75$  to  $-85^\circ$  range of angle of attack, but a rapid increase between  $-85$  and  $-105^\circ$  was observed because of flow separation at the slat's forward surface and below the leading-edge-door hinge line (fig. 16). Figure 16c shows the effect of angle of attack on drag coefficient for three different slat positions. The sensitivity to angle of attack may result in undesirable variations of download during hover in gusty air. It would also appear that, the configuration-j slat when retracted for cruise flight, could produce a spanwise discontinuity in the airfoil contour at the intersection of the slat and the upper surface door (which would hinge downward to provide the slot opening during hover operations). This spanwise line could adversely affect the airplane mode performance of the wing. In view of the probable hover and airplane mode problems with this configuration, it appears unsuitable for the intended application.

### Upper Surface Slat

The upper surface slat, in the airplane flight mode, provides a continuous upper surface from the leading edge radius to the 25% chord point. This design is based on the presumption that a clean slot is obtained by providing a leading-edge fairing ahead of the forward spar that would enclose all wing hardware and systems (lines, cables, shafting, actuators, etc.). This slat allows for a less complex mechanism than the lower surface slat does in that it could be hinged from a fixed point near the wing's lower surface. Two hinge locations (configurations k and l) and a foreshortened wing leading-edge version (configurations m and n) were examined. The upper surface slat test positions are shown in figure 17.

Initially, the largest wing volume was used. In this configuration the leading-edge fairing is closely nested to the lower/aft surface of the slat. This arrangement provided a very small slot size and produced higher levels of download drag than the prior configuration provided. In addition, a strong sensitivity to angle of attack was noted. Figure 18 shows the forward-hinge-point data whereas figure 19 depicts the performance of the aft-hinge-point model. The lift- and moment-coefficients remain near zero for all test conditions. The effect of slat position (for the forward-hinge location) presented in figure 18c shows that minimum drag is obtained at approximately  $50^\circ \delta_s$  for angles of attack between  $-80$  and  $-85^\circ$ . At higher (negative) angles of attack a lower slat angle would be desired.

Figure 19c (aft-hinge location) indicates that a  $50^\circ$  slat angle would be acceptable for all tested angles of attack ( $-80$  to  $-90^\circ$ ). A comparison of the forward- and aft-hinge location effect is given in figure 20. The leading-edge-slot size was then increased as illustrated in configuration m. This arrangement would reduce the volume available for hardware forward of the wing spar. Figure 21 shows that the altered contour and larger slot not only reduced drag, but also reduced the sensitivity of the drag coefficient to the angle of attack. An additional small improvement in drag was obtained with the modified trailing-edge flap (configuration n) as shown in figure 22 in that attached flow was maintained for the  $75^\circ$  flap angle at angles of attack near  $-90^\circ$ .

This configuration appears to combine a desirable low level of download drag and a low sensitivity to angle of attack in the hover mode with a simple mechanism requirement and a favorable airplane mode geometry. Furthermore, consideration could be given to the use of this slat in improving wing lift in the low speed range for short takeoff and landing rotorcraft such as the low-speed portion of the tilt rotor flight envelope.

The final leading-edge configuration in this test series employed the altered leading-edge contour of configuration m, but deleted the leading-edge slat. The results, presented in figure 23, show that configuration o delivers a drag variation that is fairly insensitive to angle of attack and is slightly higher than the slatted airfoil in the  $-75$  to  $-90^\circ$  angle-of-attack range.

### Variations in Flap Size

#### Plain Flap, 25% c

The performance of the basic airfoil with a 25% plain flap (configuration a) is shown in figure 24a. Although the drag coefficients at flap angles below  $45^\circ$  closely resemble the values for the 30% flap (fig. 6a), separation (and the associated drag increase) occurs over a greater range of angles of attack than it does for the 30% flap. The minimum achievable drag coefficient at  $-85^\circ$  angle of attack would be approximately 1.2 (at a flap angle of about  $50^\circ$ ), compared to about 1.0 for the 30% configuration (at  $60^\circ \delta_F$ ). The greater range of separated inflow angles may be related to the additional buildup of chordwise flow due to the larger unflapped section of the airfoil.

The application of the upper surface spoiler (similar to configuration d) to alter the chordwise flow field produces a greater reduction in drag than achieved for the 30% flap (figs. 24c and d), but the minimum drag ( $C_D = 1.05$ ) remains higher than for the larger flap.

#### Plain Flap, 35% c

The variation of the aerodynamic coefficients with angle of attack at various flap angles for the 35% chord plain flap model (configuration c of fig. 3) is presented in figure 25a. The drag coefficient variation is summarized in figure 25b.



The reason why this model did not provide a further reduction in minimum drag, as compared to the 30% chord plain flap, is not understood. Observations of the flow conditions on the flap's upper surface, however, were consistent with the measured data. At a  $-90^\circ$  inflow angle, flow separation on the 35% chord flap occurred at  $60^\circ \delta_F$ . The 30% chord (producing the minimum drag) indicated separation at about  $70^\circ \delta_F$ , whereas the flow over the 25% chord plain flap separated at about  $52.5^\circ \delta_F$  for the  $-90^\circ \alpha$  condition. It is possible that the favorable aspects of the 35% chord flap as compared to the 30% chord flap (i.e., the larger flap leading-edge radius and the expected lower chordwise velocity at the flap cove) are more than offset by the longer flap chord length which is subjected to the adverse pressure field. If this rationale is correct, it suggests that in the vicinity of the minimum drag condition (or just prior to the onset of separation) flow perturbations or surface irregularities could trigger the separation phenomenon and result in higher than minimum-achievable drag values.

### Reynolds Number Effects

Each model was tested over a range of wind tunnel speeds to obtain a Reynolds number variation. Figure 26 shows the effect of Reynolds number on the drag coefficient for an array of configurations. The drag is found to be fairly insensitive to Reynolds number between the achievable values of  $0.6 \times 10^6$  to  $1.4 \times 10^6$ . Note that the Reynolds number is based on the free-stream velocity and the full (1 ft) chord dimension.

### Pressure Data

Surface pressure data was obtained during portions of the 25, 30, and 35% plain flap tests (configurations a, b, c, and d). For the 25% flap at a constant ( $-90^\circ$ ) angle of attack, a variation of flap angle produces the pressure distribution shown in figure 27. For all flap positions, the base pressure is seen to be nearly constant across the chord. A noticeable irregularity of the upper-surface pressure coefficient is observed at the leading edge of the flap. As the flap angle is increased, the flap's upper surface pressure coefficient decreases until a local separation occurs just behind the flap's leading-edge radius at  $45^\circ \delta_F$ . Further aft on the flap, the flow reattaches (as also indicated by tuft observation and by the slightly elevated surface pressure). At higher flap angles, the separation encompasses the entire flap upper surface, and the pressure remains at, or below, the lower surface value.

The effects of angle of attack on surface pressure is illustrated in figure 28. As the inflow progresses from  $-75$  to  $-100^\circ \alpha$ , the fully separated upper surface of the flap becomes partially separated (aft of the flap leading edge) at  $-95^\circ \alpha$ . At  $-100^\circ \alpha$ , local separation is still apparent, but the attached portion has grown, when compared to the  $-95^\circ \alpha$  data.

A comparison of the chordwise pressure distribution recorded with the flap slot closed and the data obtained with the flap slot open is shown in figure 29. For the

flap angle shown, sealing the flap slot increases the drag coefficient by about 1%. No significant change in the pressure distribution in the vicinity of the flap's leading edge can be seen.

The upper surface spoiler is seen (in fig. 30) to markedly affect the pressure distribution aft of the spoiler location. The reduction in flap upper-surface download pressure produces a drag reduction on the order of 15-20% of the untreated airfoil drag.

The effect of flap size is indicated in figures 31 and 32. The pressure distribution for the 0° flap angle is shown in figures 31a, b, and c, and the 60° flap data is given in figures 32a, b, and c.

In general, the drag coefficients computed from the pressure data were found to be within 2% of the drag coefficients obtained from the wind tunnel force data.

#### CONCLUDING REMARKS

Significant reductions in the two-dimensional drag of wing sections at angles of attack near -90° can be obtained by the use of leading- and trailing-edge devices. It has been demonstrated that an effective method of drag reduction involves the delay of flow separation by alteration of the basic airfoil contour. The deflected trailing-edge plain flap (modified with a curved upper surface) and a curved leading edge behind a hinged slat (configuration n) is an example of a successful geometry. The reduction of "frontal" or exposed flat plate area (resulting from flap deflection, for example), accounts for less than half of the total achievable drag reduction.

The lowest drag level was obtained with the umbrella flap design concept. However, a practical size umbrella flap would probably be smaller than the 25% chord size examined in this test series (and would therefore offer a smaller drag reduction). This, coupled with several previously noted problems in the hover and cruise modes, makes it less attractive than some of the other configurations that produce slightly greater drag values.

Drag coefficients were primarily determined from force measurements (corrected for blockage). Surface pressure data enabled the computation of a drag coefficient (less the skin friction component) which generally agreed to within 2% of the force data.

The 25% plain flap produced a minimum drag coefficient of about 1.2, whereas the 30% plain flap delivered a minimum  $C_D$  of approximately 1.0. The 35% chord plain flap did not provide a further reduction of minimum drag, when compared to the 30% flap data.

The best umbrella flap model yielded a drag coefficient of about 0.4, and the upper-surface leading-edge slat offered a minimum drag coefficient of 0.6.

The drag of many configurations was found to be sensitive to angle of attack. Sharp drag increases often occurred after the onset of flow separation from the leading- or trailing-edge surfaces.

Finally, the drag coefficients proved to be rather insensitive to Reynolds number over the  $0.6 \times 10^6$  to  $1.4 \times 10^6$  Re range tested.

## APPENDIX A

### SURFACE PRESSURE DATA REDUCTION

The surface pressure values were measured as the difference between the local and the wind tunnel static pressures and were reduced to pressure coefficient form by dividing by the average blockage-corrected dynamic pressure. These values were then plotted against chord location. Flap deflection is accommodated in the data processing and the resulting reduction of overall chord length (noted as "effective chord") is displayed on the plots. As in the force coefficient computations, the reference 1-ft chord is used in calculations of drag coefficients obtained from the surface pressure data.

Computation of the drag coefficient based on the pressure data was accomplished using a segmented computer curve-fit (applying low-order polynomials) to obtain a good point match and to accommodate flow discontinuities at the flap cove and in the case of the upper surface spoiler. The difference between the lower and upper surface pressure coefficients was integrated along the chord as follows:

$$C_D = \int_0^{1.0} (C_{P_{\text{lower}}} - C_{P_{\text{upper}}}) dx$$

The contribution to drag caused by skin friction on the bluff bodies tested in this experiment is small and was not included in this assessment. It is also noted that the surface pressures that were obtained reflected time-averaged values since the tubing length between the orifice and the pressure transducer precluded any high frequency measurements.

## APPENDIX B

### TUNNEL WALL EFFECTS CORRECTIONS

The blockage caused by the presence of a model in a closed-section wind tunnel creates an acceleration of the local flow and increases the drag. This effect is known to depend primarily on the drag and on the physical size of the model. Although many investigations have been made of the phenomenon, as seen in reference 5, no completely satisfactory method exists for correcting wind tunnel data to free-air conditions. Two of the most successful theoretical approaches to date are the Image Method, e.g., Allen and Vincenti (ref. 6) and Pankhurst and Holder (ref. 7), and the Momentum Method of Maskell (ref. 8).

Although references 6 through 8 differ in their approaches and basic assumptions, each predicts that the blockage correction for a two-dimensional bluff body is determined primarily by the "blockage parameter"  $bC_{D_o}$ , where  $b$  is the ratio of the lateral dimension of the wind tunnel, and  $C_{D_o}$  is the measured drag coefficient. To a first approximation, each analysis yields the following expression for bluff bodies with high drag and low lift:

$$\frac{C_D}{C_{D_o}} \approx 1 - \epsilon b C_{D_o} \quad (B1)$$

$$\frac{C_P - 1}{C_{P_o} - 1} = \frac{C_D}{C_{D_o}} \quad (B2)$$

where  $\epsilon$  is a constant,  $C_D$  is the corrected, "free-air" drag coefficient, and  $C_P$  and  $C_{P_o}$  are the corrected and uncorrected values of the pressure coefficient, respectively.

In references 6 and 7,  $\epsilon = 0.50$  for incompressible flow and is independent of the shape of the body. In Maskell's analysis (ref. 8),  $\epsilon$  depends strongly upon the aspect ratio of the model and weakly upon its cross-sectional shape;  $\epsilon$  is of order unity for two-dimensional cases. The numerous previous wind tunnel measurements that are cited in references 5 and 9, for cylinders of various cross sections, suggest values somewhere between 0.5 and 1.0, depending upon the details of the particular wind tunnel installation and the shape and complexity of the model. Therefore, the basic form of equations (B1) and (B2) is indicated to be appropriate here, provided that a reasonable estimate of  $\epsilon$  can be obtained for the range of values of the blockage parameter  $bC_{D_o}$  that was encountered in the present airfoil tests.

To determine a suitable value of the empirical constant  $\epsilon$  for the present experimental setup, two models having equilateral-triangular cross sections and chords of 8.5 and 12 in. were tested at two different orientations, with the apex

pointing upstream and pointing downstream, thus providing four combinations of the blockage parameter  $bC_{D_o}$ . The data so obtained were found to be independent of Reynolds number over the range explored,  $0.6$  to  $1.4 \times 10^6$ , to within measurement accuracy.

The corresponding free-air drag coefficients for wedges have been documented to within  $\pm 5\%$  in reference 9; i.e.,  $C_D = 2.0$  with the flat face forward and  $C_D = 1.3$  for the apex of an equilateral triangle facing forward. With these values for  $C_D$  and the measured values of  $C_{D_o}$  for 15 combinations of Reynolds numbers, sizes, and orientations, the values of  $\epsilon$  as shown in table B1 were computed from the following rearrangement of equation (B1):

$$\epsilon = \frac{C_{D_o} - C_D}{b(C_{D_o})^2} \quad (B3)$$

The mean value of  $\epsilon$  is  $0.60$ , in good agreement with the various independent studies cited above.

The experimental results for the triangles are summarized in table B2. All of the results are in excellent agreement with Hoerner (ref. 9). It is interesting to note that the corrected base pressure coefficient,  $C_{P_{base}}$ , is essentially independent of the orientation of the triangle, even though  $C_D$  is not.

For the present airfoil sections with  $b = 0.10$ , the following formulae were used to correct the measured data:

$$C_D = C_{D_o} (1 - 0.06C_{D_o}) \quad (B4)$$

$$C_P - 1 = (C_{P_o} - 1)(1 - 0.06C_{D_o}) \quad (B5)$$

The blockage correction to the drag coefficient, therefore, is seen to be about 10% of the nominal values for the higher drag configurations examined in this test series. The validity of that magnitude of correction was tested by Allmaras (ref. 10) using a two-dimensional revision to the three-dimensional wall-pressure signature method devised by Hackett, Wilsden, and Lilley (ref. 11). Wall-pressure data for that study were obtained from a subsequent wind tunnel entry using the same equalateral-triangle cross-sectional bodies discussed above. Allmaras concluded that the blockage corrections derived from the wall-pressure method were in good agreement with the simpler methods used for the subject investigation.

No corrections were applied to account for the corner flow condition at the model/endplate interface.

Flow observations using wool tufts, comparisons of the three spanwise surface pressure measurements, and wake surveys indicated that the flow was uniform in the spanwise direction to within the accuracy of the measurements despite the fact that

the aspect ratios of the large triangle and the full chord airfoil models were only 5.

TABLE B1.- BLOCKAGE CORRECTION FACTOR  $\epsilon$  DERIVED  
FROM DATA ON TRIANGLES









Configuration	$C_D$ (from ref. 9)	b	$C_{D_o}$	$\epsilon$
→  figure 3q	2.00	0.10	2.31	0.581
→  figure 3p	2.00	0.071	2.24	0.675
→  figure 3s	1.30	0.10	1.41	0.553
→  figure 3r	1.30	0.071	1.38	0.593

TABLE B2.- SUMMARY OF RESULTS FOR THE EQUILATERAL TRIANGLES

Configuration	$C_{D_o}$	$C_D$	$C_D$ (from ref. 9)	$C_{p_{base}}$	$C_{p_{base}}$ (from ref. 9)
→  figure 3q	2.31	1.99	2.00 1.98 <sup>a</sup>	-1.17	-1.13 <sup>a</sup>
→  figure 3p	2.25	2.03	2.00 1.98 <sup>a</sup>	-1.24	-1.13 <sup>a</sup>
→  figure 3s	1.41	1.29	1.30	-1.12	-1.13 <sup>a</sup>
→  figure 3r	1.38	1.30	1.30	-1.18	-1.13 <sup>a</sup>

<sup>a</sup>Flat plate normal to flow.

## References

1. Koenig, D. G.: Low-Speed Tests of Semispan-wing Models at Angles of Attack from  $0^\circ$  to  $180^\circ$ ". NASA Memorandum 2-27-59A, April 1959.
2. Critzos, C. C.; Heyson, H. H.; and Boswinkle, Jr., R. W.: Aerodynamic Characteristics of NACA-0012 Airfoil Section at Angles of Attack from  $0^\circ$  to  $180^\circ$ . NACA TN 3361, 1955.
3. Pope, A.: Forces and Pressures over an NACA-0015 Airfoil Through  $180^\circ$  of Angle of Attack. Georgia Tech. Report No. E102, 1947.
4. Stansby, P. K.: The Effects of End Plates on The Base Pressure of a Circular Cylinder. Aeronautical J., vol. 78, no. 1, 1974, pp. 36-37.
5. Anon.: Blockage Corrections for Bluff Bodies in Confined Flows. Engineering Sciences Data Item No. 80024, Nov. 1980 (Great Britain).
6. Allen, H. J.; and Vincenti, W. G.: Wall Interference in Two-Dimensional Flow Wind Tunnel with Consideration of the Effect of Compressibility. NACA Report 782, 1944.
7. Pankhurst, R. C.; and Holder, D. W.: Wind Tunnel Techniques. Pitman, 1952.
8. Haskell, E. C.: A Theory of the Blockage Effects on Bluff Bodies and Stalled Wings in a Closed Wind Tunnel. Aero. Res. Coun. R2M 3400, 1963.
9. Hoerner, S. F.: Fluid-Dynamic Drag. Published by the author, 1965.
10. Allmaras, S. R.: On Blockage Corrections for Two-Dimensional Wind Tunnel Tests Using the Wall-Pressure Signature Method. NASA TM 86759, 1986.
11. Hackett, J. E.; Wilsden, D. J.; and Lilley, D. E.: Estimation of Tunnel Blockage from Wall Pressure Signatures: A Review and Data Correlation. NASA CR-15224, 1979.



ORIGINAL PAGE IS  
OF POOR QUALITY



Figure 1.- Smoke flow visualization of two-dimensional flow conditions on a tilt-rotor wing during tie-down (hover-mode) operations.

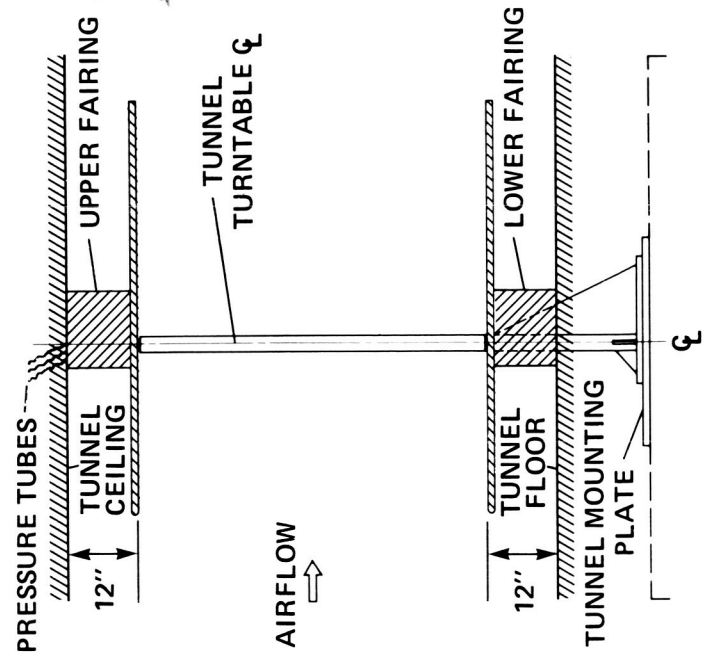
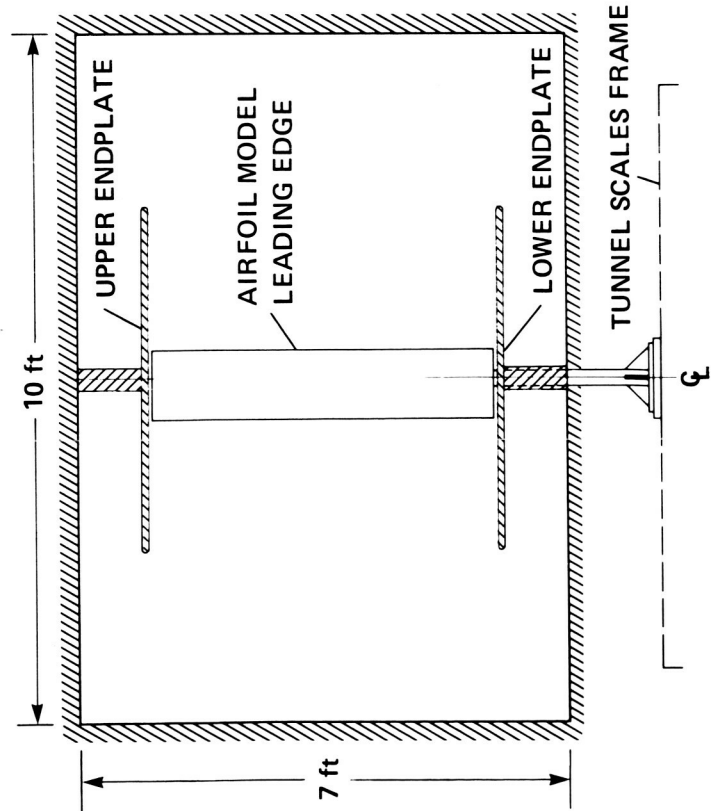
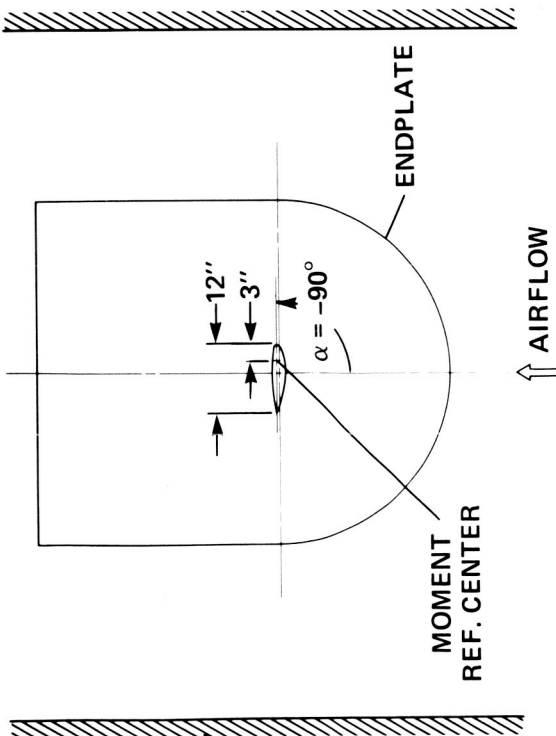
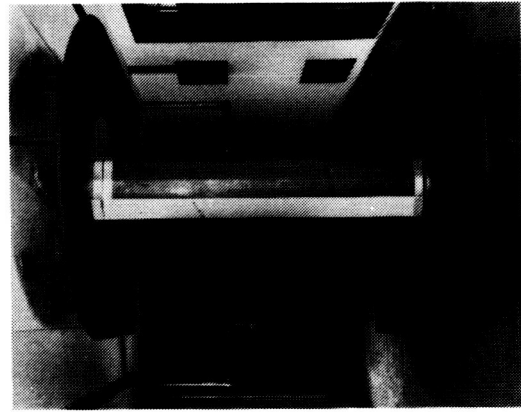


Figure 2.- Model installation in Ames Research Center 7- by 10-Foot (No. 2) Wind Tunnel.

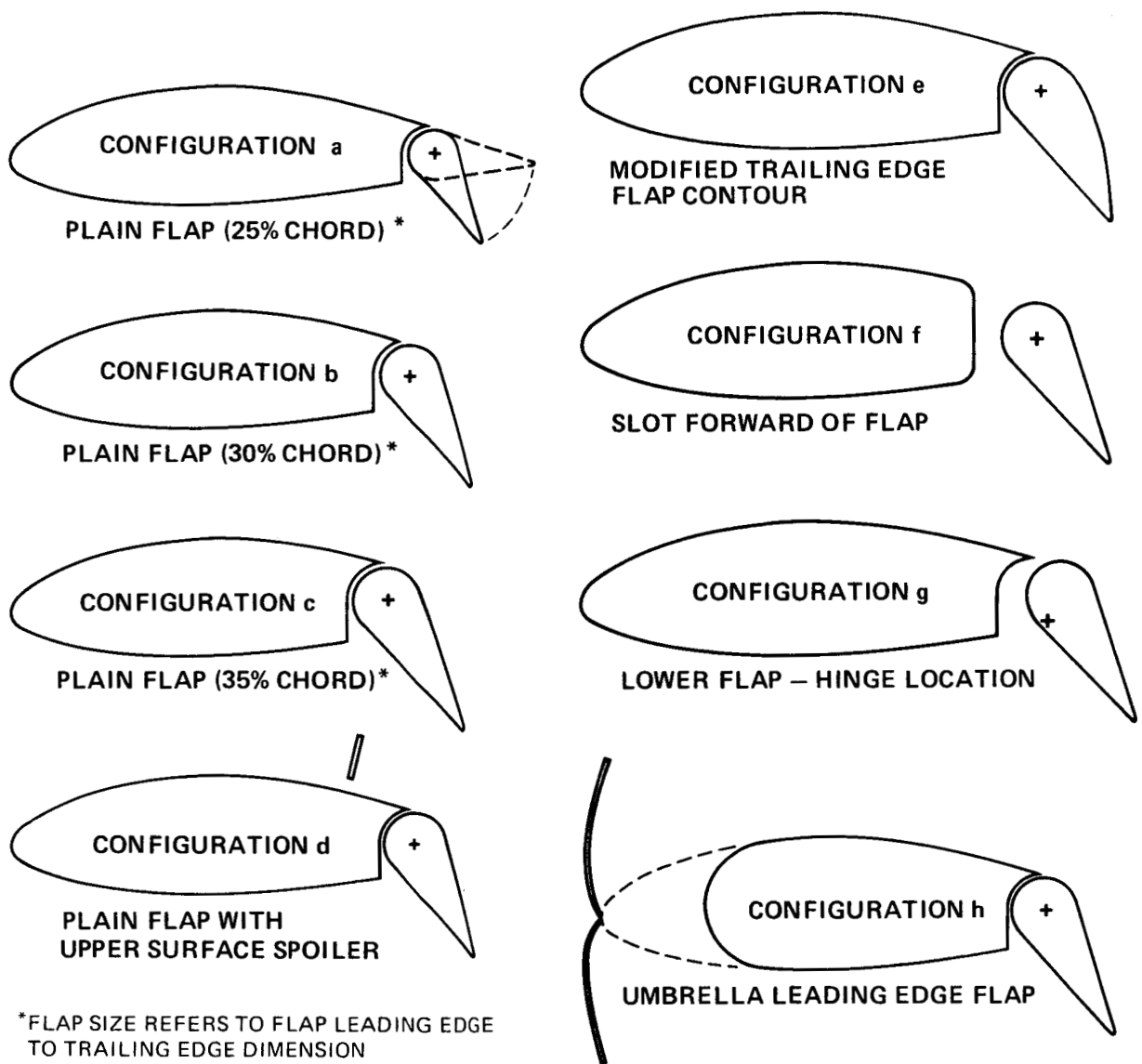


Figure 3.- Model configurations.

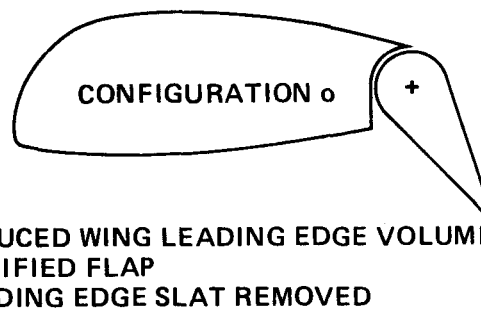
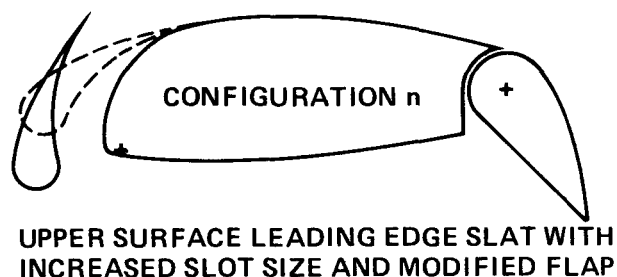
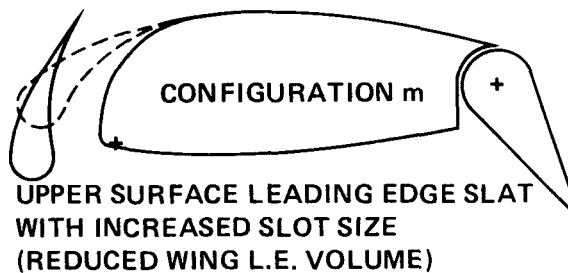
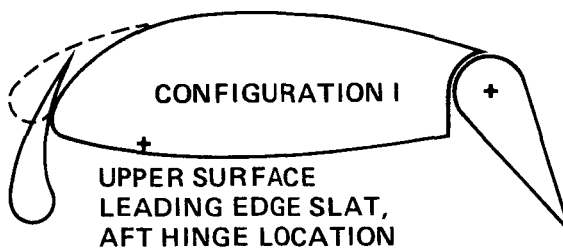
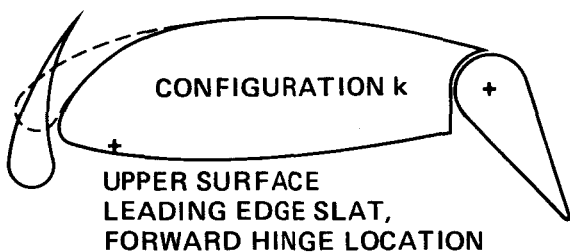
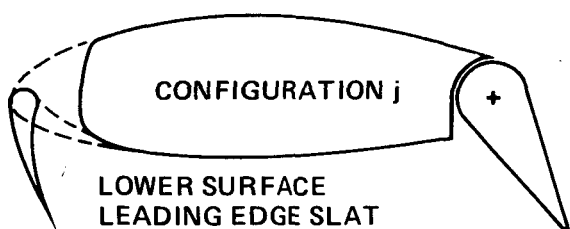
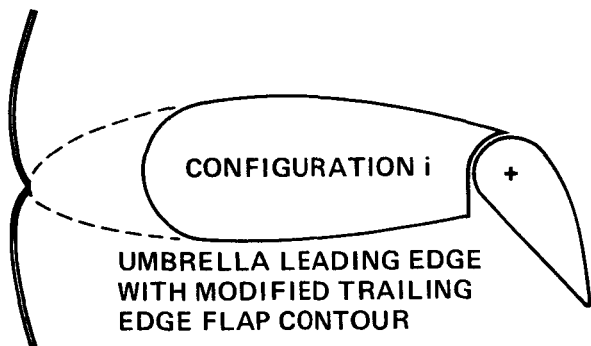


Figure 3.- Continued.

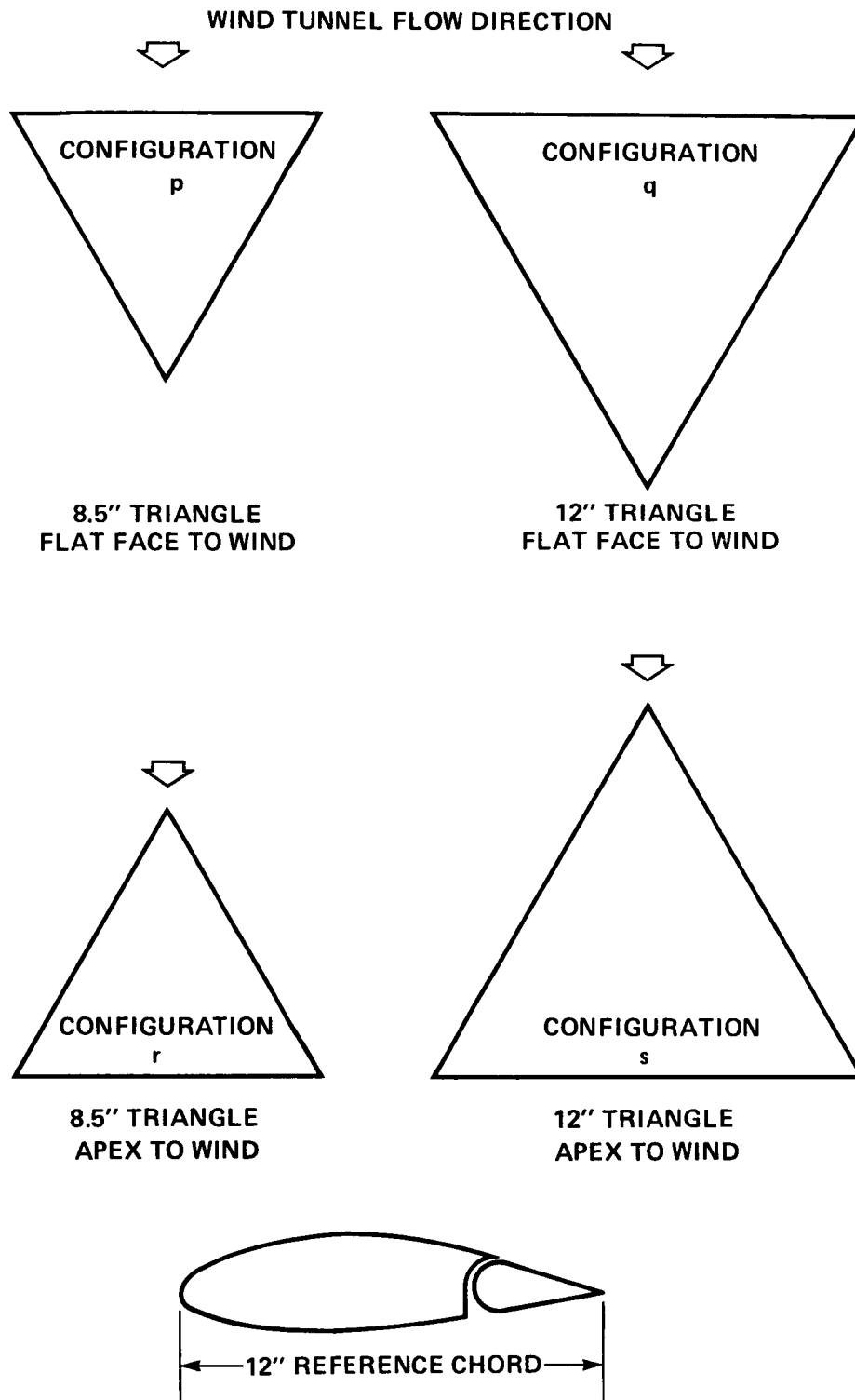
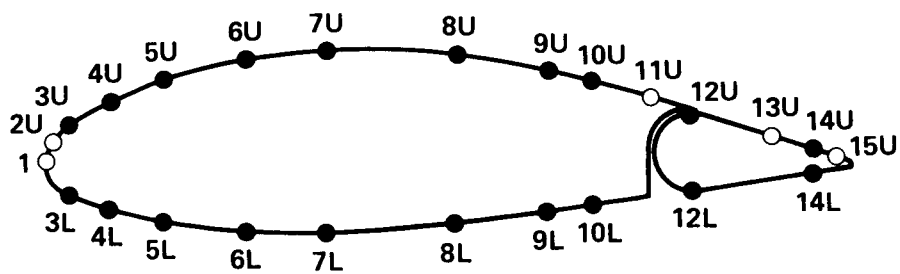
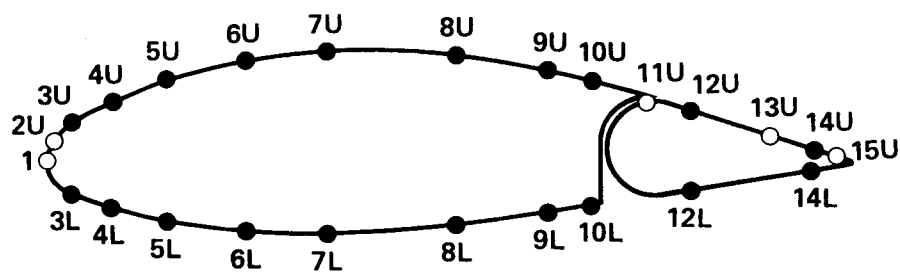


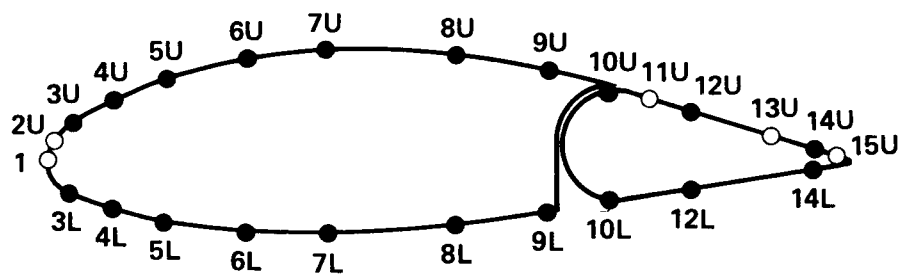
Figure 3.- Concluded.



(a) 25% FLAP CHORD



(b) 30% FLAP CHORD



(c) 35% FLAP CHORD

○ UPPER SURFACE ONLY  
● UPPER AND LOWER SURFACE PAIRS

ORIFICE NUMBER	1	2	3	4	5	6	7	8	9	10	11	12	13	14	15
% CHORD LOCATION	0	1	3	8	15	25	35	51	62.5	68*	75	80	90	95	98

\*70% FOR 35% CHORD FLAP

Figure 4.- Pressure orifice locations for plain-flap configurations.

XV-15 N703

GROUND RUN 176B, MAY 1983

PHOTO. TUFT SURVEY -

16 PHOTO. FRAMES

163 TUFT READINGS

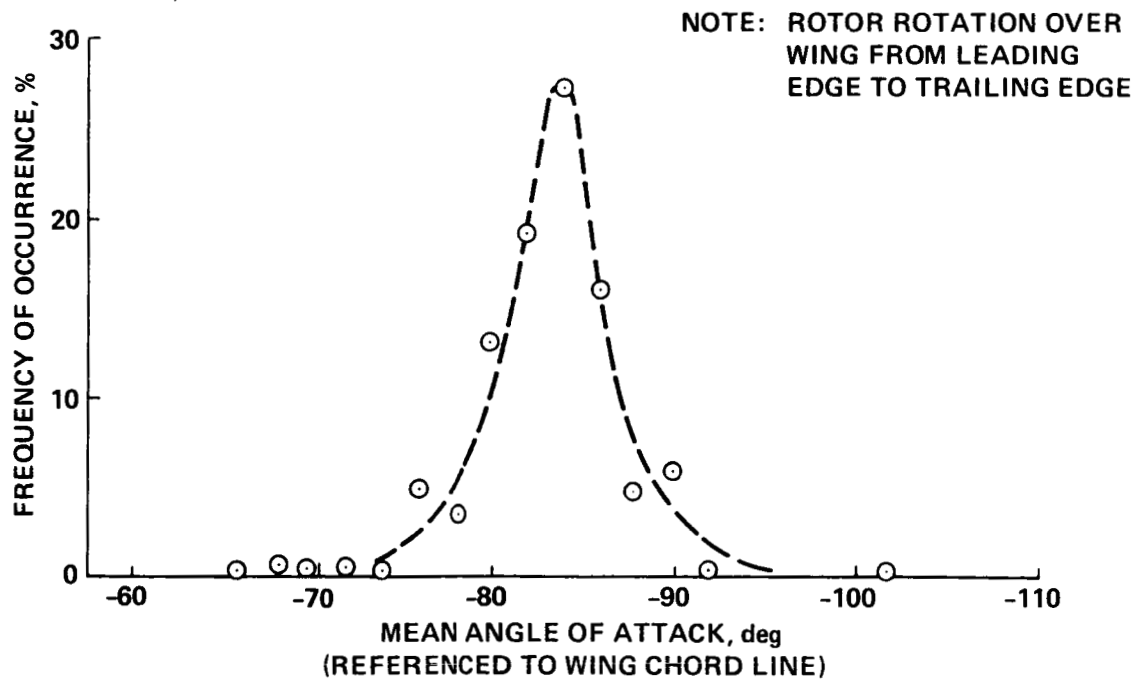
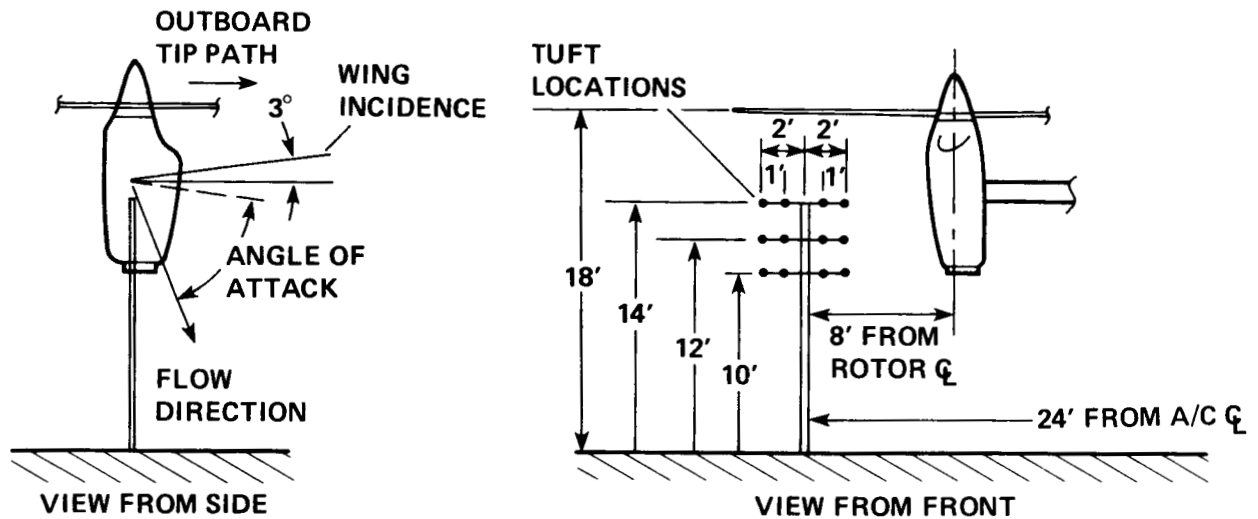
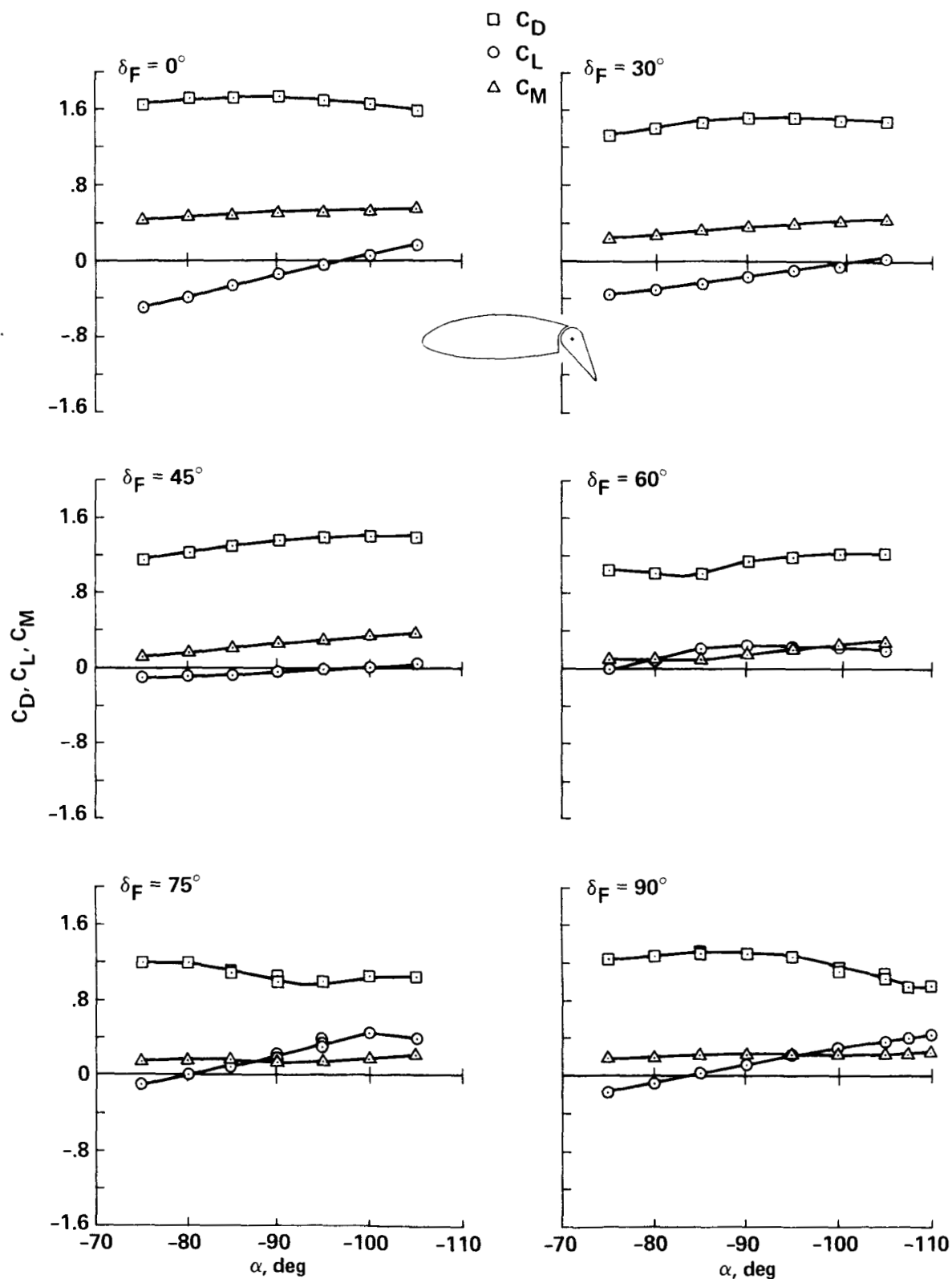


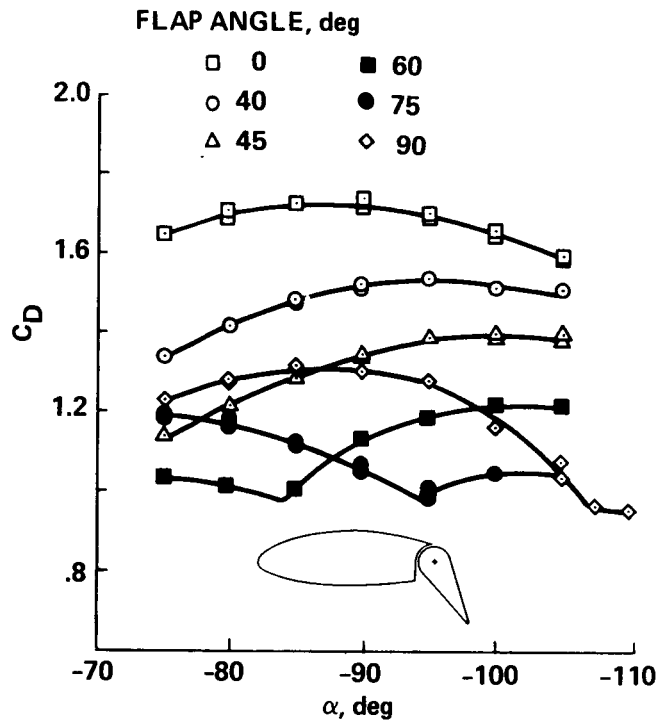
Figure 5.- Flow orientation in near-rotor wake.



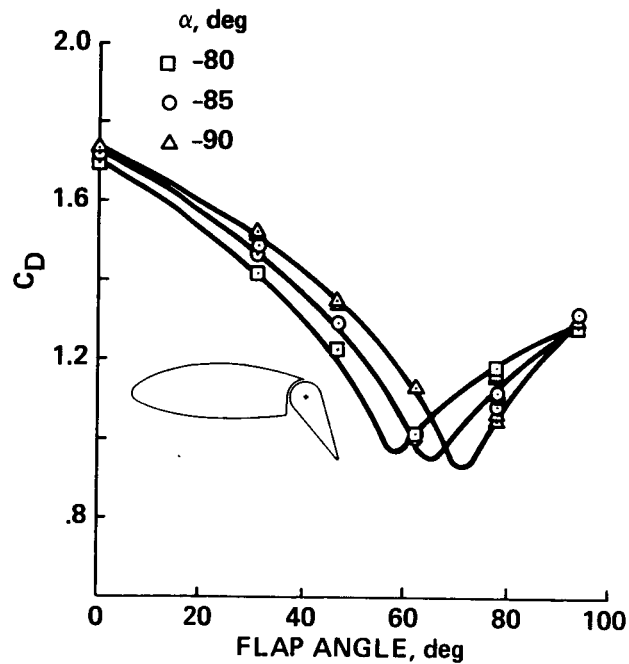
(a) Lift, drag, and moment coefficients for various flap angles.

Figure 6.- Aerodynamic characteristics of a two-dimensional wing at angles of attack near  $-90^\circ$ ; basic leading edge, 30% chord plain flap (configuration b).



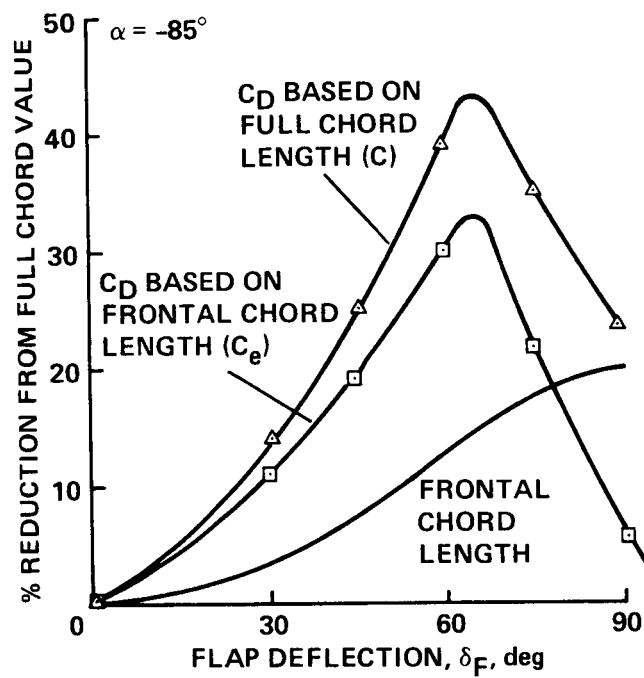


(b) Effect of angle of attack on drag coefficient for various flap angles.



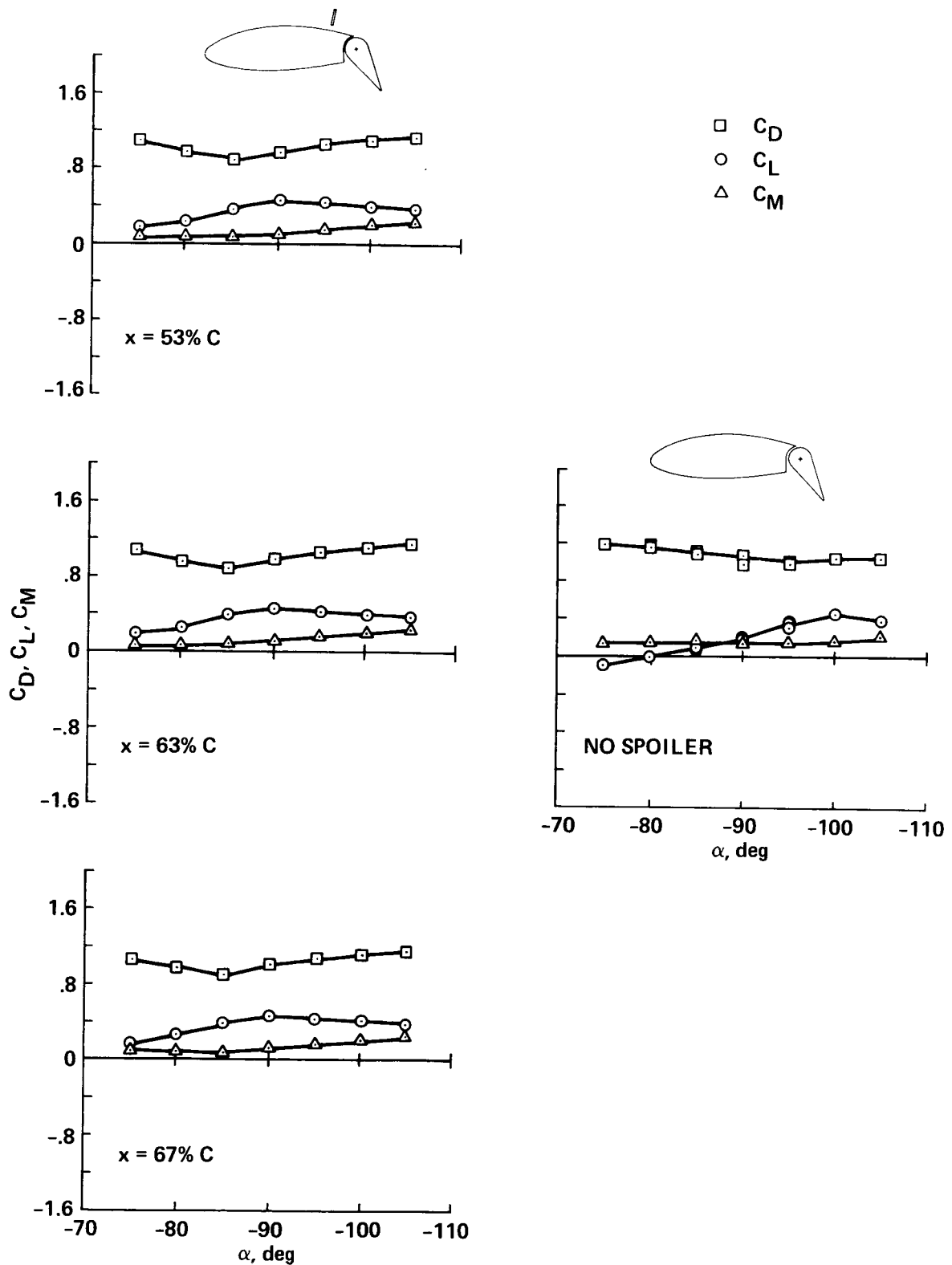
(c) Effect of flap angle on drag coefficient for various angles of attack.

Figure 6.- Continued.



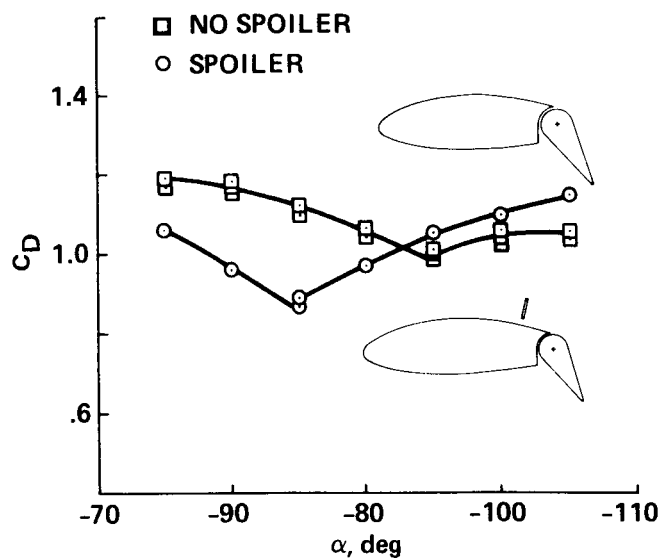
(d) Effect of flap angle on reduction of chord length and drag coefficient.

Figure 6.- Concluded.

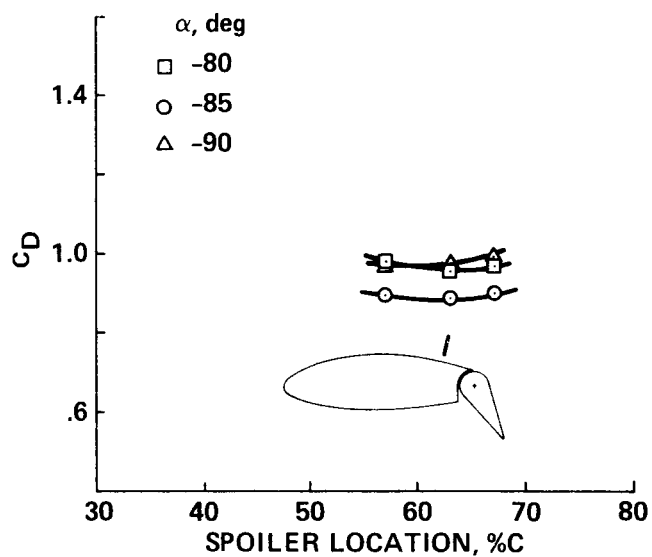


(a) Effect of spoiler location,  $75^\circ$  flap angle.

Figure 7.- Aerodynamic characteristics of a two-dimensional wing at angles of attack near  $-90^\circ$ ; basic leading edge, 30% chord plain flap, upper surface spoiler (configuration d).

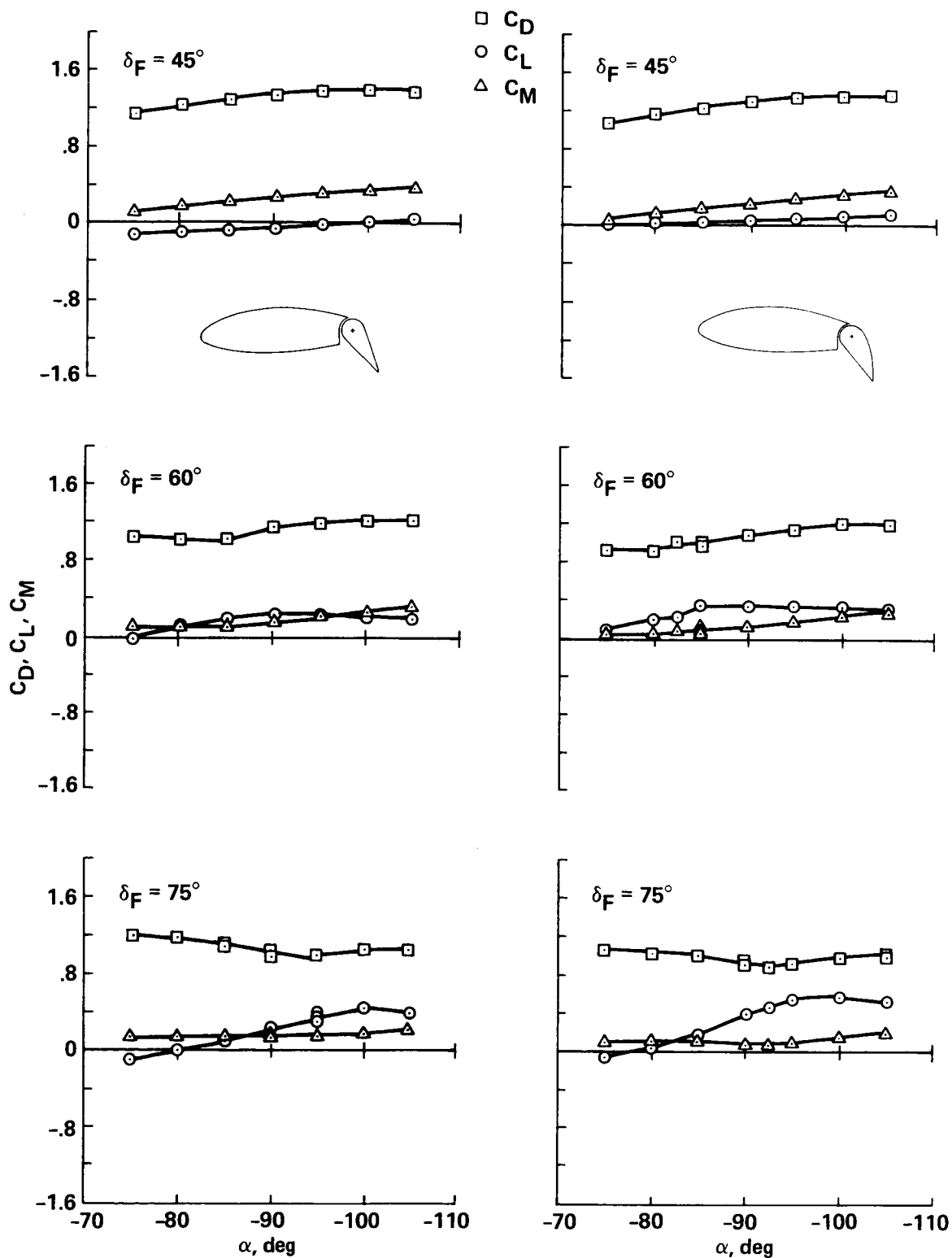


(b) Effect of upper surface spoiler on drag coefficient, 75° flap angle.



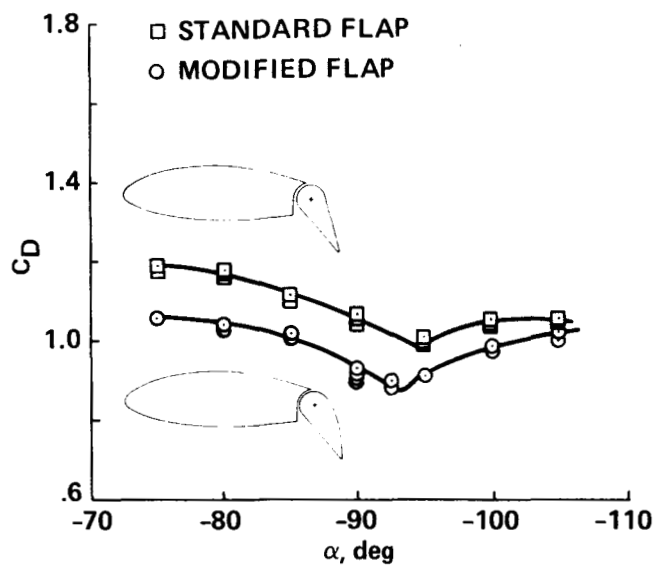
(c) Effect of upper surface spoiler on drag coefficient, 75° flap angle.

Figure 7.- Concluded.



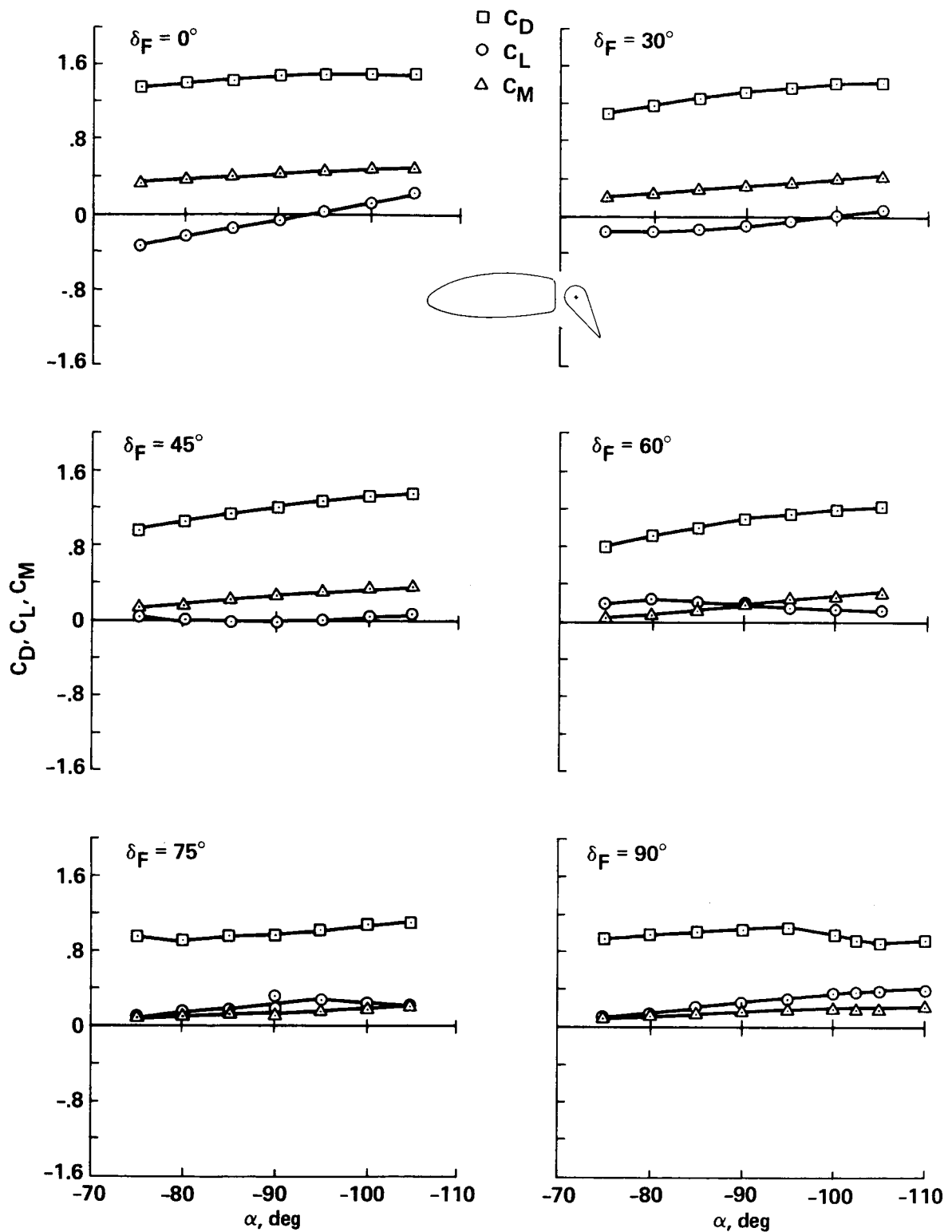
(a) Lift, drag, and moment coefficients for various flap angles (plain flap and modified flap).

Figure 8.- Comparison of the aerodynamic characteristics of configuration e (modified trailing-edge flap contour) with configuration b (30% chord plain flap).



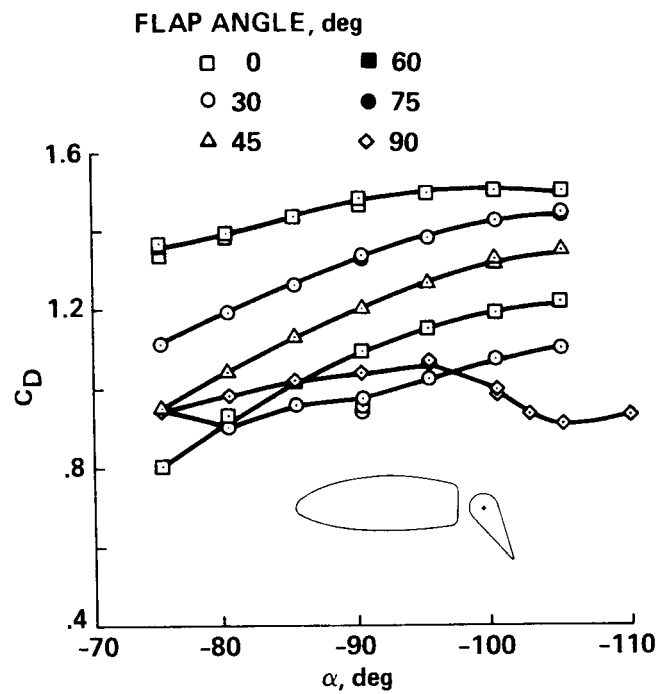
(b) Effect of modified trailing-edge flap contour on drag coefficient, 75° flap angle.

Figure 8.- Concluded.



(a) Lift, drag, and moment coefficients for various flap angles.

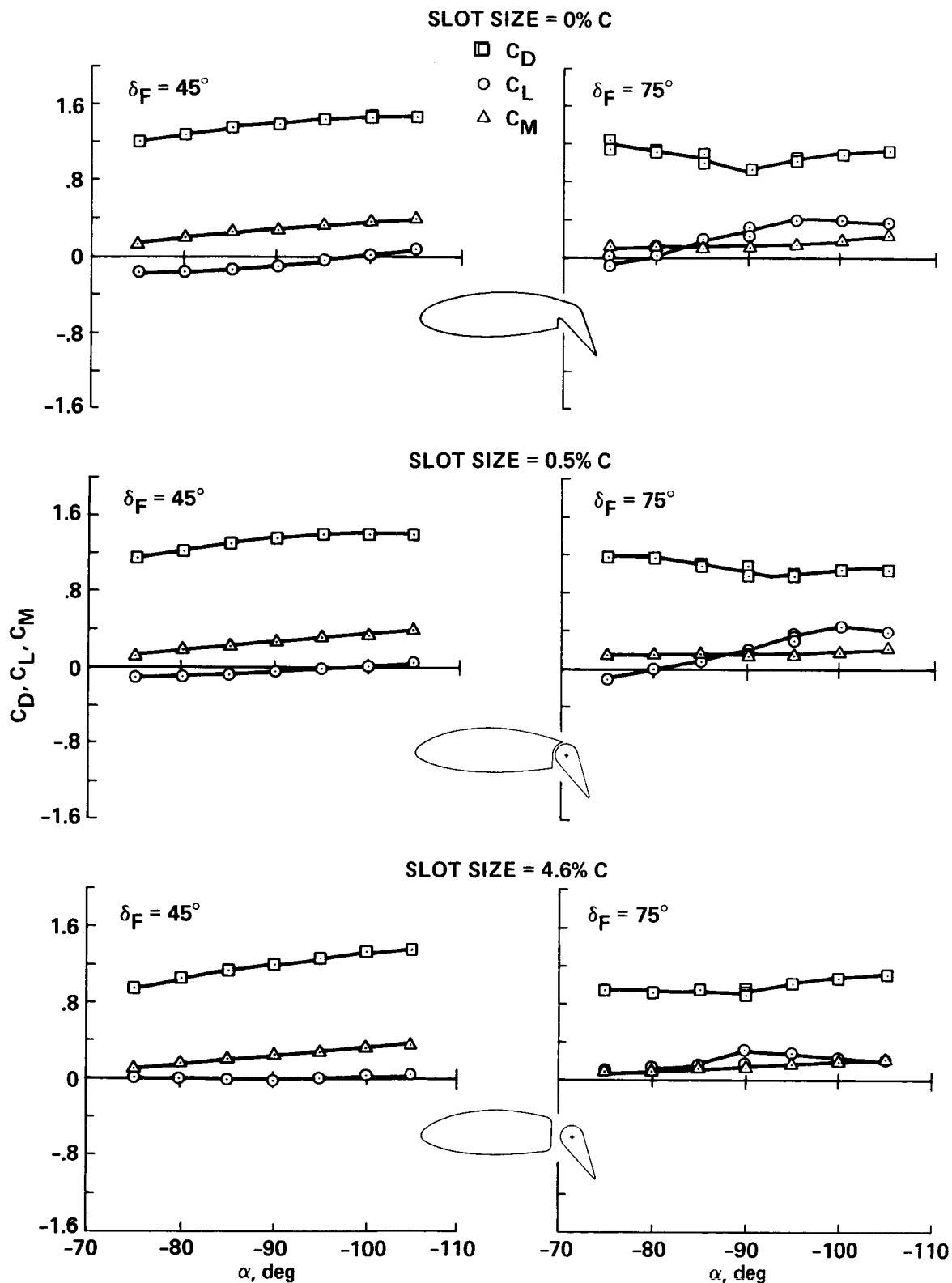
Figure 9.- Aerodynamic characteristics of a two-dimensional wing at angles of attack near  $-90^\circ$ ; basic leading edge, 30% chord plain flap, slot forward of flap (configuration f).



(b) Effect of angle of attack on drag coefficient for various flap angles.

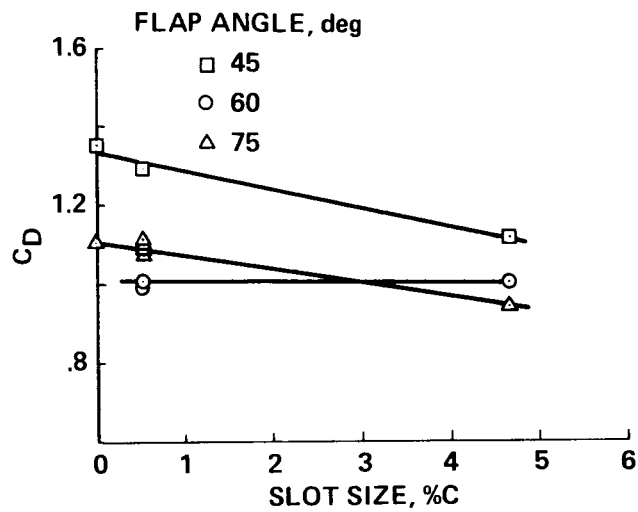
Figure 9.- Concluded.





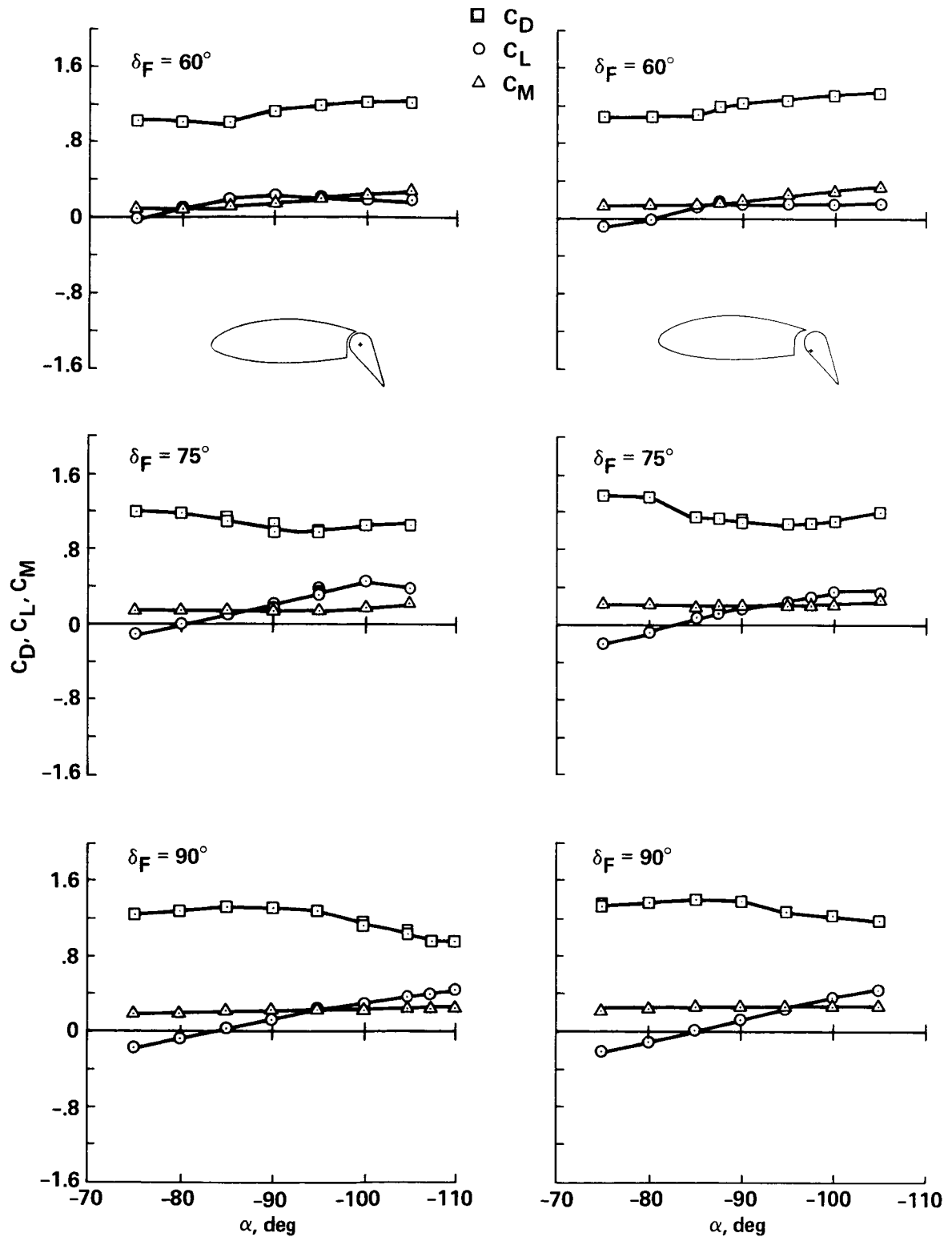
(a) Effect of slot size forward of flap for various flap angles.

Figure 10.- Comparison of the aerodynamic characteristics of configuration f (slot forward of flap) with configuration b (30% chord plain flap).



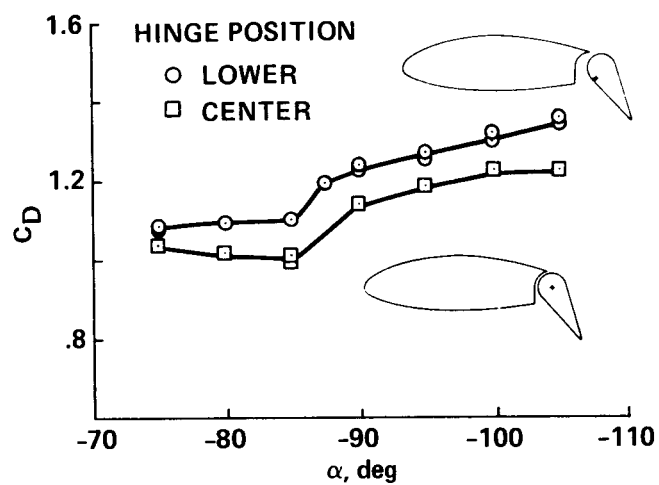
(b) Effect of slot size on drag coefficient for various flap angles,  $-85^\circ$  angle of attack.

Figure 10.- Concluded.



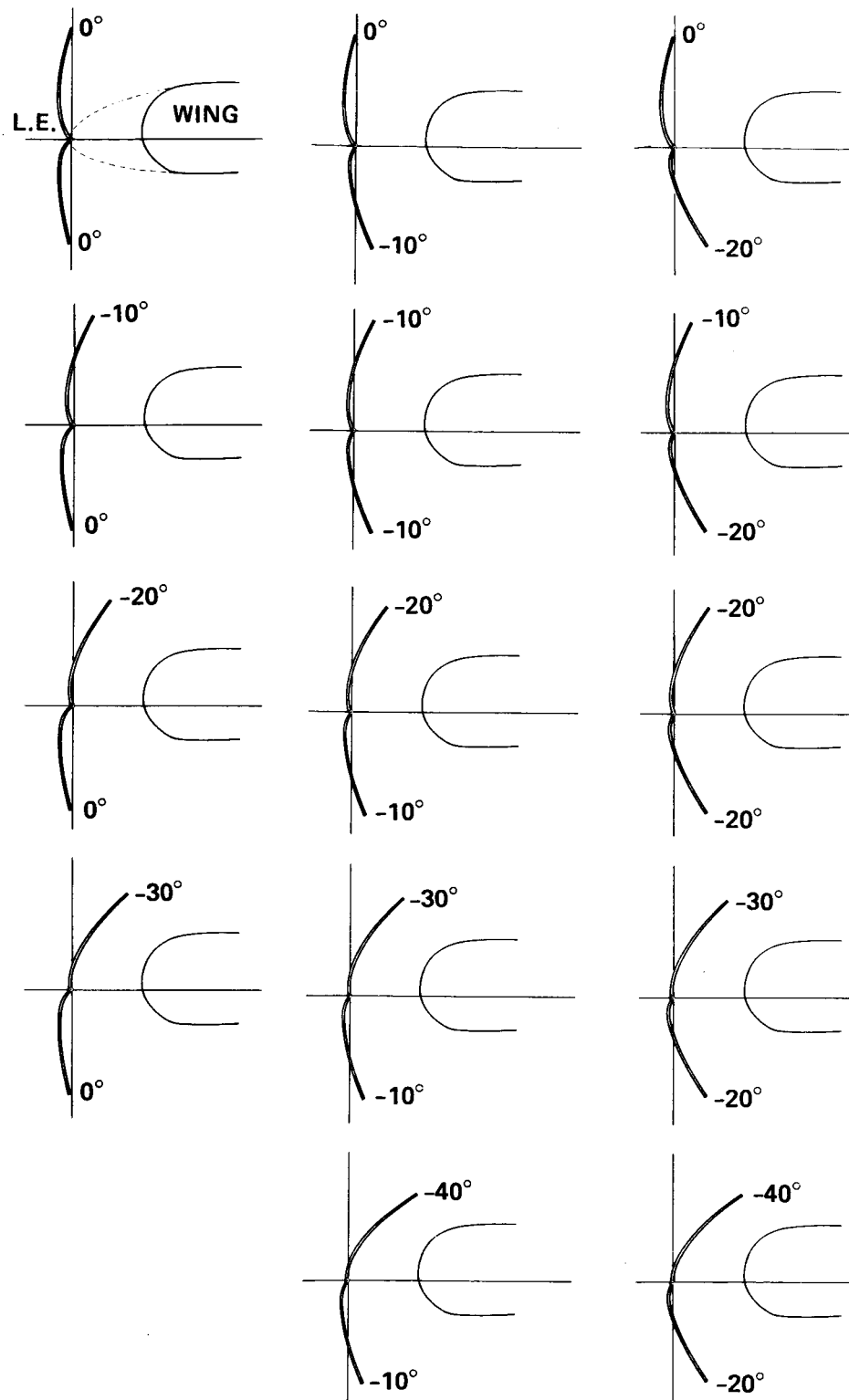
(a) Lift, drag, and moment coefficient variations for various flap angles (center hinge and lower hinge).

Figure 11.- Comparison of the aerodynamic characteristics of configuration g (lower hinge location) with configuration b (center hinge location).



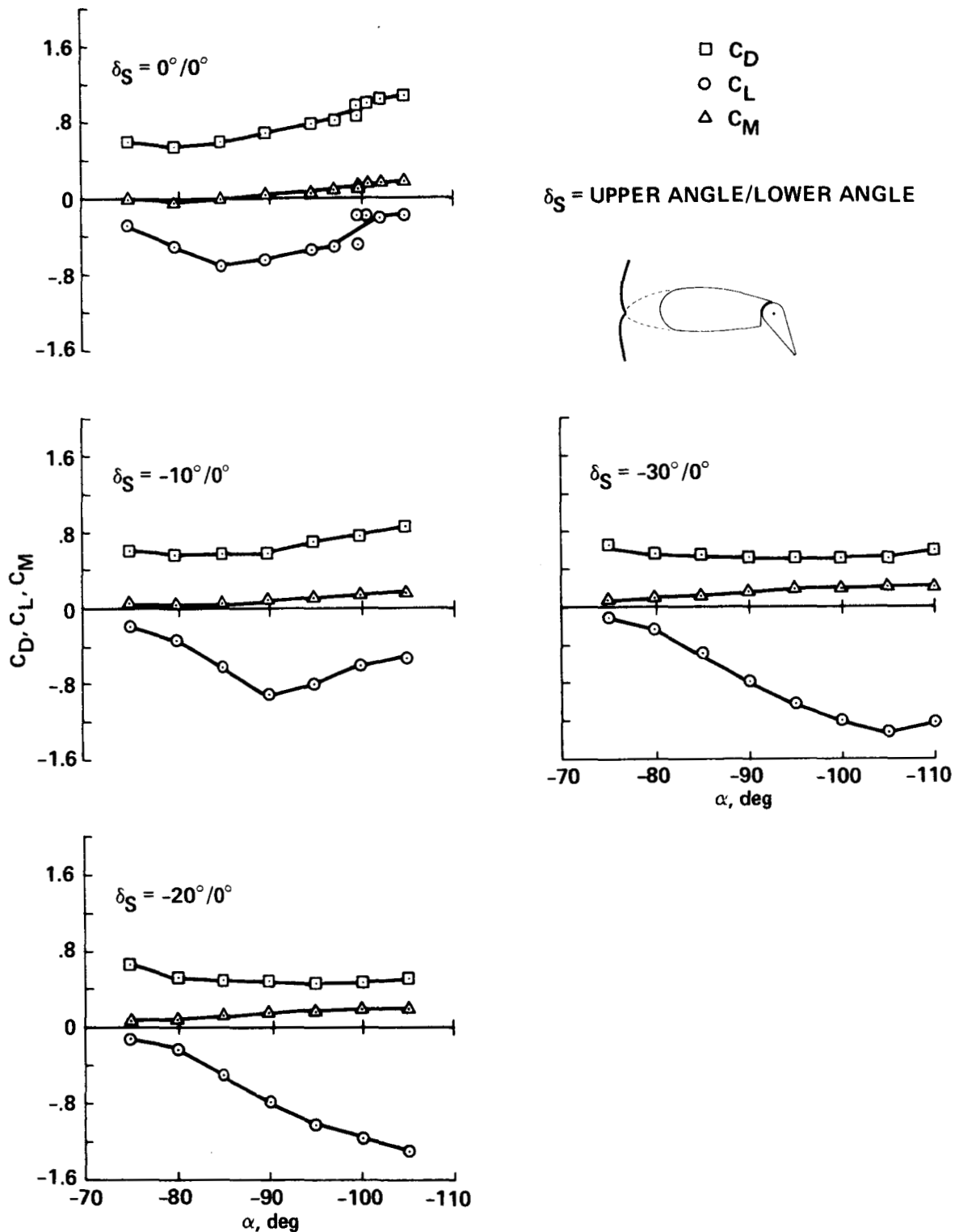
(b) Effect of hinge location on drag coefficient, 60° flap angle.

Figure 11.- Concluded.



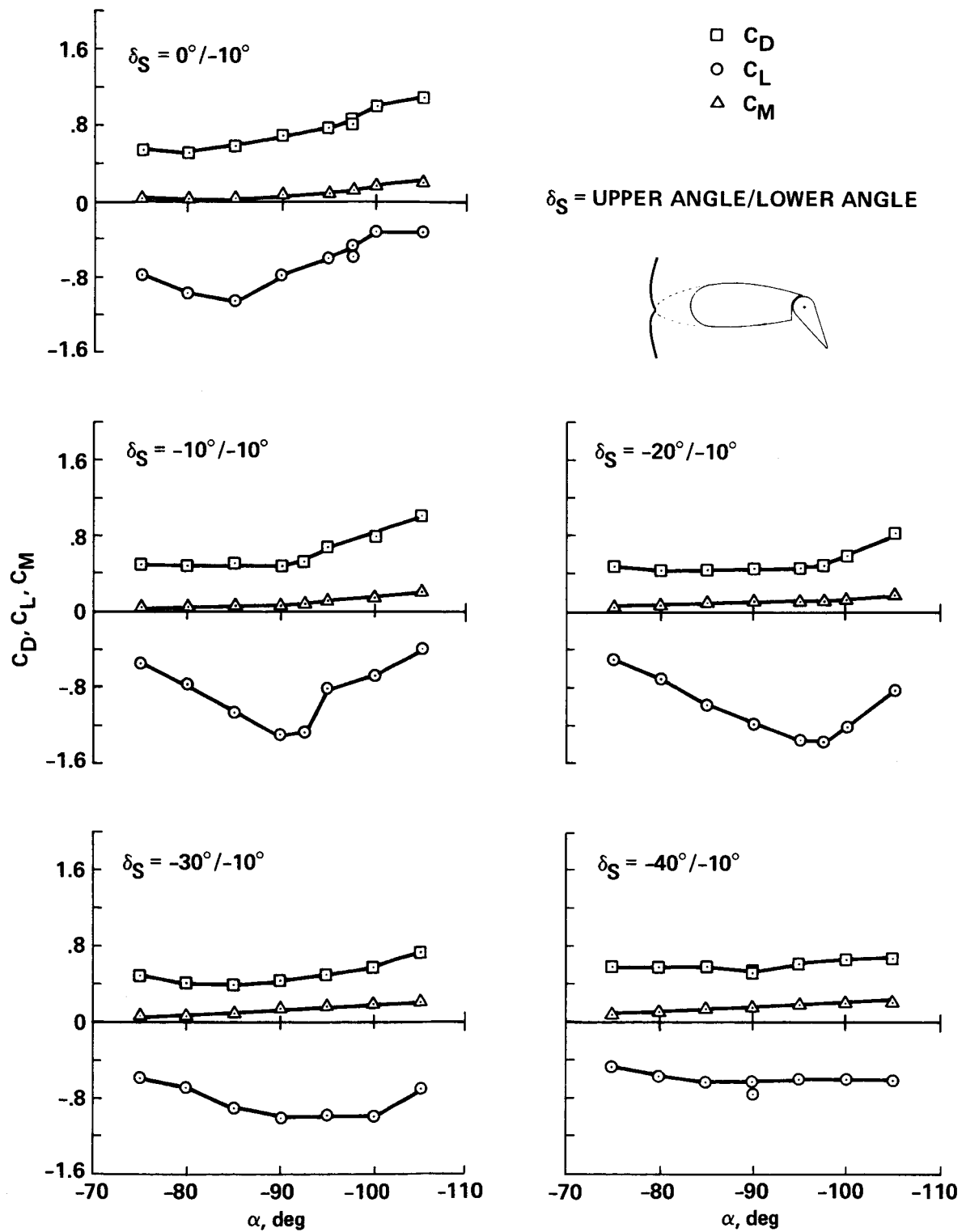
$\delta_s$  — UPPER ANGLE/LOWER ANGLE

Figure 12.- Test positions for umbrella leading-edge flap surfaces.



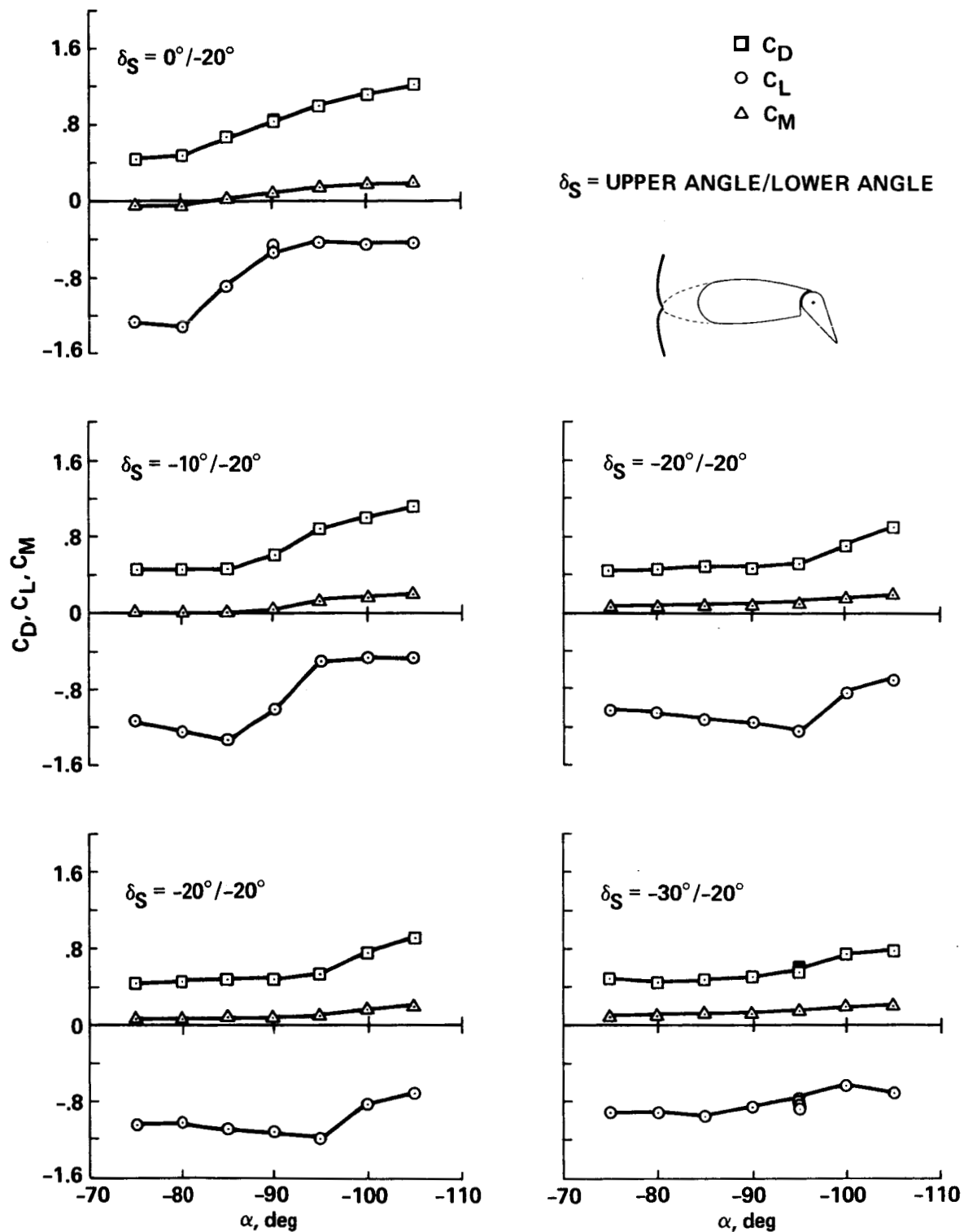
(a) Aerodynamic coefficient variations,  $0^\circ$  lower leading-edge flap angle and  $60^\circ$  trailing-edge flap angle.

Figure 13.- Aerodynamic characteristics of a two-dimensional wing at angles of attack near  $-90^\circ$ ; umbrella leading-edge flap, 30% chord plain flap (configuration h).



(b) Aerodynamic coefficient variations,  $-10^\circ$  lower leading-edge flap angle and  $60^\circ$  trailing-edge flap angle.

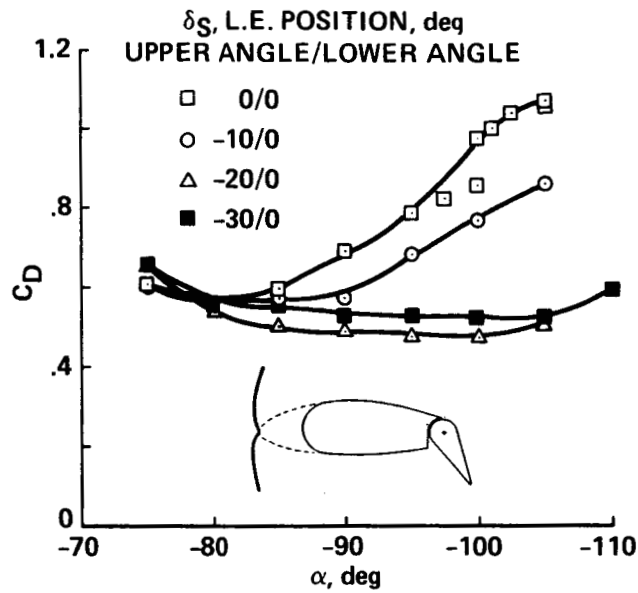
Figure 13.- Continued.



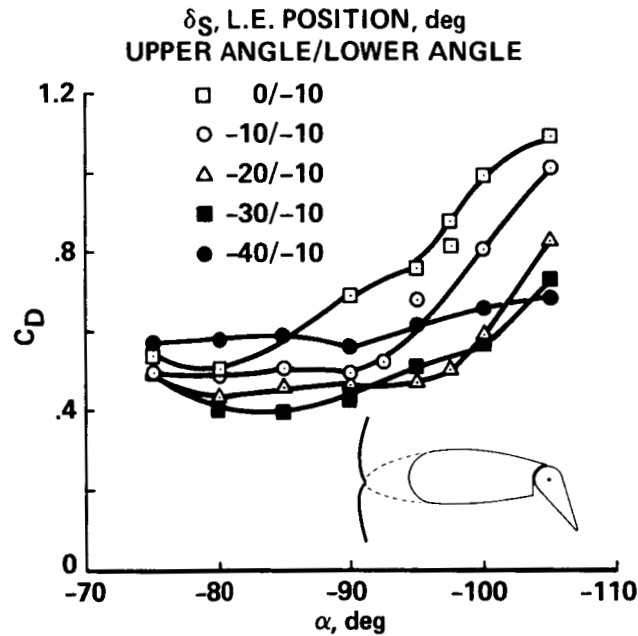
(c) Aerodynamic coefficient variations,  $-20^\circ$  lower leading-edge flap angle and  $60^\circ$  trailing-edge flap angle.

Figure 13.- Continued.



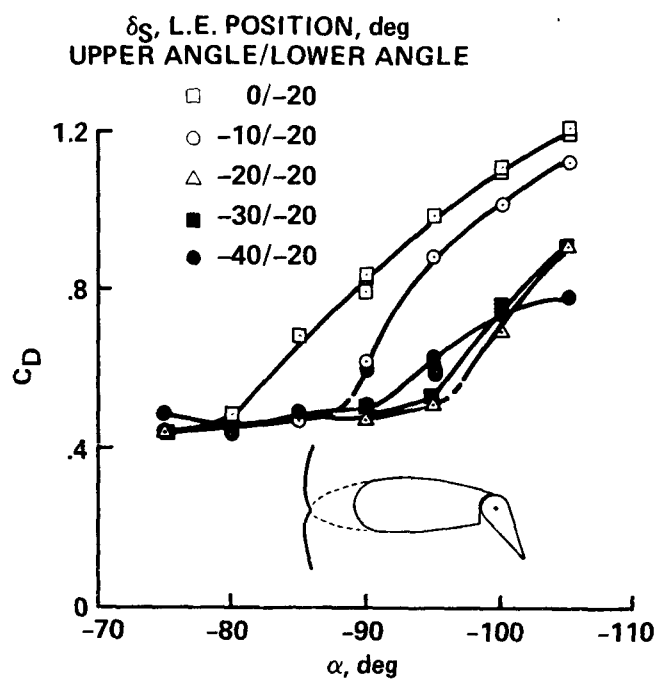


(d) Effect of angle of attack on drag coefficient for various upper leading-edge flap angles, 0° lower leading-edge flap angle and 60° trailing-edge flap angle.

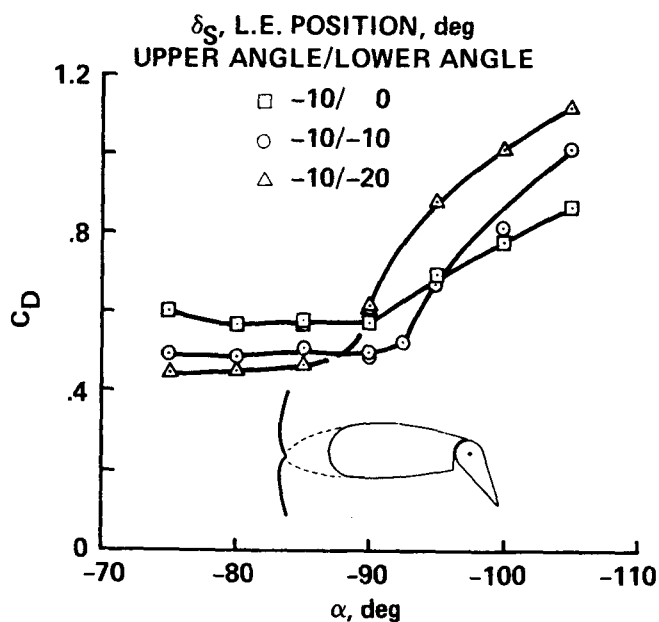


(e) Effect of angle of attack on drag coefficient for various upper leading-edge flap angles, -10° lower leading-edge flap angle and 60° trailing-edge flap angle.

Figure 13.- Continued.

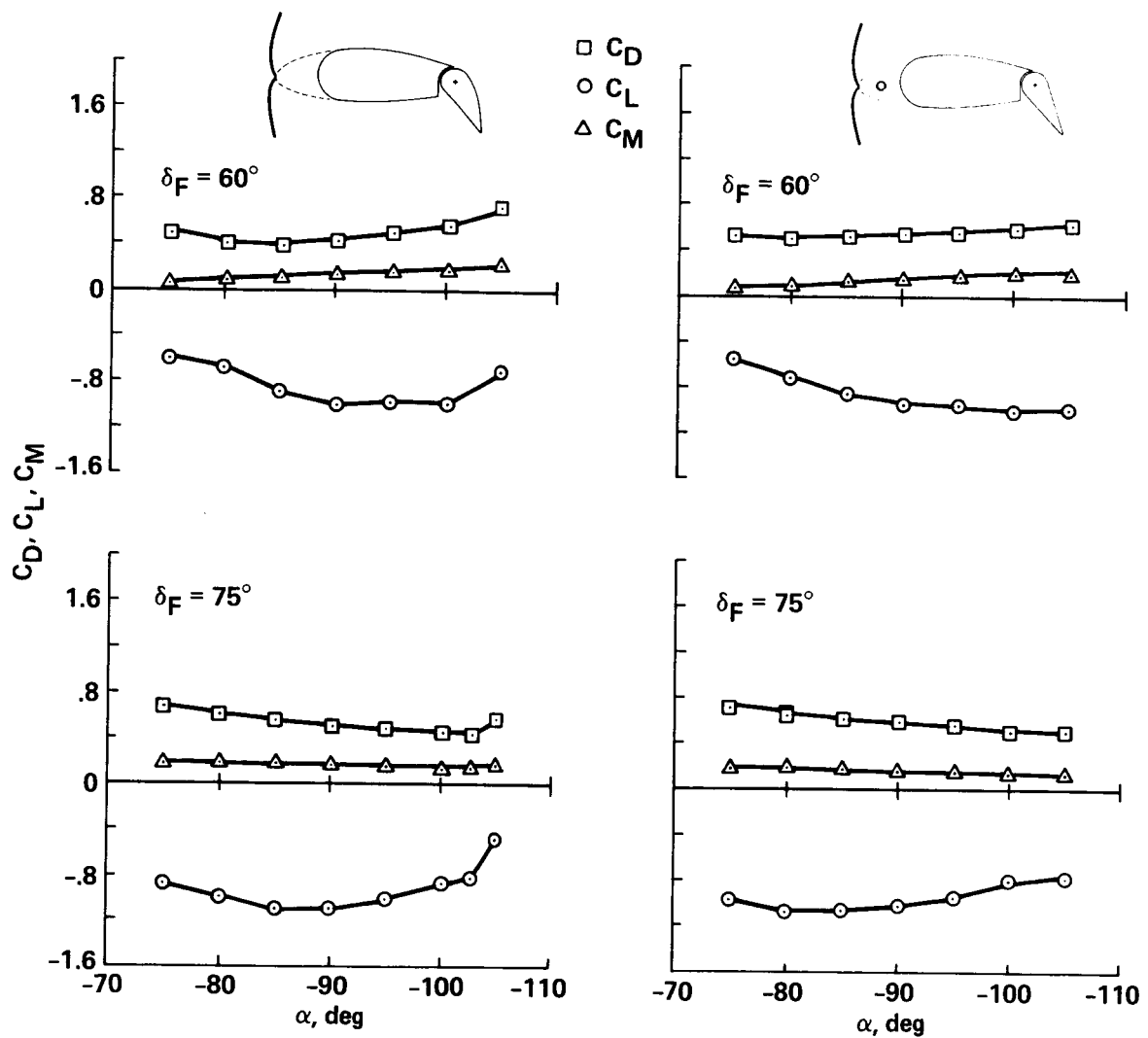


(f) Effect of angle of attack on drag coefficient for various upper leading-edge flap angles,  $-20^\circ$  lower leading-edge flap angle and  $60^\circ$  trailing-edge flap angle.



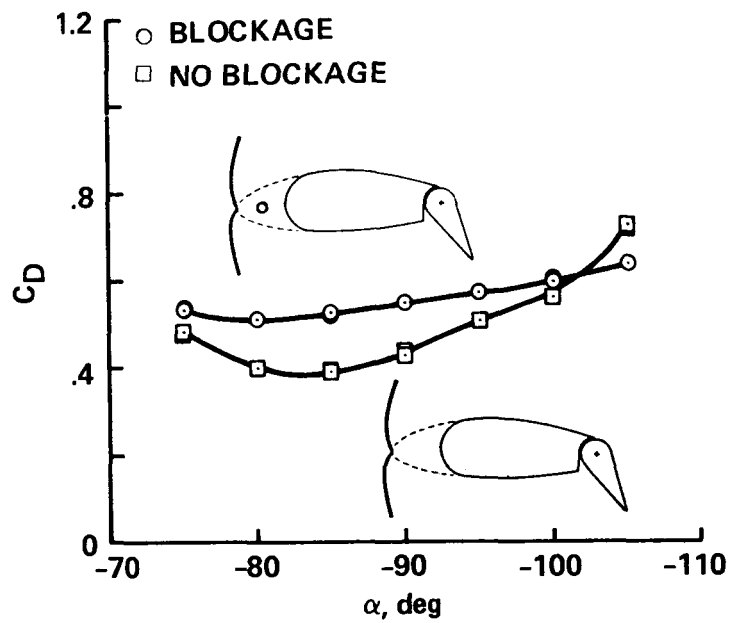
(g) Effect of angle of attack on drag coefficient for various lower leading-edge flap angles,  $-10^\circ$  upper leading-edge flap angle and  $60^\circ$  trailing-edge flap angle.

Figure 13.- Continued.



(h) Effect of blockage in leading-edge slot on aerodynamic characteristics for leading-edge flap angle of  $-30/-10^\circ$ .

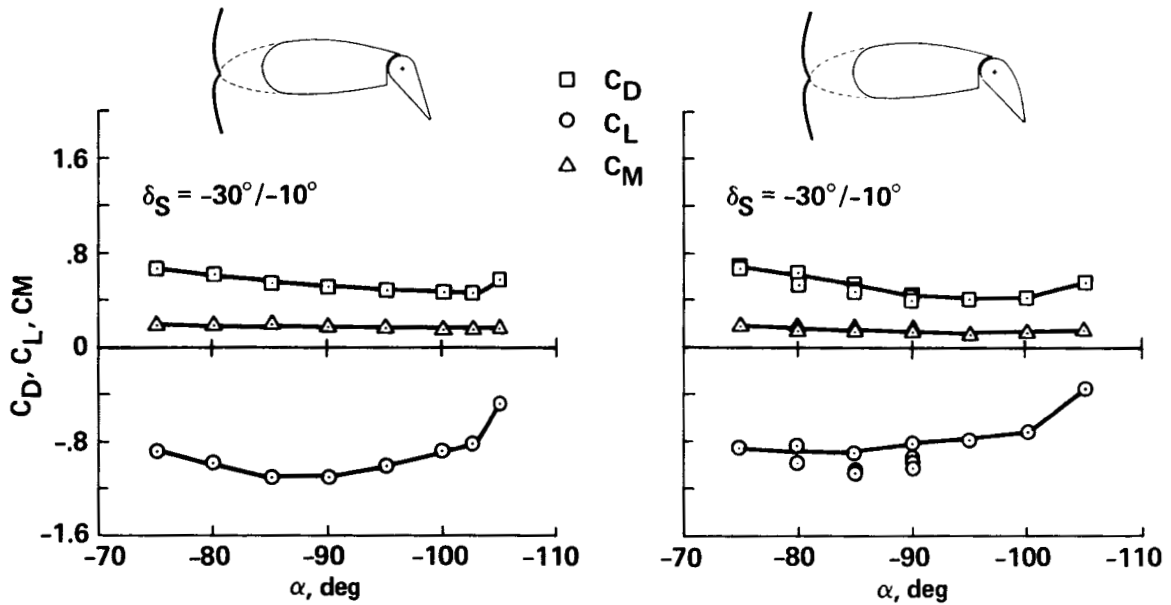
Figure 13.- Continued.



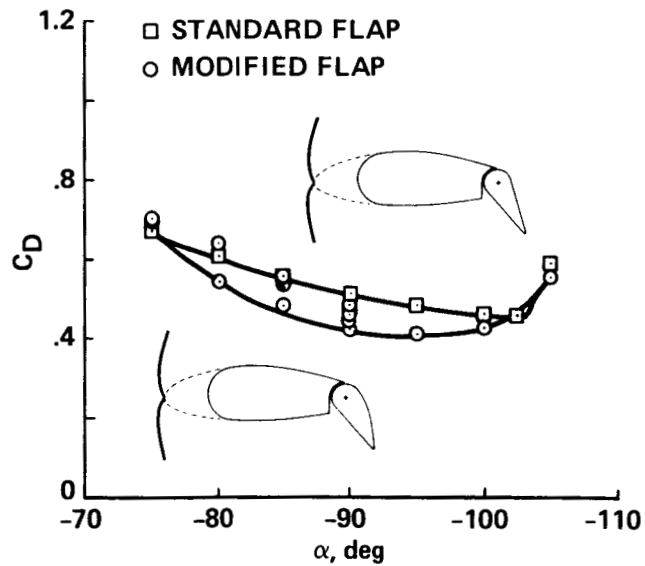
(i) Effect of blockage in leading-edge slot on drag coefficient for leading-edge flap angle of  $-30/-10^\circ$ ,  $60^\circ$  trailing-edge flap angle.

Figure 13.- Concluded.

$\delta_S = \text{UPPER ANGLE/LOWER ANGLE}$



(a) Lift, drag, and moment coefficient comparison for modified flap contour and plain flap,  $75^\circ$  flap angle.



(b) Effect of modified trailing-edge flap contour on drag coefficient,  $-30/-10^\circ$  leading-edge flap angle and  $75^\circ$  trailing-edge flap angle.

Figure 14.- Comparison of the aerodynamic characteristics of configuration i (umbrella leading-edge/modified flap contour) and configuration h (plain flap).

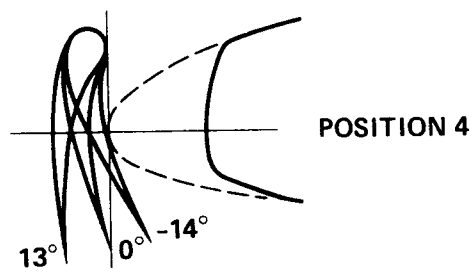
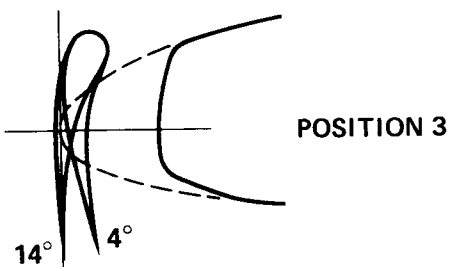
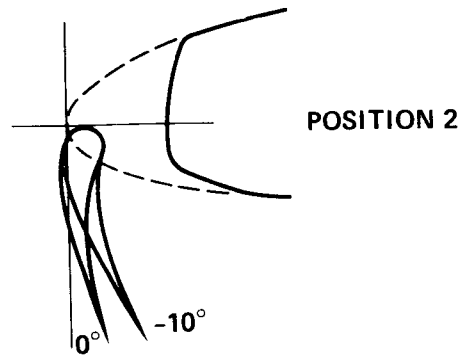
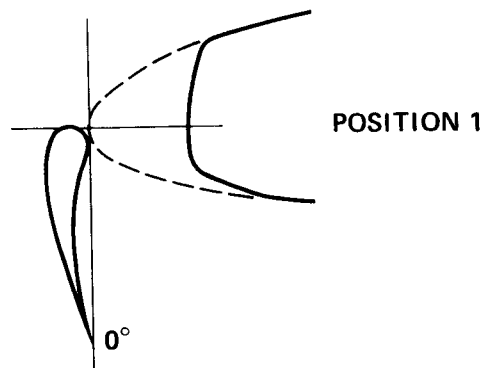
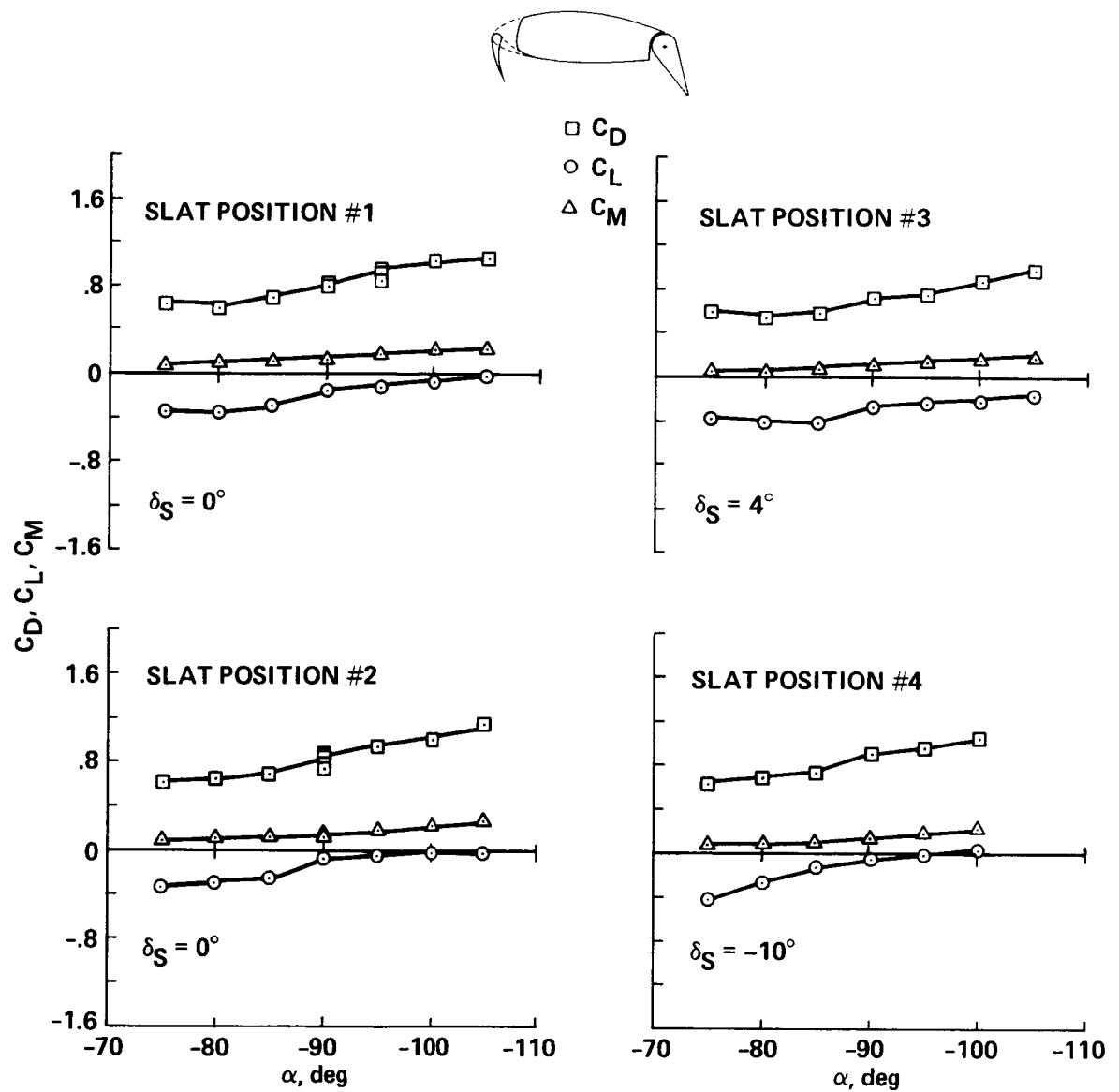
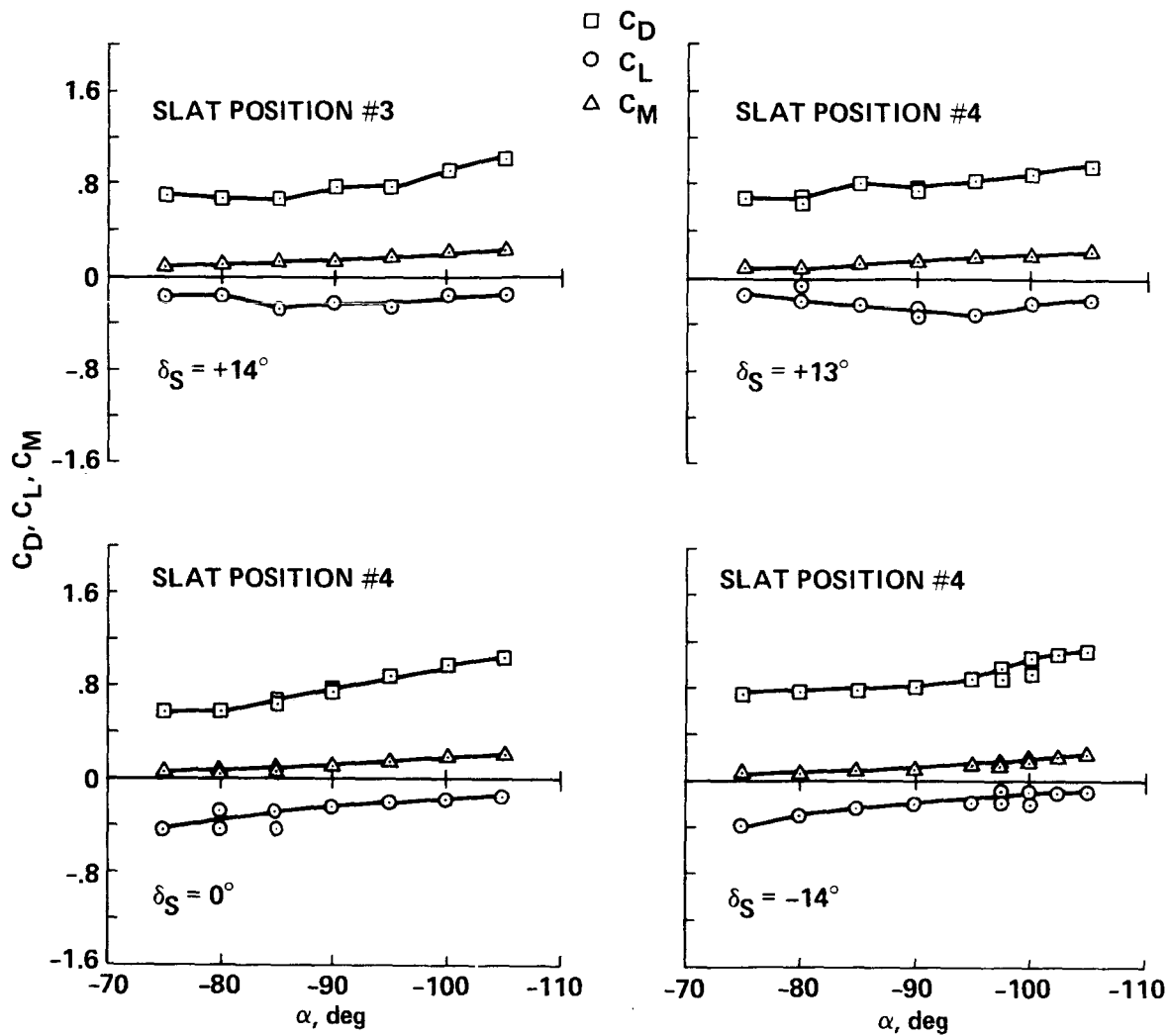
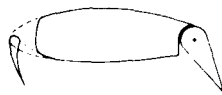


Figure 15.- Test positions for lower-surface-leading-edge slat.



(a) Lift, drag, and moment coefficients for various leading-edge lower surface slat positions,  $60^\circ$  trailing-edge flap angle.

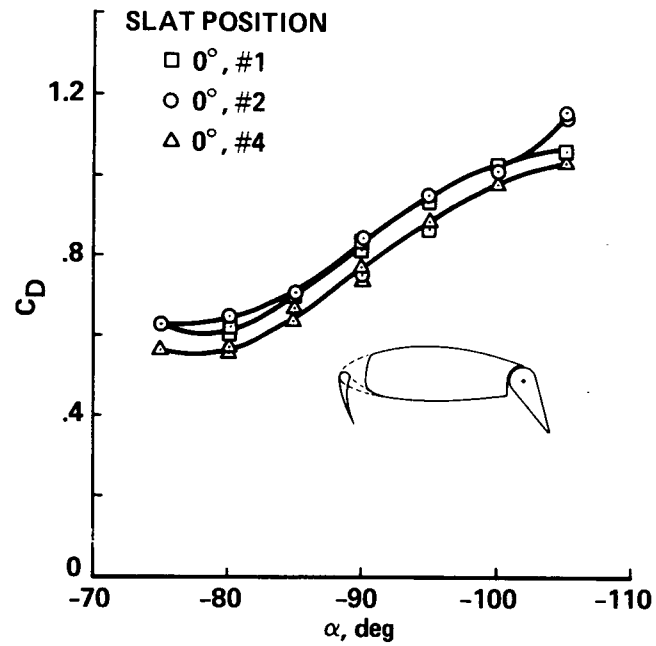
Figure 16.- Aerodynamic characteristics of a two-dimensional wing at angles of attack near  $-90^\circ$ ; leading-edge lower surface slat, 30% chord plain flap (configuration j).



(b) Lift, drag, and moment coefficients for various lower surface slat positions, 60° flap angle.

Figure 16.- Continued.





(c) Effect of angle of attack on drag coefficient for various slat positions, 60° flap angle.

Figure 16.- Concluded.

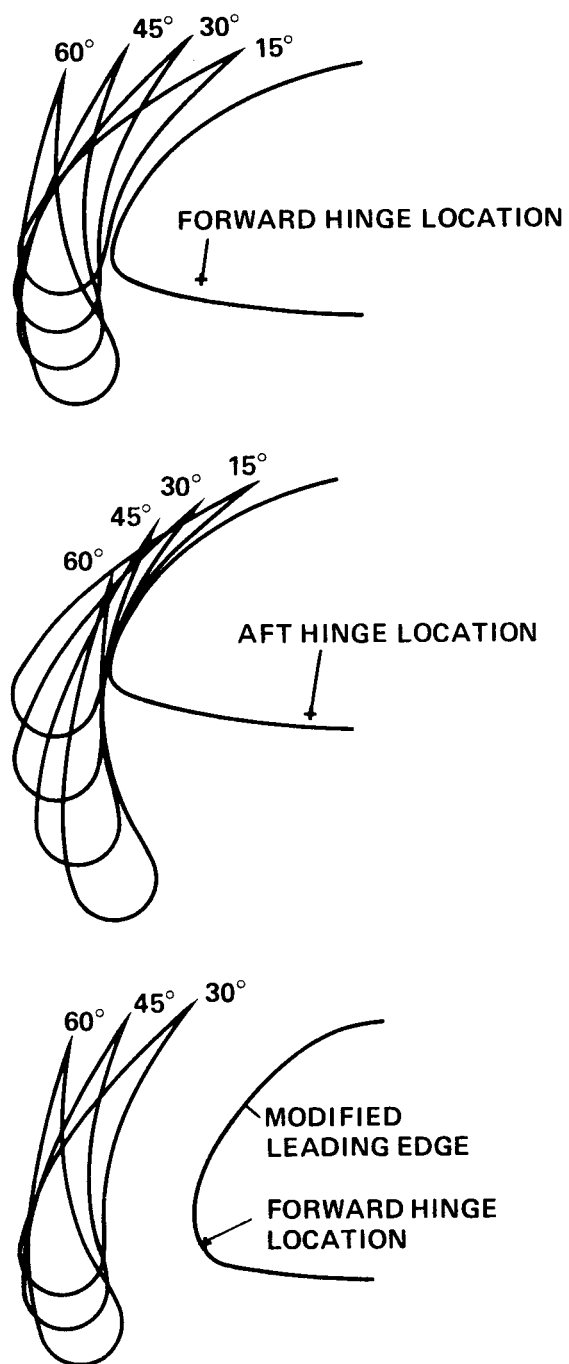
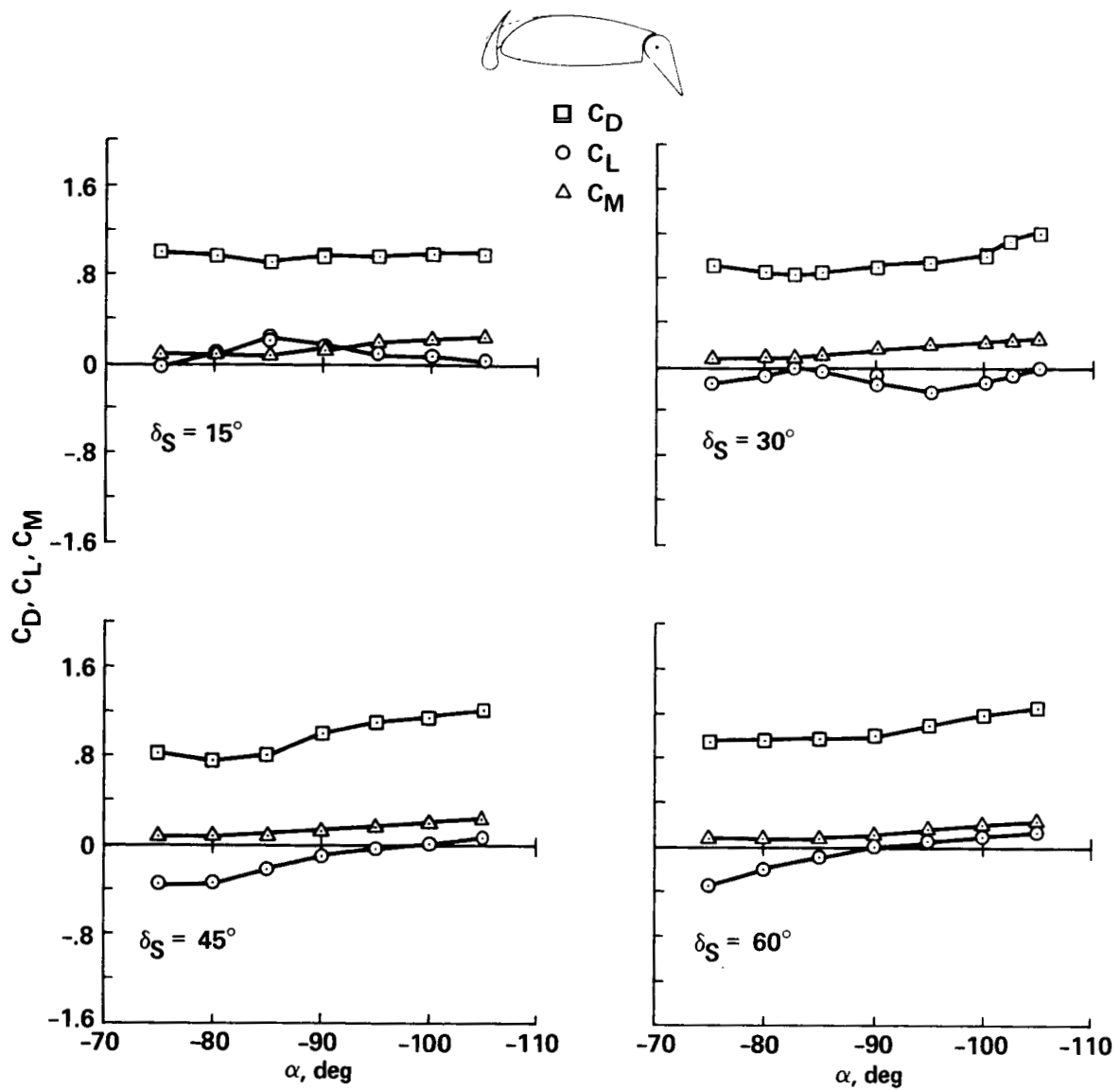
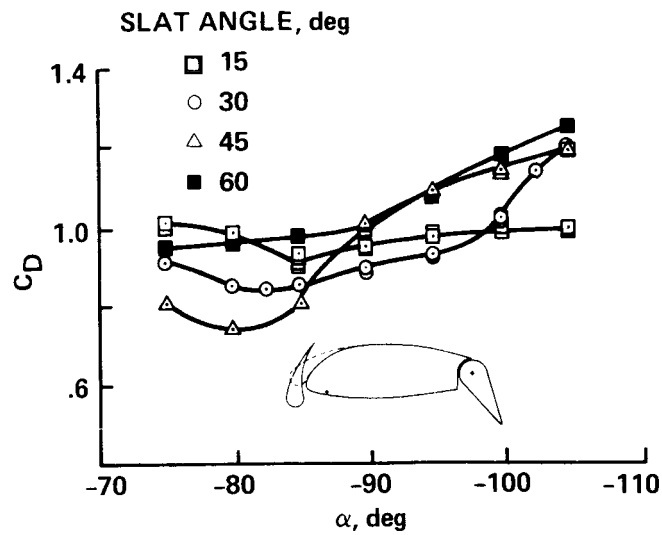


Figure 17.- Test positions for upper surface leading-edge slat.

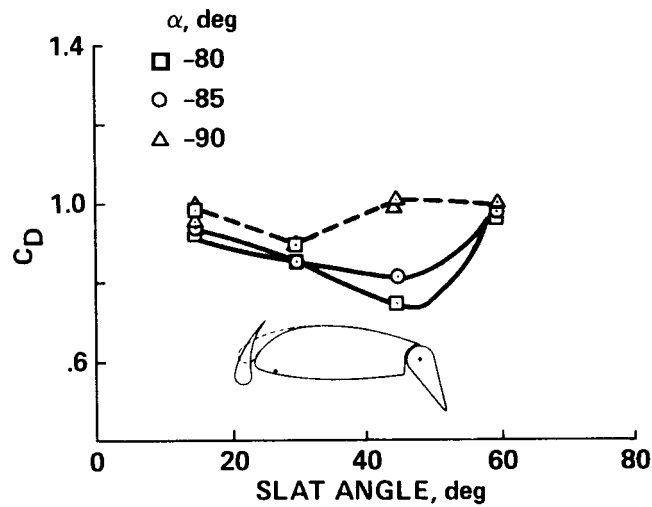


(a) Lift, drag, and moment coefficients for various leading-edge upper surface slat angles,  $60^\circ$  flap angle.

Figure 18.- Aerodynamic characteristics of a two-dimensional wing at angles of attack near  $-90^\circ$ ; upper-surface leading-edge slat forward hinge, 30% chord plain flap (configuration k).

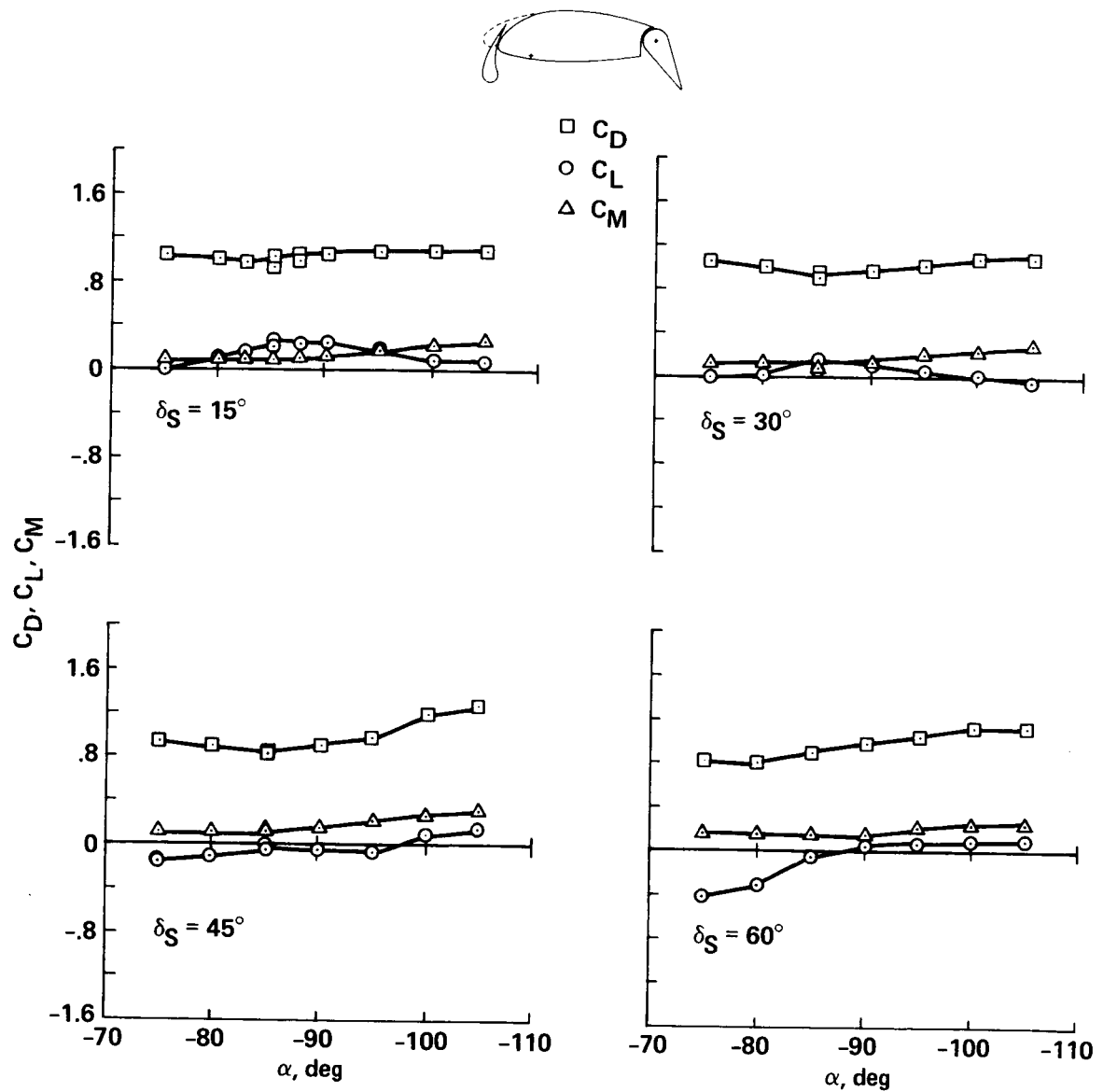


(b) Effect of angle of attack on drag coefficient for various slat angles, 60° flap angle.



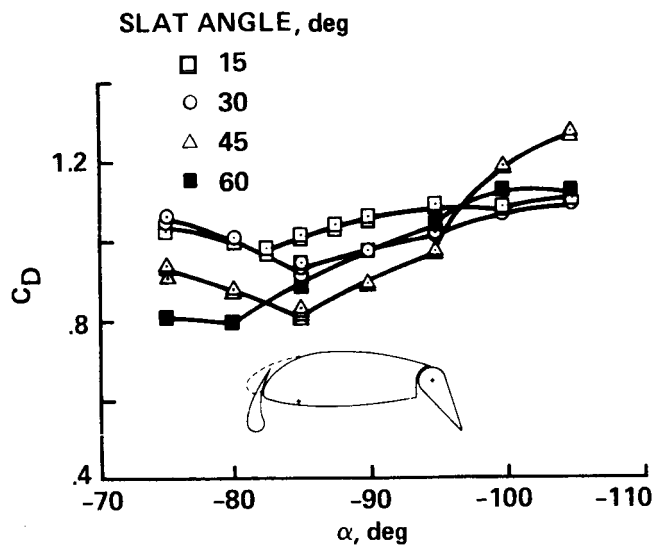
(c) Effect of slat angle on drag coefficient for various angles of attack, 60° flap angle.

Figure 18.- Concluded.

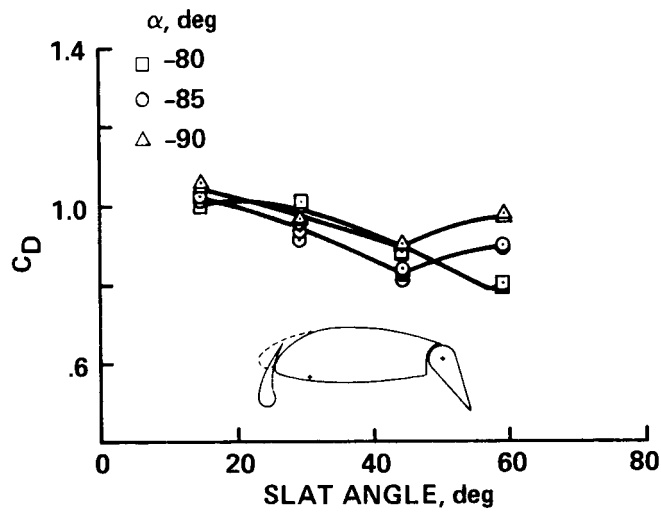


(a) Lift, drag, and moment coefficients for various leading-edge upper surface slat angles,  $60^\circ$  flap angle.

Figure 19.- Aerodynamic characteristics of a two-dimensional wing at angles of attack near  $-90^\circ$ ; upper surface leading-edge slat aft hinge, 30% chord plain flap (configuration 1).



(b) Effect of angle of attack on drag coefficient for various slat angles, 60° flap angle.



(c) Effect of slat angle on drag coefficient for various angles of attack, 60° flap angle.

Figure 19.- Concluded.

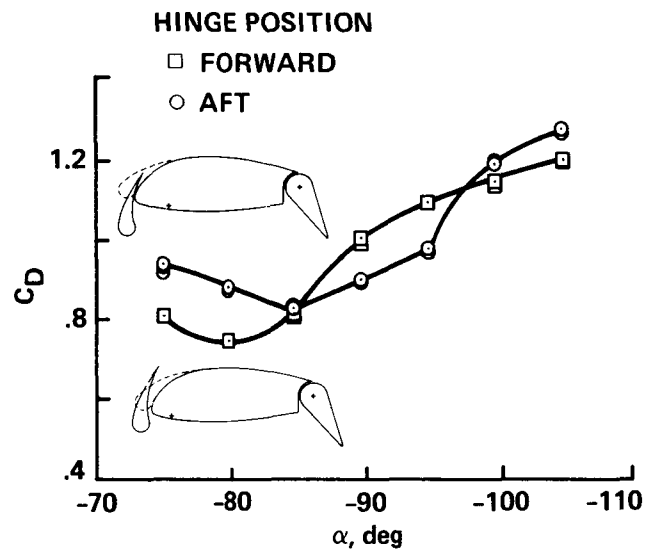
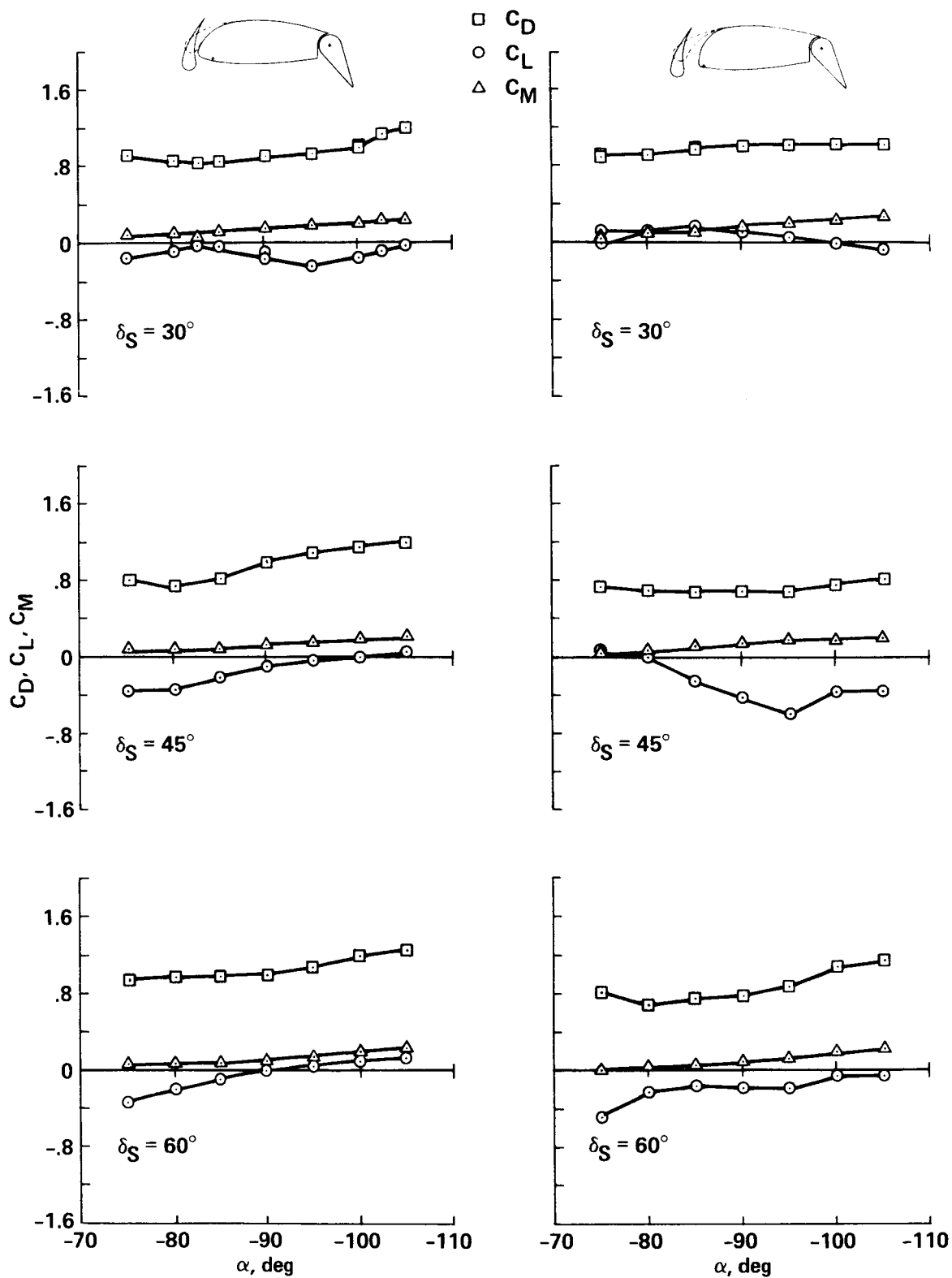


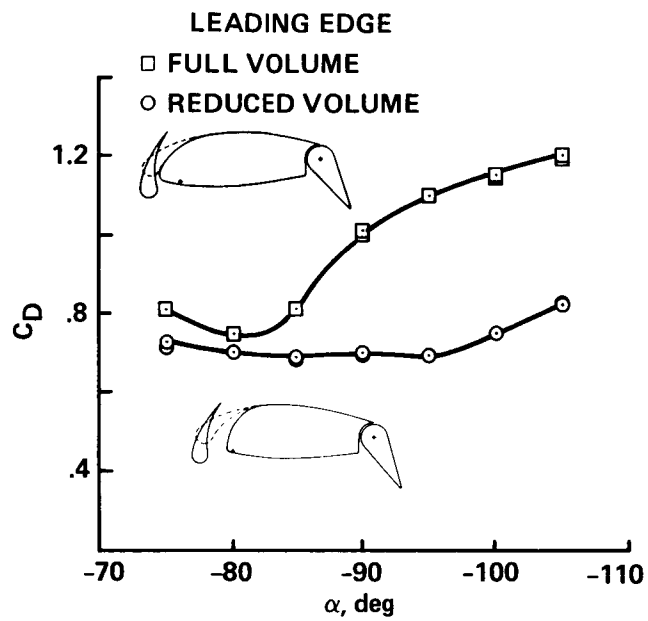
Figure 20.- Effect of leading-edge upper surface hinge location on drag coefficient for  $45^\circ$  slat angle and  $60^\circ$  flap angle (configuration k and configuration l).



(a) Lift, drag, and moment coefficients for various leading-edge slat angles, 60° flap angle.

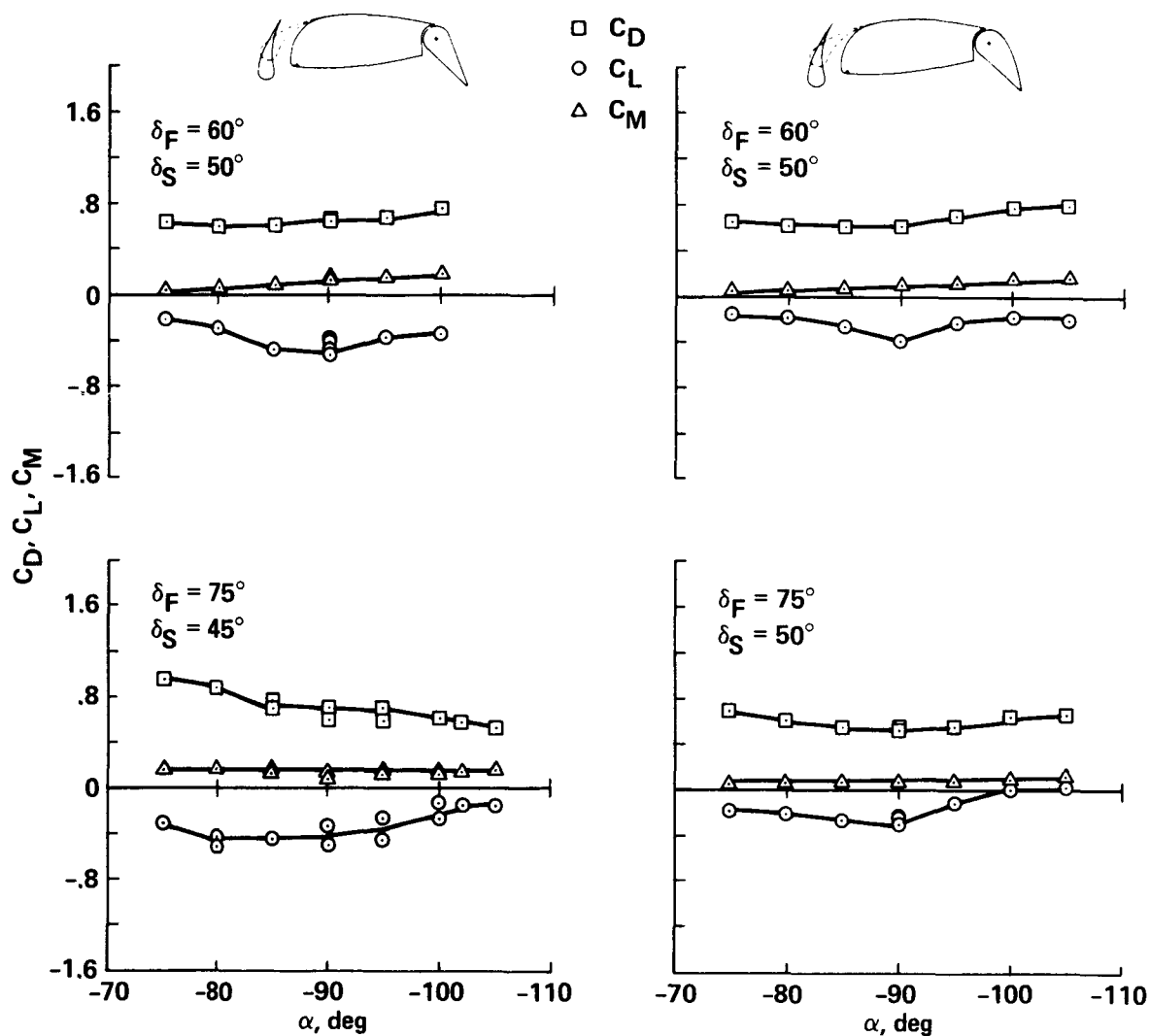
Figure 21.- Effect of wing leading-edge shape on aerodynamic characteristics for various flap angles (configuration k and configuration m).





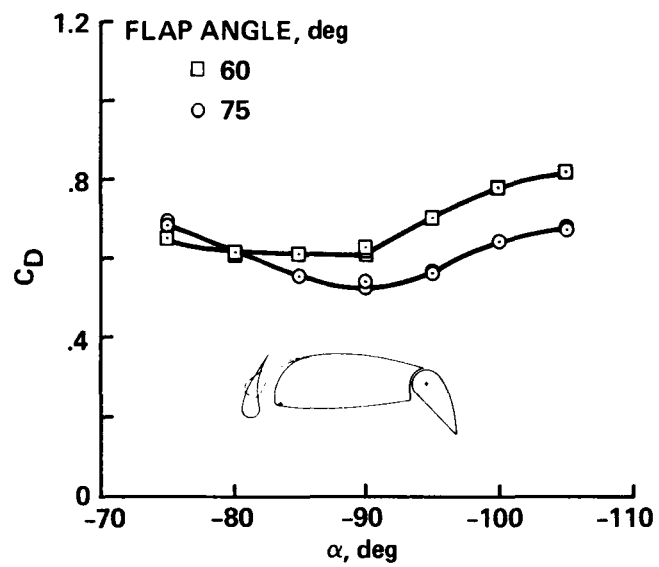
(b) Effect of wing leading-edge shape on drag coefficient, 45° slat angle and 60° flap angle.

Figure 21.- Concluded.



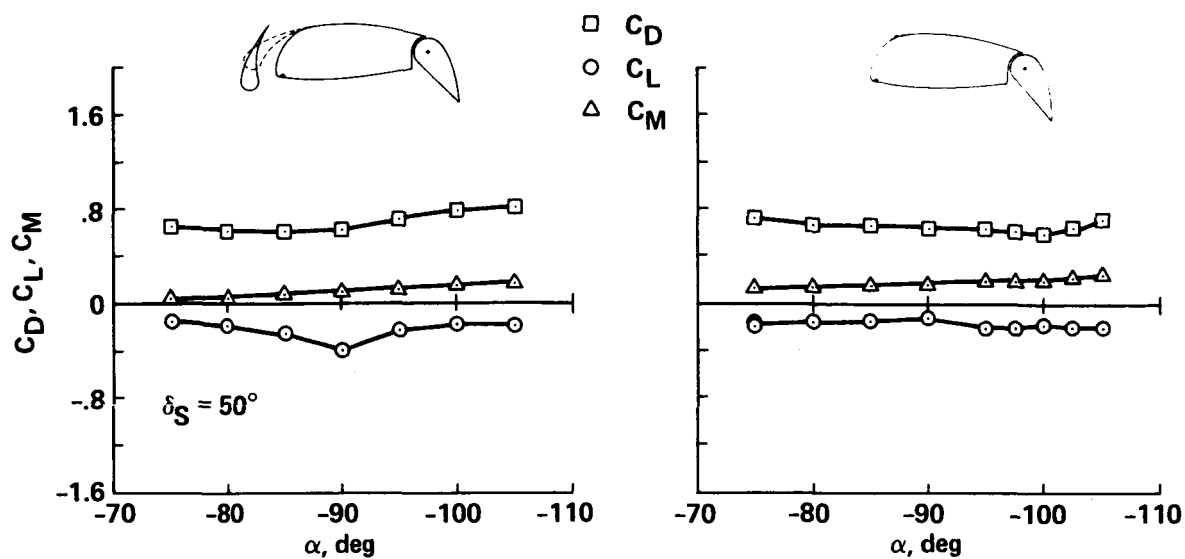
(a) Effect of modified flap contour on lift, drag, and moment coefficients for various slat and flap angles.

Figure 22.- Comparison of the aerodynamic characteristics of configuration n (modified trailing-edge flap contour) and configuration m (30% chord plain flap).

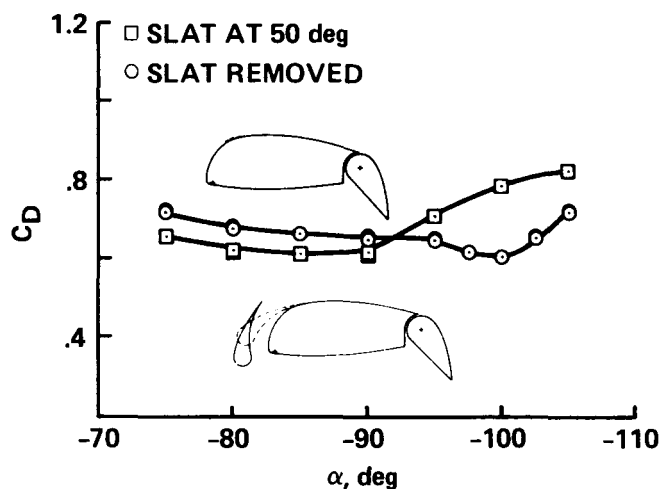


(b) Effect of angle of attack on drag coefficient for the reduced leading-edge volume and the modified flap, 50° slat angle.

Figure 22.- Concluded.

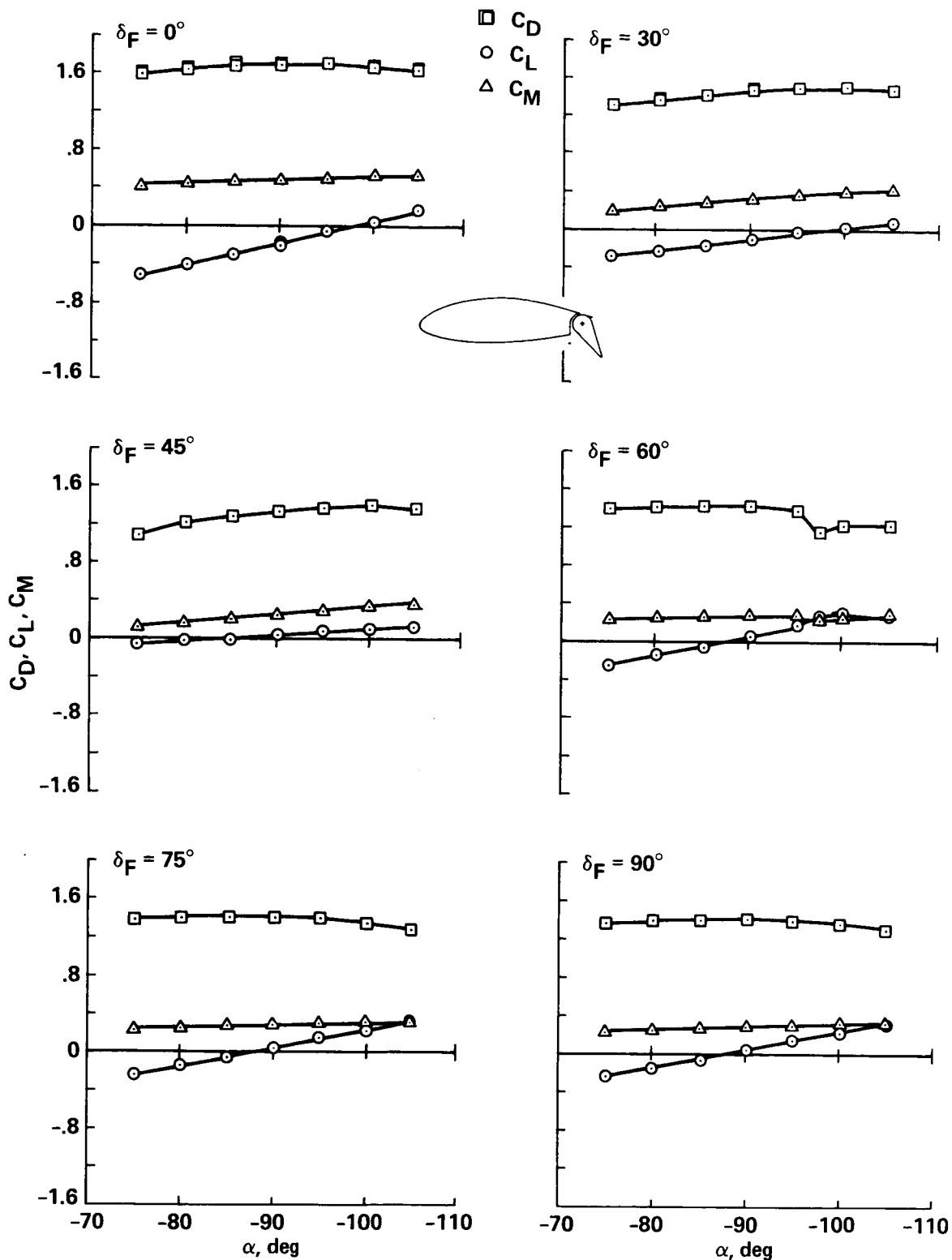


(a) Lift, drag, and moment coefficient variations for the reduced volume leading-edge with and without slat,  $60^\circ$  flap angle.



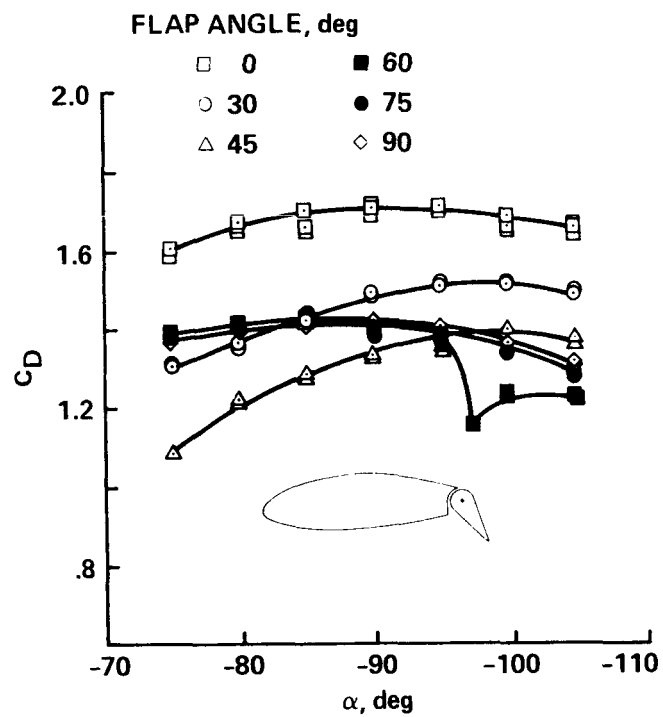
(b) Effect of slat on drag coefficient for a range of angles of attack,  $60^\circ$  flap angle.

Figure 23.- Comparison of aerodynamic characteristics for configuration n (reduced leading-edge volume/modified flap contour with slat) and configuration o (slat removed).



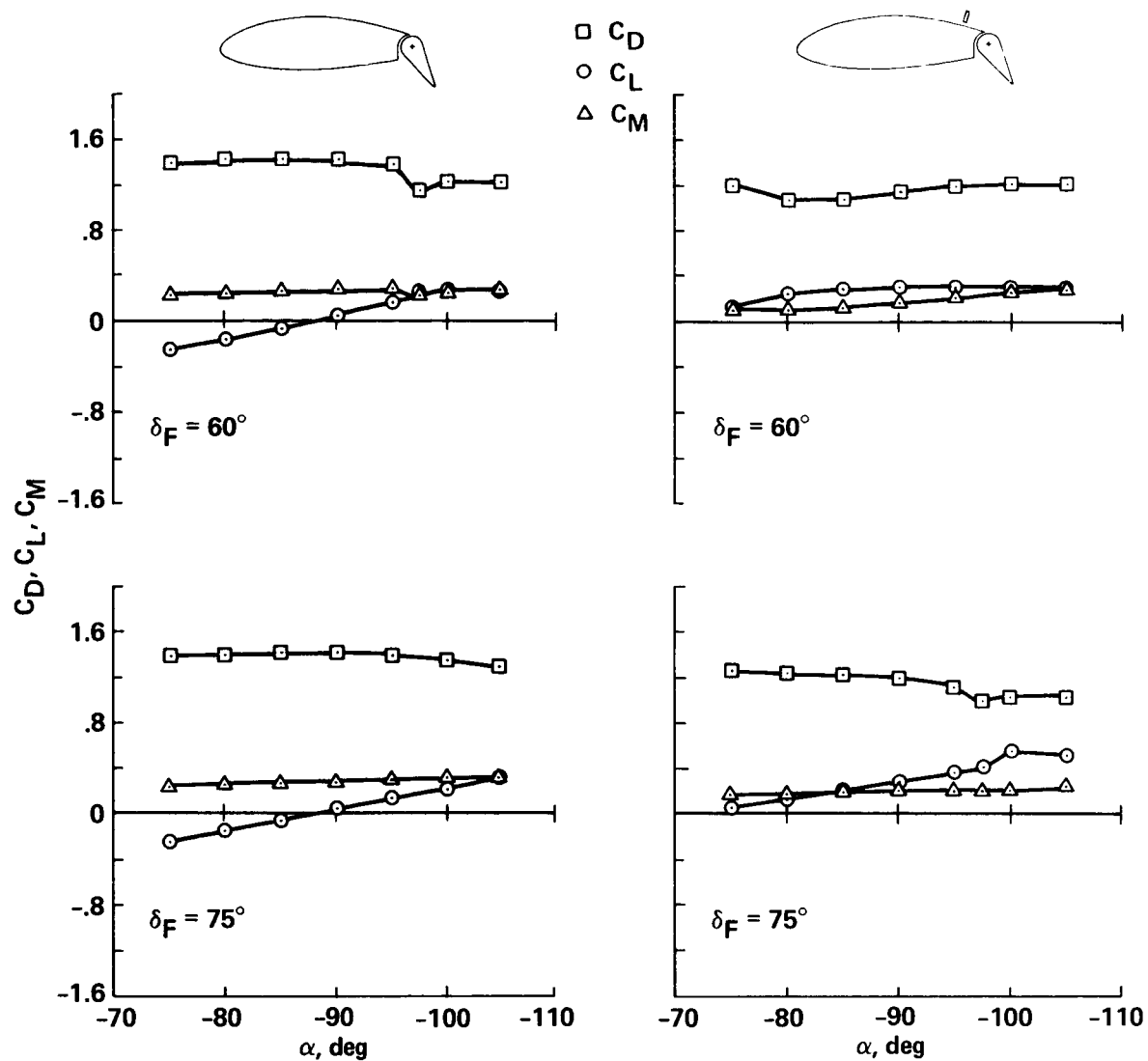
(a) Lift, drag, and moment coefficients for various flap angles.

Figure 24.- Aerodynamic characteristics of a two-dimensional wing at angles of attack near  $-90^\circ$ ; basic leading edge, 25% chord plain flap (configuration a).



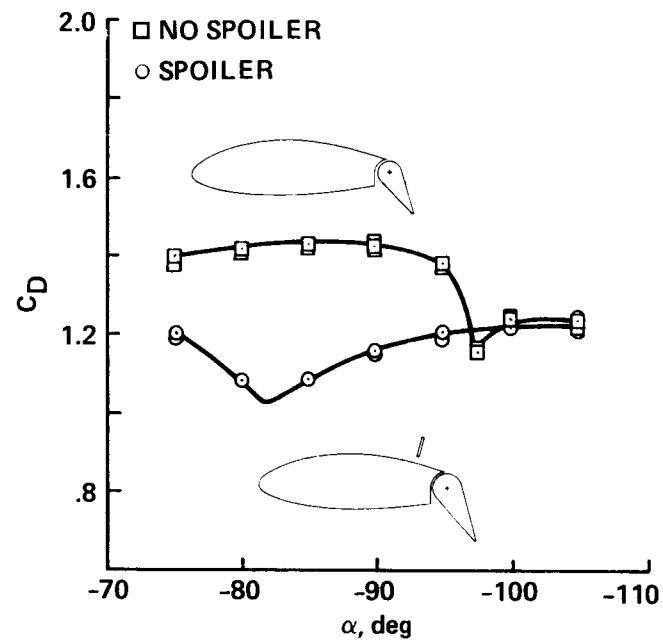
(b) Effect of angle of attack on drag coefficient for various flap angles.

Figure 24.- Continued.



(c) Effect of upper surface spoiler on aerodynamic characteristics for various flap angles.

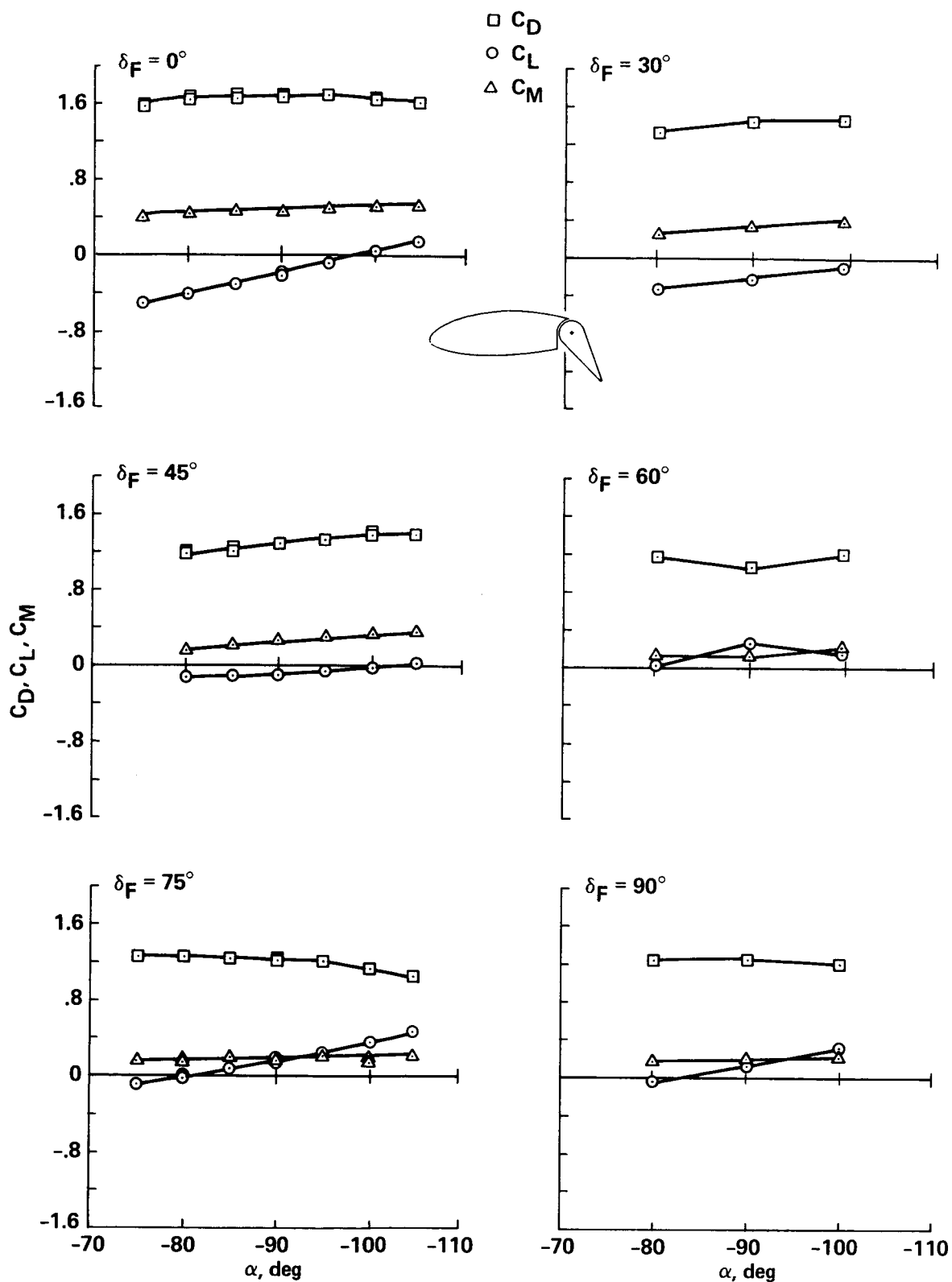
Figure 24.- Continued.



(d) Effect of upper surface spoiler on drag coefficient, 60° flap angle.

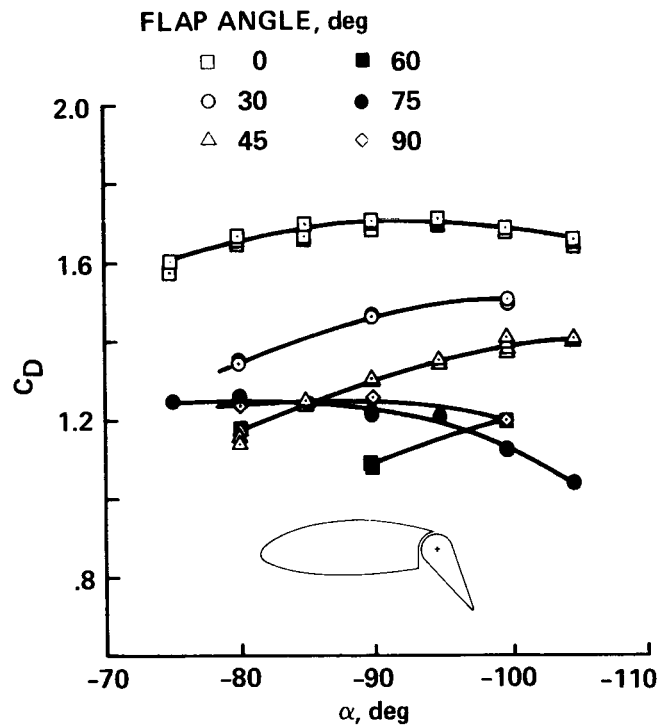
Figure 24.- Concluded.





(a) Lift, drag, and moment coefficients for various flap angles.

Figure 25.- Aerodynamic characteristics of a two-dimensional wing at angles of attack near  $-90^\circ$ ; basic leading edge, 35% chord plain flap (configuration c).



(b) Effect of angle of attack on drag coefficient for various flap angles.

Figure 25.- Concluded.

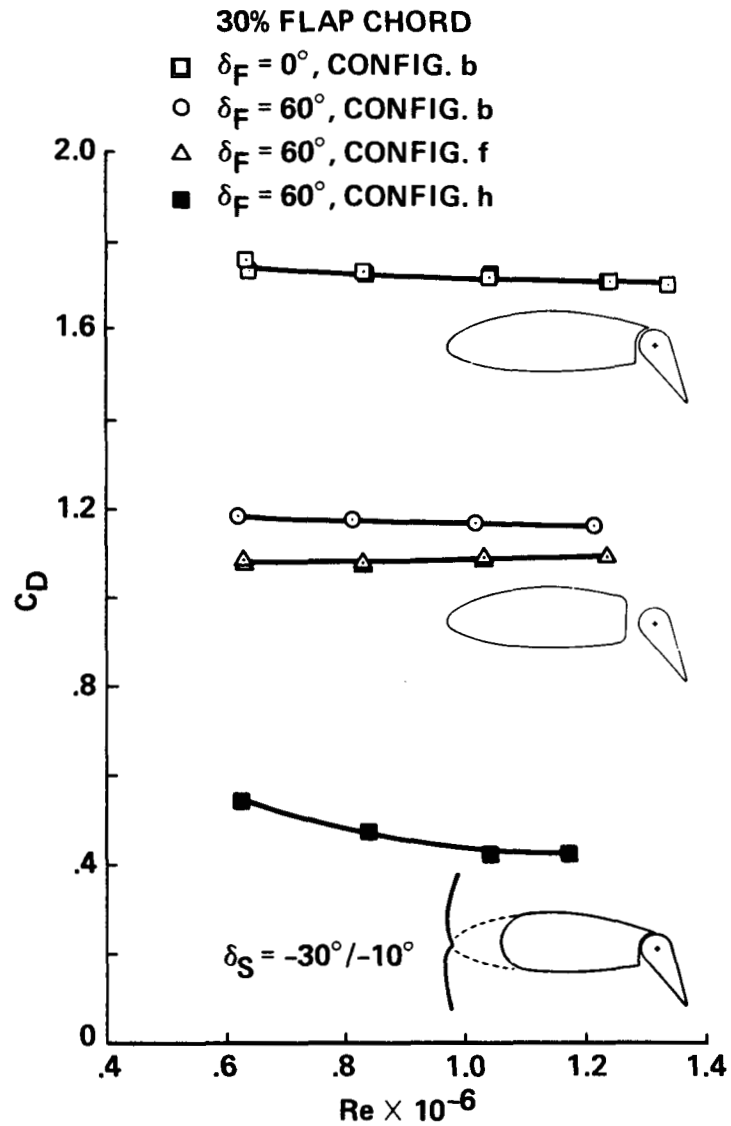


Figure 26.- Effect of Reynolds number on drag coefficient for a wide range of drag levels at  $-90^\circ$  angle of attack.

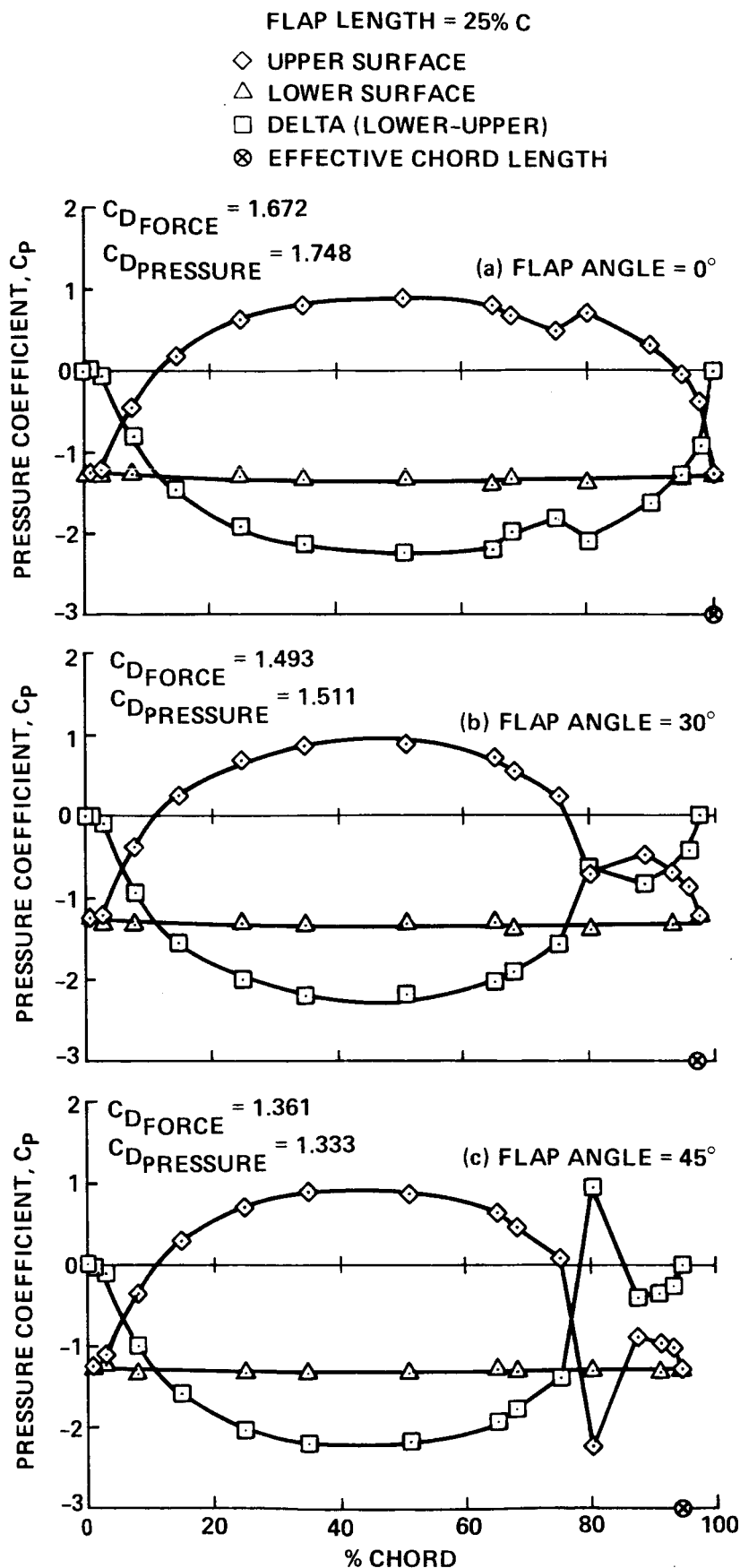


Figure 27.- Effect of flap angle on surface pressure distribution, angle of attack  $\alpha = -90^\circ$ .

FLAP LENGTH = 25% C

- ◇ UPPER SURFACE
- △ LOWER SURFACE
- DELTA (LOWER-UPPER)
- ⊗ EFFECTIVE CHORD LENGTH

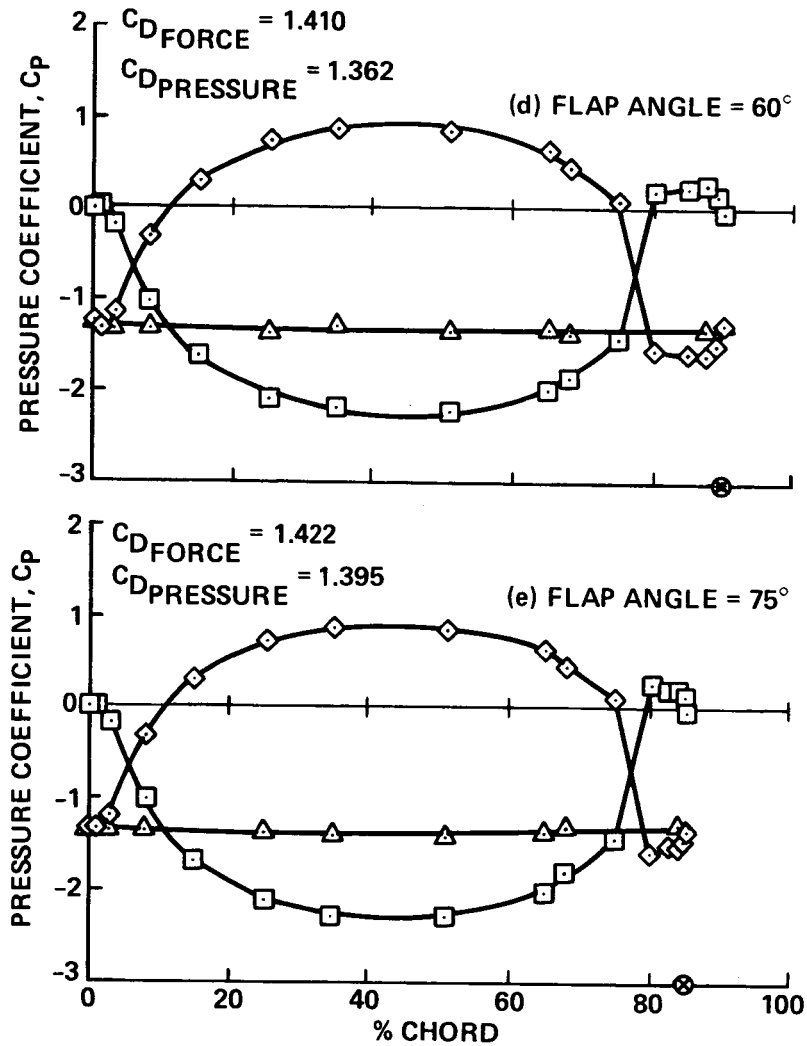


Figure 27.- Concluded.

FLAP LENGTH = 25% C

- ◇ UPPER SURFACE
- △ LOWER SURFACE
- DELTA (LOWER-UPPER)
- ⊗ EFFECTIVE CHORD LENGTH

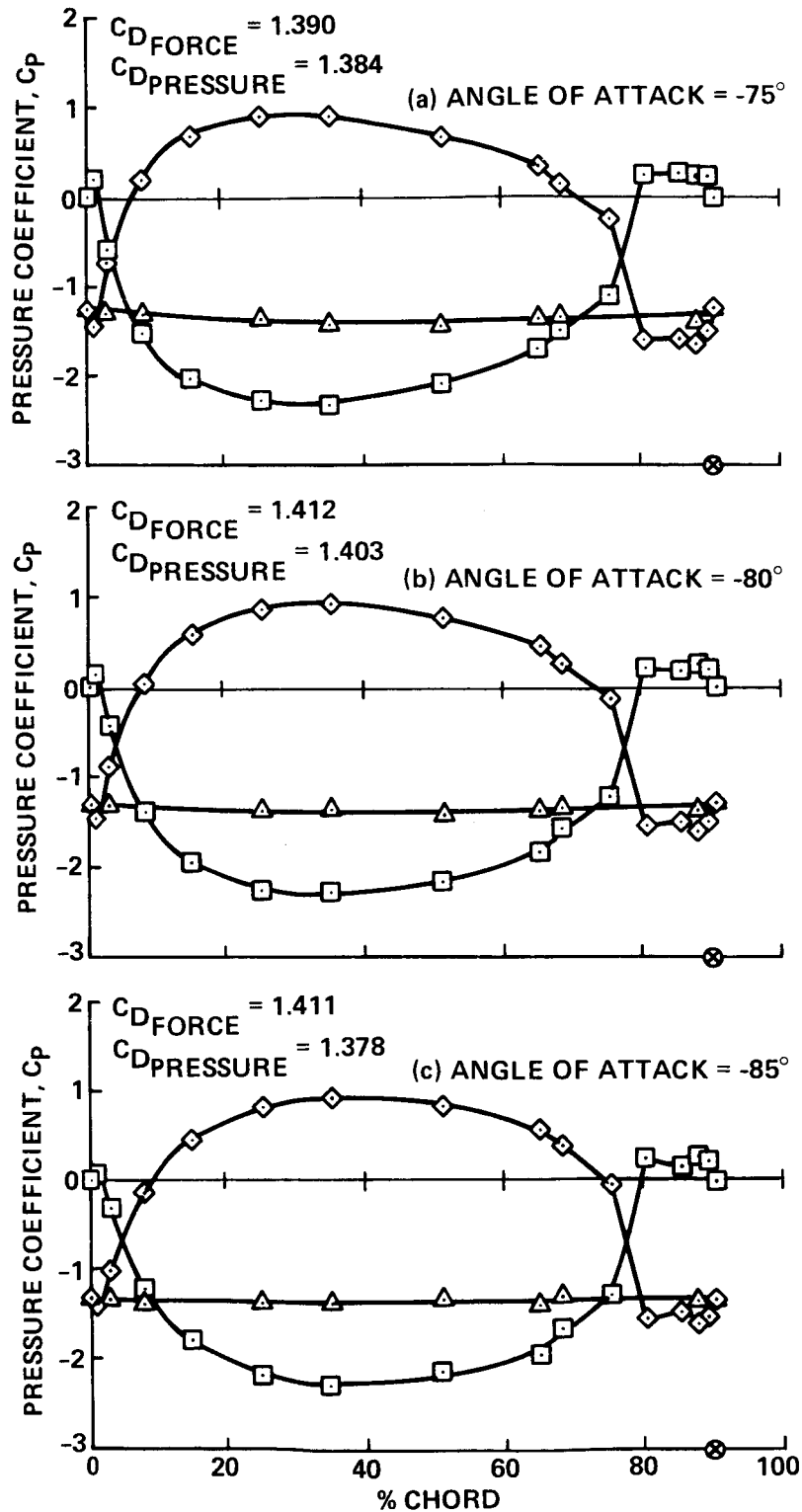


Figure 28.- Effect of angle of attack on surface pressure distribution, flap angle =  $60^\circ$ .

FLAP LENGTH = 25% C

- ◇ UPPER SURFACE
- △ LOWER SURFACE
- DELTA (LOWER-UPPER)
- ⊗ EFFECTIVE CHORD LENGTH

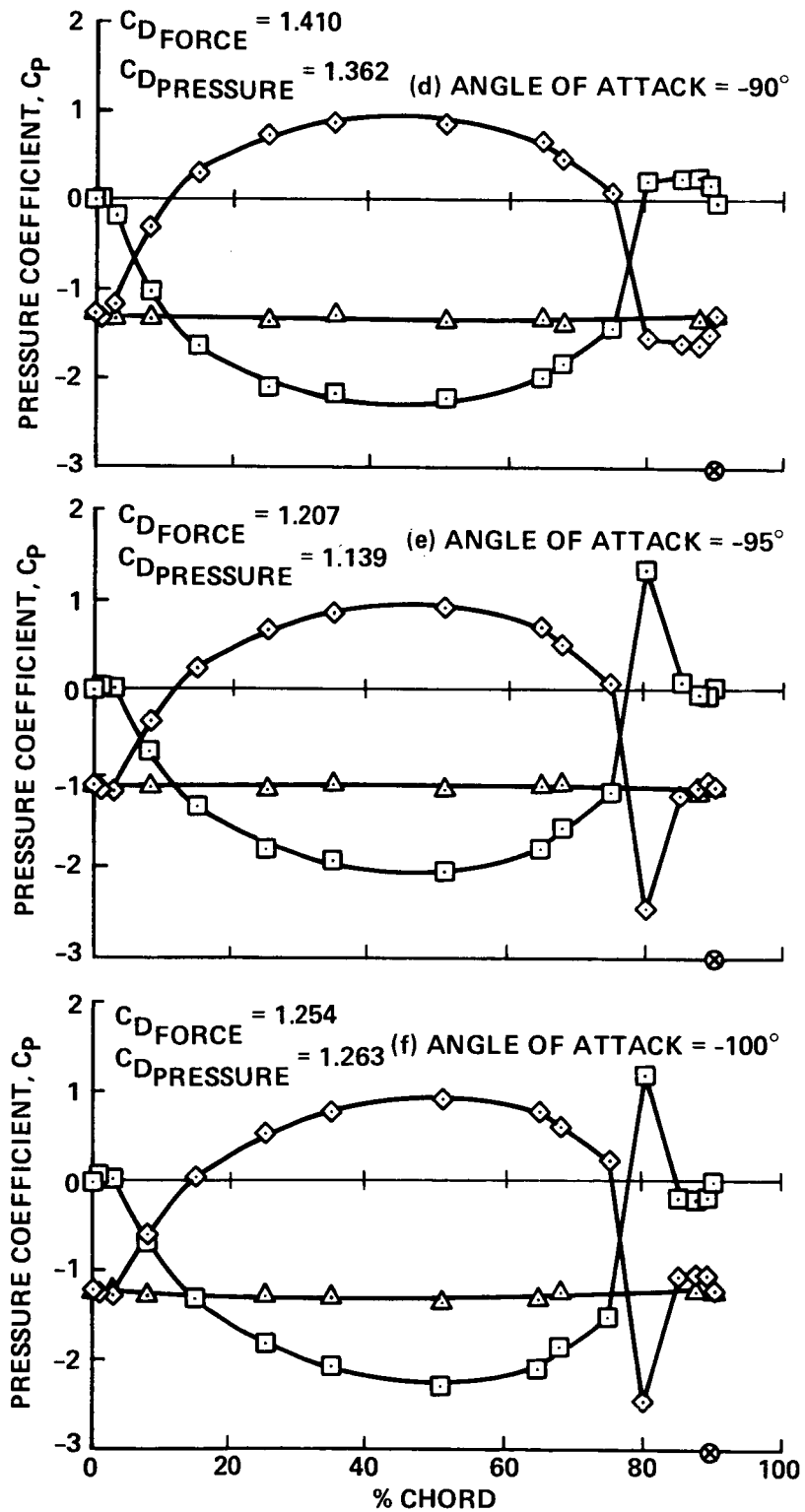


Figure 28.- Concluded.

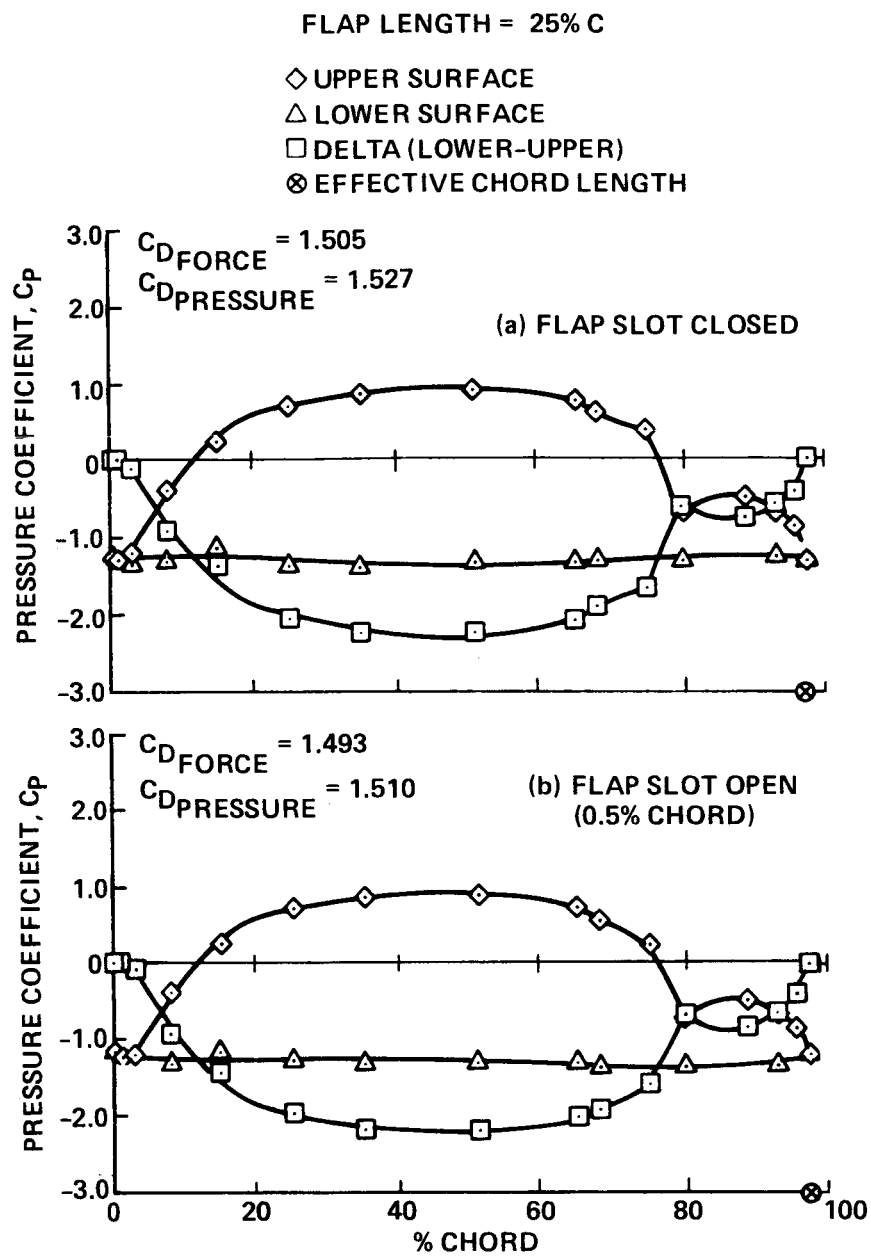


Figure 29.- Effect of flap slot on pressure distribution.



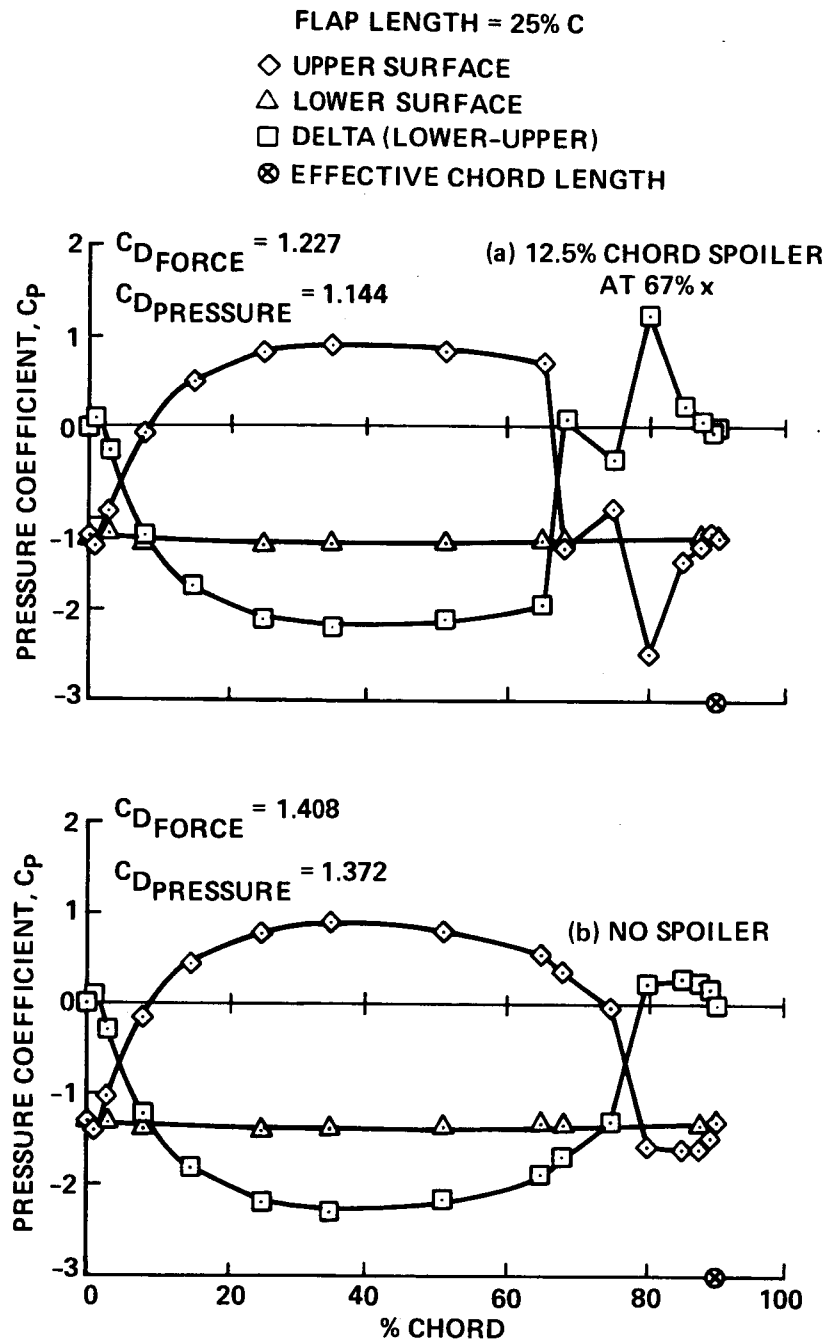


Figure 30.- Effect of upper-surface spoiler on surface pressure distribution  
flap angle =  $60^\circ$ , angle of attack =  $-85^\circ$ .

- ◇ UPPER SURFACE
- △ LOWER SURFACE
- DELTA (LOWER-UPPER)
- ⊗ EFFECTIVE CHORD LENGTH

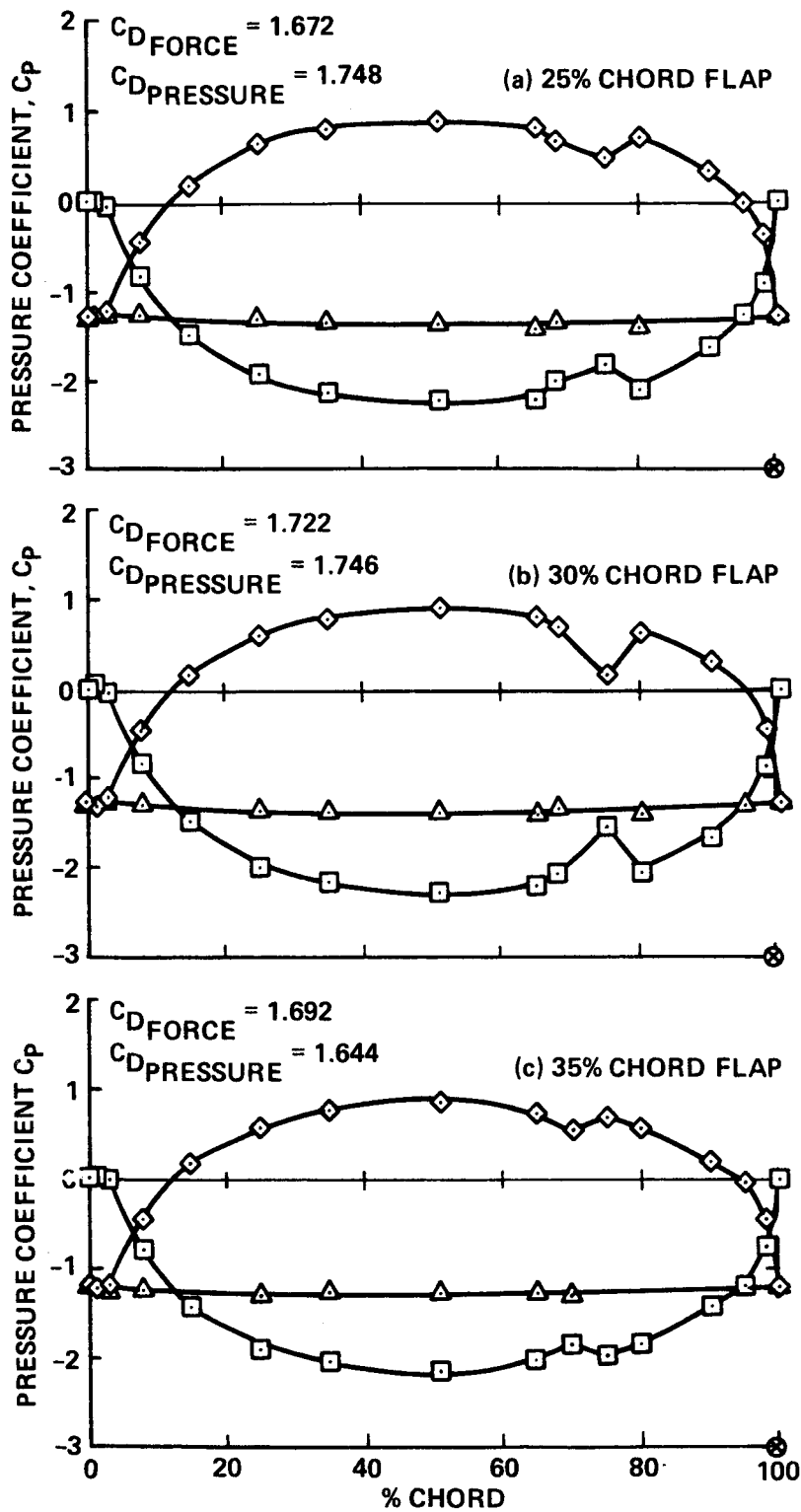


Figure 31.- Effect of flap size on surface pressure distribution, flap angle =  $0^\circ$ , angle of attack =  $-90^\circ$ .

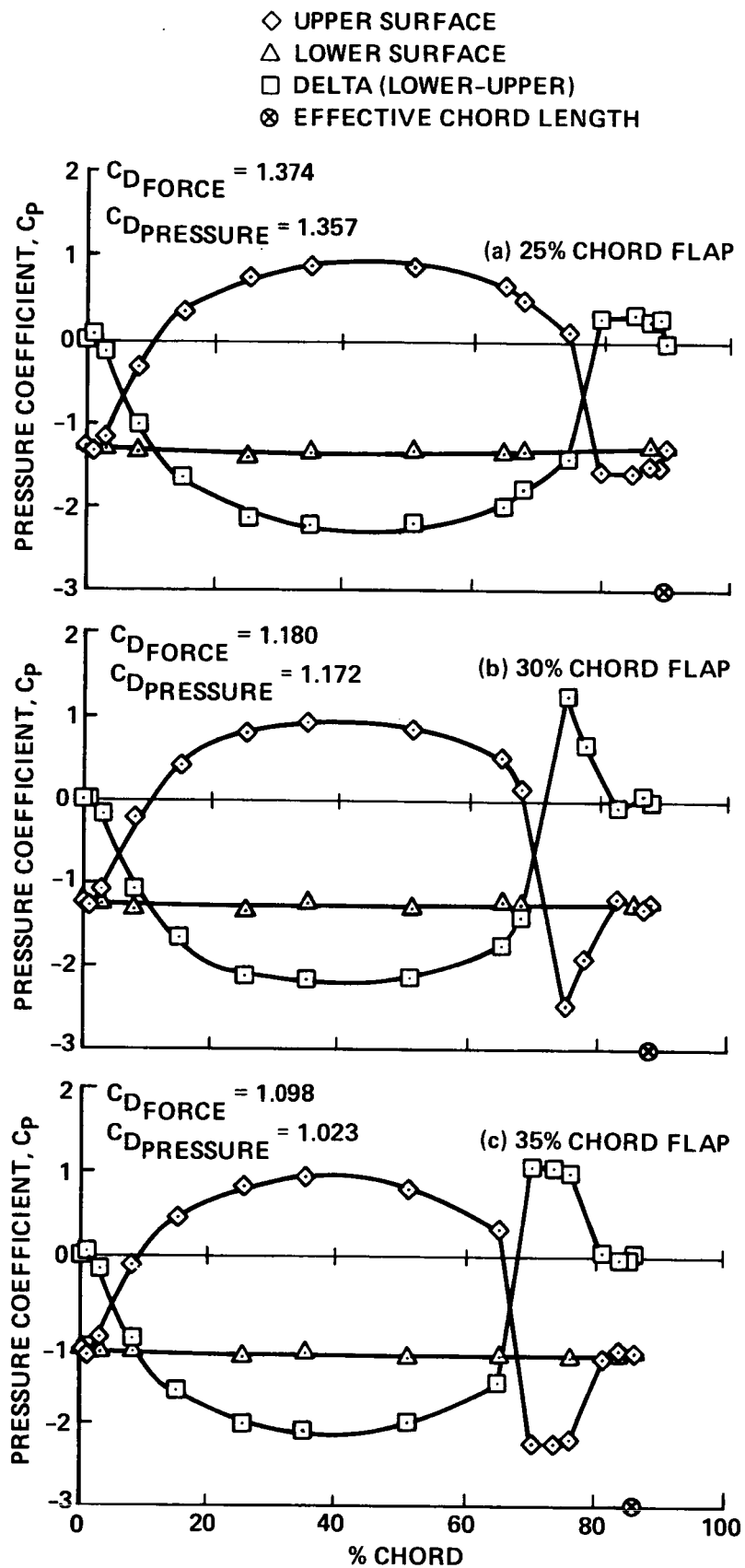


Figure 32.- Effect of flap size on surface pressure distribution, flap angle =  $60^\circ$ , angle of attack =  $-90^\circ$ .

1. Report No. NASA TM-88373 USAVSCOM TM-86-A-8		2. Government Accession No.		3. Recipient's Catalog No.	
4. Title and Subtitle AERODYNAMIC CHARACTERISTICS OF TWO-DIMENSIONAL WING CONFIGURATIONS AT ANGLES OF ATTACK NEAR -90°				5. Report Date December 1986	
				6. Performing Organization Code	
7. Author(s) Martin Maisel, Georgene Laub, and W. J. McCroskey				8. Performing Organization Report No. A-86427	
9. Performing Organization Name and Address Aeroflightdynamics Directorate, U.S. Army Aviation Research and Technology Activity, Ames Research Center, Moffett Field, CA 94035				10. Work Unit No.	
				11. Contract or Grant No.	
12. Sponsoring Agency Name and Address National Aeronautics and Space Administration, Washington, D.C. 20546 and U.S. Army Aviation Systems Command, St. Louis, MO 63120				13. Type of Report and Period Covered Technical Memorandum	
				14. Sponsoring Agency Code 532-06-11	
15. Supplementary Notes  Point of contact: M. Maisel, MS 237-5, Ames Research Center, Moffett Field, CA 94035 (415) 694-6372 or FTS 464-6372					
16. Abstract  Wind tunnel tests were conducted to determine the drag of two-dimensional wing sections operating in a near-vertical flow condition. Various leading- and trailing-edge configurations, including plain flaps of 25, 30, and 35% chord were tested at angles of attack from -75 to -105°. Reynolds numbers examined ranged from approximately $0.6 \times 10^6$ to $1.4 \times 10^6$ . The data were obtained using a wind tunnel force and moment balance system and arrays of chordwise pressure orifices. The results showed that significant reductions in drag, beyond what would be expected by virtue of the decreased frontal area, were obtainable with geometries that delayed flow separation. Rapid changes in drag with angle of attack were noted for many configurations. The results, however, were fairly insensitive to Reynolds number variations. Drag values computed from the pressure data generally agreed with the force data within 2%.					
17. Key Words (Suggested by Author(s))  Download, Two-dimensional wing, Wind tunnel testing, Drag, Wing leading edge, Wing trailing edge, Wing flap, Wing slots, Wing slats, Wing spoiler			18. Distribution Statement  Unlimited - Unclassified  Subject category - 02		
19. Security Classif. (of this report) Unclassified		20. Security Classif. (of this page) Unclassified		21. No. of Pages 83	
				22. Price* A03	

1. Report No. NASA TM-88373 USAVSCOM TM-86-A-8		2. Government Accession No.		3. Recipient's Catalog No.	
4. Title and Subtitle AERODYNAMIC CHARACTERISTICS OF TWO-DIMENSIONAL WING CONFIGURATIONS AT ANGLES OF ATTACK NEAR -90°				5. Report Date December 1986	
				6. Performing Organization Code	
7. Author(s) Martin Maisel, Georgene Laub, and W. J. McCroskey				8. Performing Organization Report No. A-86427	
9. Performing Organization Name and Address Aeroflightdynamics Directorate, U.S. Army Aviation Research and Technology Activity, Ames Research Center, Moffett Field, CA 94035				10. Work Unit No.	
				11. Contract or Grant No.	
12. Sponsoring Agency Name and Address National Aeronautics and Space Administration, Washington, D.C. 20546 and U.S. Army Aviation Systems Command, St. Louis, MO 63120				13. Type of Report and Period Covered Technical Memorandum	
				14. Sponsoring Agency Code 532-06-11	
15. Supplementary Notes  Point of contact: M. Maisel, MS 237-5, Ames Research Center, Moffett Field, CA 94035 (415) 694-6372 or FTS 464-6372					
16. Abstract <p><i>@ ASD</i> Wind tunnel tests were conducted to determine the drag of two-dimensional wing sections operating in a near-vertical flow condition. Various leading- and trailing-edge configurations, including plain flaps of 25, 30, and 35% chord were tested at angles of attack from -75 to <del>-90</del>. Reynolds numbers examined ranged from approximately <math>0.6 \times 10^6</math> to <math>1.4 \times 10^6</math>. The data were obtained using a wind tunnel force and moment balance system and arrays of chordwise pressure orifices. The results showed that significant reductions in drag, beyond what would be expected by virtue of the decreased frontal area, were obtainable with geometries that delayed flow separation. Rapid changes in drag with angle of attack were noted for many configurations. The results, however, were fairly insensitive to Reynolds number variations. Drag values computed from the pressure data generally agreed with the force data within 2%.</p> <p><i>@ ASD Duthon.</i></p> <p><i>- 105 deg.</i></p> <p><i>10 to the 6th power</i></p>					
17. Key Words (Suggested by Author(s))  Download, Two-dimensional wing, Wind tunnel testing, Drag, Wing leading edge, Wing trailing edge, Wing flap, Wing slots, Wing slats, Wing spoiler				18. Distribution Statement  Unlimited - Unclassified  Subject category - 02	
19. Security Classif. (of this report) Unclassified		20. Security Classif. (of this page) Unclassified		21. No. of Pages 83	
				22. Price* A03	